SECURITY INFORMATION

AUTHOR'S PERSONAL COPY

CONFIDENTIAL

Copy 410
RM L53I21

NACA RM L53I21

NACA

RESEARCH MEMORANDUM

AN INVESTIGATION AT MACH NUMBER 2.40 OF FLAP-TYPE CONTROLS EQUIPPED WITH OVERHANG NOSE BALANCES

By James N. Mueller

Langley Aeronautical Laboratory
Langley Field, Va.

CLASSIFICATION CHANGED TO UNCLASSIFIED
AUTHORITY: NACA RESEARCH ABSTRACT NO. 120
EFFECTIVE DATE: SEPTEMBER 13, 1957 WHL

CLASSIFIED DOCUMENT

This material contains information affecting the National Defense of the United States within the meaning of the espionage laws, Title 18, U.S.C., Secs. 793 and 794, the transmission or revelation of which in any manner to an unauthorized person is prohibited by law.

NATIONAL ADVISORY COMMITTEE
FOR AERONAUTICS

WASHINGTON

November 17, 1953

CONFIDENTIAL

NATIONAL ADVISORY COMMITTEE FOR AERONAUTICS

RESEARCH MEMORANDUM

AN INVESTIGATION AT MACH NUMBER 2.40 OF FLAP-TYPE CONTROLS EQUIPPED WITH OVERHANG NOSE BALANCES

By James N. Mueller

SUMMARY

Some of the factors affecting the two-dimensional characteristics of flap-type controls equipped with overhang nose balances have been investigated at a Mach number of 2.40. The effects of changing nose-balance overhang, altering the shape of the nose balance, beveling the afterbody of the basic wing forward of the flap nose, varying wing-flap gap size, fixing transition, and varying the flap trailing-edge thickness were evaluated.

The results of the investigation indicated that low values of both hinge moments due to flap deflection and hinge moments due to angle of attack could be obtained for a flap attached to a blunt-base wing with a gap of 0.033c when the balance overhang was about 80 percent of the flap chord rearward of the hinge line. The primary effect of beveling the rear section of the basic wing or increasing wing-flap gap size was to minimize the wing-wake—boundary-layer effects over the flap so that the nose-balance effectiveness was increased. The lifting effectiveness of the flap was not appreciably affected by overhang balance. The effects of fixing transition and changing flap overhang nose shape on the balancing characteristics were negligible. Increasing flap trailing-edge thickness resulted in increased control heaviness.

A method for estimating the aerodynamic loading over trailing-edge flap-type controls equipped with overhang nose balances is shown to give good results.

INTRODUCTION

At supersonic speeds, unbalanced controls have large hinge moments that require heavy and complex mechanical booster systems. A reduction in hinge moments by use of aerodynamic balance is desirable to reduce

the size and weight of the boost system required and in some cases to provide controls that can be operated manually in an emergency.

For some time the National Advisory Committee for Aeronautics has been conducting investigations of the balancing characteristics at transonic speeds of various control arrangements (refs. 1 to 6). At supersonic speeds, however, experimental data on the aerodynamic balancing of flap-type controls are relatively meager and adequate theory is not available for predicting balancing characteristics.

An investigation, therefore, has been made in the Langley 9-inch supersonic tunnel at a Mach number of 2.40 of some of the factors affecting the balancing characteristics of flap-type controls equipped with plain overhang nose balances. This study is similar to that reported in references 7 and 8 but was made in a two- rather than three-dimensional flow field and utilized pressure distributions rather than force tests so as to determine the nature of the flow fields about the wing-flap configurations.

A preliminary-data report (ref. 9) has been published relating to the initial phases of the test program which encompassed tests with different amounts of flap nose overhang balance and several wing-flap gap sizes. Subsequent tests included the effect of beveling the afterbody of the basic wing forward of the flap nose, fixed transition studies, the effect of balance nose shape, and the effect of flap trailing-edge thickness. The present paper presents all the pertinent data obtained in this investigation together with a more complete analysis than that of reference 9.

SYMBOLS

p_l	local static pressure
p	stream static pressure
M	stream Mach number
γ	ratio of specific heats for air, 1.4
q	stream dynamic pressure, $\frac{\gamma}{2} M^2 p$
P	pressure coefficient, $\frac{p_l - p}{q}$
P_R	resultant pressure coefficient, $P_L - P_U$

P_L	lower-surface pressure coefficient
P_U	upper-surface pressure coefficient
c_f	flap chord back of hinge line
c_b	chord of balance forward of hinge line
c_t	total flap chord, $c_b + c_f$
c	model chord, main wing plus flap and exclusive of gap
h	section hinge moment of flap, positive when it tends to deflect trailing edge of flap downward
n	section normal force, positive upward
m	section pitching moment about midchord, positive when it tends to rotate the leading edge of airfoil upward
d	section chord force, positive rearward
c_h	section hinge moment, h/qc_f^2
$c_h\left(\frac{c_f}{c_t}\right)^2$	section hinge-moment-coefficient parameter
c_n	section normal-force coefficient of complete configuration, n/qc
c_m	section pitching-moment coefficient of complete configuration, m/qc^2
c_c	section chord-force coefficient of complete configuration, d/qc
V	free-stream velocity
R	Reynolds number, $\rho Vc/\mu$
t	maximum thickness of model
t_B	flap trailing-edge thickness
x/c	chordwise distance from leading edge of wing in terms of model chord, positive rearward

c_{h_δ} rate of change of flap section hinge-moment coefficient with flap deflection, $\left(\frac{\partial c_h}{\partial \delta}\right)_\alpha$

c_{h_α} rate of change of flap section hinge-moment coefficient with angle of attack, $\left(\frac{\partial c_h}{\partial \alpha}\right)_\delta$

c_{n_δ} rate of change of flap section normal-force coefficient with flap deflection, $\left(\frac{\partial c_n}{\partial \delta}\right)_\alpha$

ρ mass density of free stream

μ absolute coefficient of viscosity

α wing angle of attack

δ deflection of flap chord with respect to airfoil chord, positive when trailing edge is down

θ included angle of flap nose

ϕ included angle of flap trailing edge

APPARATUS AND METHODS

Wind Tunnel

The investigation was conducted in the Langley 9-inch supersonic tunnel, which is a continuous-operation closed-return type of tunnel with provisions for the control of the humidity and pressure of the enclosed air. Eleven fine-mesh screens in the relatively large settling chamber ahead of the nozzles aid in keeping the turbulence in the tunnel test section at a low level. For qualitative visual-flow observations, a schlieren optical system is provided. During the tests, the quantity of water vapor in the tunnel air was kept sufficiently low so that the effects of water condensation in the supersonic nozzle were negligible.

Models

General.- Presented in figure 1 are the wing-flap configurations tested in this investigation. No data are presented for those configurations shown shaded. (See explanation under "Results.") Also included

in the figure is pertinent information relative to each of the configurations. The majority of the flaps tested had diamond-shaped profiles; others included a flap with an elliptical-shaped overhang and one with a full-blunt trailing edge. All the flaps had plain overhang nose balances having c_b/c_f values of 0.38, 0.60, and 0.82. The maximum thickness locations of the flaps were coincident with the hinge lines and the total flap chords were 30 percent of the chord of the wing-flap combination (exclusive of any wing-flap gap). The thickness ratio of the combinations was 6 percent. Variations in the wing-flap gap size were obtained by translating the flap rearward from the basic wings.

The artificial roughness seen near the nose of some of the configurations of figure 1 (see for example, configuration 6(a)) are fixed transition strips used to produce turbulent boundary-layer flow and therefore to simulate higher Reynolds number flow. The fixed transition or roughness strips were prepared by sprinkling common table salt, ground to an average grain size of slightly less than 0.01 inch, onto a thin layer of dope that had been sprayed on the wing just prior to the application of the salt grains. The chordwise thickness of the strips was approximately 3/16-inch and were located approximately at 19 percent chord.

The models were machined from steel with the sharp leading and trailing edges ground to a thickness of less then 0.002 inch. The wing and flap surfaces were cut to within 0.002 inch of the specified values and were generally free of scratches and well-polished.

Figure 2 shows the general arrangement and basic dimensions of the pressure distribution and schlieren models. Also illustrated is the method used for coupling the flaps to the wings. As shown on figure 2, two basic wings differing only in profile shape were employed in these tests. Basic wing 1 consisted of a 30-percent-chord nose section of double-wedge shape and sharp leading edge followed by a slab-type afterbody section with a full blunt trailing edge. Basic wing 2 differed from basic wing 1 in that the afterbody was beveled to a sharp edge at the base. (The term "afterbody" as used herein refers to the section of the basic wing rearward of the nose section.) All models had 3-inch chords (for zero wing-flap gap) and rectangular plan forms. The flap chords in all cases were 30 percent of the model chord.

Pressure-distribution models.- Figure 3 is a dimensional sketch of the pressure-distribution models illustrating the manner in which the models were mounted in the tunnel for testing. For convenience in carrying pressure leads from the wings to the outside of the tunnel and in setting angles of attack, the models were mounted in the tunnel directly from circular end plates which replaced the tunnel observation windows.

The pressure-distribution models were equipped with static-pressure orifices on both the upper and lower wing and flap surfaces at the midspan

station only as shown in figure 3. This location afforded an essentially two-dimensional-flow region relatively free from the disturbances which originate from the inboard edges of the wing-flap linkage plates. Two pressure orifices were located on the base of basic wing 1. Except for the orifices near the sharp leading and trailing edges of the wings and flaps, all orifices were drilled on a line normal to the wing leading edge. In order to establish some orifices as close to the leading and trailing edges as possible, these particular orifices were slightly staggered spanwise. All pressure leads from the orifices were ducted to the outside of the tunnel internally through the model.

Wing angle of attack was changed by rotating the circular end plates and measured by means of a clinometer attached to one of the rotating plates. The flaps were deflected with the aid of 1/16 diameter wire cables attached to the flaps and a manually actuated mechanism. In order to indicate flap-angle settings, the hinge pin, fixed relative to the flap, was extended through the circular end plate and equipped with an indicator hand which traversed a circular scale.

Schlieren model.- Figure 4 shows the schlieren model mounted for visual-flow observation and schlieren photography. The model was supported by two struts which in turn were attached to support trunnions which pierced the tunnel side walls. The angle of attack of the model was changed by rotating these support trunnions from outside the tunnel; thus the angle of attack could be changed while the tunnel was in operation. On the other hand the flap angle had to be set while the tunnel was inoperative. The span of the model was slightly less than the tunnel width in order to permit model movement in the pitch direction without damaging the observation windows.

Pressure Measurements and Reduction of Data

The pressures on the wing and flap surfaces and the total pressure in the tunnel settling chamber were recorded simultaneously by photographing a multiple-tube mercury manometer on which the pressures were indicated. Subsequently, the pressures were read directly from the film as pressure coefficients through use of a film reader.

Section aerodynamic coefficients were obtained by integrating the pressure distributions. The chordwise forces were computed in a similar manner by plotting the pressures normal to a line which was perpendicular to the wing or flap chord. No attempt was made to include viscous effects in any of the aerodynamic coefficients.

Range of Tests

Most of the pressure-distribution tests were made at angles of attack of 2° and 8° and through a flap deflection range of $\pm 20^\circ$ in increments of 4°. Additional pressure distributions were usually obtained at $\alpha = 0^\circ$, 4°, 6°, and 10° and at flap deflections of 0° and $\pm 12^\circ$ only. Schlieren photographs were obtained usually at $\alpha = 2^\circ$ and 8° at $\delta \approx 0^\circ$, $\delta \approx \pm 12^\circ$, and $\delta \approx \pm 20^\circ$. The tests were made at a Reynolds number of 0.78×10^6 based on the model chord of 3 inches.

Precision of Data

Stream surveys obtained with an empty test section indicate that the mean value of the Mach number in the region occupied by the test configurations is 2.40 and that the variation about this mean is about ±0.01. Other surveys have indicated that any deviations in stream-flow direction in the test section are small.

Estimates of the precision of the test variables are as follows:

Hinge-moment coefficient, c_h	±0.008
Normal-force coefficient, c_n	±0.005
Pitching-moment coefficient, c_m	±0.004
Chord-force coefficient, c_c	±0.004
Angle of attack, α, deg	±0.10
Flap angle, δ, deg	±0.25
Pressure coefficient, P	±0.01

RESULTS

The results of this investigation are presented in the form of section aerodynamic coefficients, pressure-distribution diagrams, schlieren photographs, slope parameters, and loading diagrams in figures 5 to 12, figures 13 to 21, figures 22 to 28, figures 29 to 31, and figures 32 and 33, respectively. Table I shows the configurations for which data are presented along with corresponding figure numbers. No data are shown for: (1) Configurations 3, 8, and 10 because the results obtained are intermediate to data which are presented; (2) configurations 6a, 6b, 14a, and 14b because tests of these configurations showed that, when the wing-flap gap was large (0.333c), fixing transition produced negligible results; and (3) configurations 13a and 13b because the results obtained are comparable to those results presented for the sharp-nose flaps.

The parameter $c_h\left(\frac{c_f}{c_t}\right)^2$, used in the presentation of hinge-moment data, is equivalent to a hinge-moment coefficient based on overall flap chord, c_t. Since c_t remained constant in all the tests, the values of this parameter afford a direct comparison of the hinge-moments for the various test configurations.

All pressure-distribution diagrams are shown for a zero wing-flap gap condition for convenience and in order to preserve uniformity among plots when comparisons are being made. The theoretical pressure distributions included on the pressure-distribution diagrams (figs. 13 to 21) were calculated from shock-expansion theory (ref. 10) for the basic wings only. (Because of the mixed-type flow which probably occurs over the flaps, no attempt was made to include theoretical pressure distributions over these surfaces. However, it will be shown in a subsequent section of this paper that reasonably good predictions of the pressure distributions over the flaps can be obtained by using a method based on shock-expansion theory.)

The flow on the strut side of the models shown in the schlieren photographs must be discounted because of interference effects from the supporting member.

The slope parameters, normally taken as tangents to the curves at $\delta = 0^\circ$ when the angle of attack was held fixed and at $\alpha = 2^\circ$ when the flap angle was held constant, are shown primarily to indicate the general trends of the two-dimensional slope parameters of overhang-balanced flaps. Included for comparative purposes are the two-dimensional hinge-moment parameters of a plain, unbalanced trailing-edge flap on a 6-percent-thick circular-arc wing (ref. 11), and the slope parameters of a three-dimensional wing-flap model (refs. 7 and 8) having flaps with geometrical characteristics similar to those of the present tests.

DISCUSSION

The discussion of the results of this investigation has been divided into the following sections: Effect of flap nose overhang, effect of wing-flap gap size, effect of fixed transition, effect of flap nose overhang shape, effect of flap trailing-edge thickness, and estimation of control-surface loading. The effects of altering the profile of the wing afterbody from a constant-thickness, blunt-base shape to a double-wedge, sharp-base shape are discussed under each section with the exception of the section on "effect of flap trailing-edge thickness," where the effects of basic-wing-afterbody shape were not evaluated.

Effect of Flap Nose Overhang

Figure 5 shows the effect of different amounts of flap nose overhang on the variation of the section aerodynamic coefficients with flap deflection at $\alpha = 2^\circ$ and $\alpha = 8^\circ$. The aerodynamic characteristics are shown for both the blunt (basic wing 1) and beveled (basic wing 2) wing-flap configurations.

In figures 6 and 7 are shown the variations of the section hinge-moment and normal-force coefficients with angle of attack at $\delta = -12^\circ$, 0°, and 12°, for the blunt and beveled wing-flap configurations, respectively.

All configurations have a wing-flap gap size of 0.033c.

Blunt wing.- The decrease in slopes of the hinge-moment curves at $\alpha = 2^\circ$ (fig. 5(a)) as the flap nose overhang is increased from $0.38c_f$ to $0.82c_f$ can be largely attributed to the fact that the least-balanced flap has most of its overhang balance immersed in the wing wake, and "unporting" (nose of flap rises above the wing surfaces) does not occur until the flap deflection exceeds 20°. The pressure-distribution diagrams of figure 13(a) (and to some extent, the schlieren photographs of figure 22(a)) show this effect. Conversely, when the overhang balance is moderately large (82 percent), its effectiveness increased because it was possible for the expanded flow around the wing base on the lower surface to impinge on a greater portion of the balance surface. (Compare the hinge-moment slope parameter c_{h_δ} (fig. 29) of the various balanced configurations.)

At $\alpha = 8^\circ$, the detrimental effects of the wing wake on the effectiveness of the overhangs is decreased (see, for example, figs. 13(b) and 22(b)); however, the relative reduction in the hinge moments between the configurations (configurations 1a, 7a, and 9a) having different amounts of flap nose overhang is comparable to those at $\alpha = 2^\circ$, as seen in figure 5(a) because the loads to the rear of the flap hinge lines also increased. (This effect is also illustrated in fig. 29, which shows the hinge-moment slope parameter c_{h_δ} measured at $\alpha = 8^\circ$.)

In figure 6(a), which shows the variation of the hinge-moment coefficient with angle of attack, the slopes of the curves at all flap deflections are seen to be relatively small (all c_{h_α} values falling within a range of 0.001 to -0.006). (See also the hinge-moment parameter c_{h_α} of fig. 29.) At $\delta = 0^\circ$, the 82-percent-balanced flap (configuration 9a) shows a very slight amount of overbalance (positive value of c_{h_α}). At $\delta = 12^\circ$, a considerable reduction in hinge moments is obtained as the flap balance is increased from 38 percent to 82 percent.

Normal-force-coefficient variations with flap deflections (fig. 5(b)) and normal-force-coefficient variations with angle of attack (fig. 6(b)) are not significantly affected by change in amount of flap nose overhang.

Pitching-moment characteristics (fig. 5(c)) show trends similar to the hinge-moment variations (fig. 5(a)) previously discussed, and indicate a loss of pitching effectiveness c_{m_δ} with increase in percent of flap nose overhang. This loss is probably caused by a forward shift in flap center of pressure due to the increase in load on the overhang.

Chord-force characteristics (fig. 5(d)) exhibit only slight changes with change in amount of flap nose overhang.

Beveled wing.- Figure 5(a) shows that, at a low angle of attack ($\alpha = 2^\circ$), beveling the afterbody of the wing ahead of the flap nose (configurations 1b, 7b, and 9b) resulted in no significant reductions in the slopes of the hinge-moment curves (that is, increase in aerodynamic balance) relative to those of the blunt-wing—flap configurations. (See c_{h_δ} slope values, fig. 29.) The reason for this lack of improvement in aerodynamic balance can be seen from the pressure-distribution diagrams of figure 14(a), which show that, although there is an increase in load on the overhang balance, the loads to the rear of the hinge line have also increased.

At a moderate angle of attack $\alpha = 8^\circ$ (fig. 5(a)), the effectiveness of the overhang balance increased markedly when the wing afterbody was beveled as is indicated by the overbalanced conditions (positive values of c_{h_δ}, generally in the negative-flap-deflection region) produced on the 60- and 82-percent-balanced flap-wing configurations (configurations 7b and 9b); also see fig. 29).

Figure 7(a) shows the hinge-moment-coefficient variation with angle of attack for the beveled wing-flap configurations (configurations 1b, 7b, and 9b). At $\delta = 0^\circ$, both the 60- and 82-percent-balanced configurations (configurations 7b and 9b, respectively) exhibit overbalance tendencies (c_{h_α} positive), whereas the least-balanced configuration (configuration 1b) is slightly underbalanced ($c_{h_\alpha} = -0.0014$). (See hinge-moment slope parameter c_{h_α} fig. 29.) At $\delta = 12^\circ$ all the flap configurations have positive floating tendencies (positive c_{h_α}) in the low angle-of-attack range (up to $\alpha = 6^\circ$ or $\alpha = 8^\circ$). At the higher angles of attack, the converse is true.

The increase in rate of change of normal force with flap deflection c_{n_δ} of the beveled-wing—flap configurations (fig. 5(b)) over that of

the blunt-wing—flap configurations was appreciable at both $\alpha = 2^\circ$ and $\alpha = 8^\circ$, at least up to about $\delta = 14^\circ$. Above $\delta = 14^\circ$, the slopes of the curves become zero and tend to exhibit reversals. This loss in lifting effectiveness c_{n_δ} can be attributed to the rather severe flow separation from the wing, as seen in the pressure-distribution diagrams of figure 14, rather than to a loss in flap lifting ability.

The variations of the normal-force coefficients with angle of attack (fig. 7(b)) reveal that, at all flap deflections shown, the slopes of the curves are approximately equal. This result indicates that the lifting effectiveness c_{n_α} of the wing-flap configurations (configurations 1b, 7b, and 9b) is not significantly altered with change in amount of flap nose overhang $\left(\text{at least within the scope of the present tests, } \frac{c_b}{c_f} = 0.38 \text{ to } \frac{c_b}{c_f} = 0.82\right)$. It was also found that the slope values are comparable to those obtained on the blunt-wing—flap configurations.

Pitching-moment characteristics (fig. 5(c)) follow closely the trends of the hinge-moment curves. At $\alpha = 8^\circ$, unstable pitching-moment variations occur over a small range of flap deflection for the 60- and 82-percent-balanced flaps (configurations 7b and 9b).

Chord-force characteristics (fig. 5(d)) show no appreciable difference between wing-flap configurations at $\alpha = 2^\circ$ or $\alpha = 8^\circ$. However, the chord-force of the beveled-wing—flap configurations is generally higher than the blunt-wing—flap configurations, and in particular at $\alpha = 8^\circ$ where the chord-force rise with positive flap deflection is very rapid.

Comparison of two- and three-dimensional slope parameters.- In figure 29 is shown a comparison between two-dimensional hinge-moment slope parameters obtained from the present tests and reference 11, and the three-dimensional hinge-moment slope parameters obtained from test data of references 7 and 8. The hinge-moment slope values c_{h_δ} and c_{h_α} of the three-dimensional tests and the present two-dimensional tests correlate reasonably well. Although the flaps of the three-dimensional tests were attached to a half-span delta wing having a subsonic leading edge (sweep angle of 75°), the hinge-line sweep (which was 0°), flap geometry (hinge-line location and profile shape), and wing-flap gap size of the three-dimensional tests were similar to those of the present tests.

On the basis of this brief comparison it appears that the geometrical parameters of the flap (as stated above) are the primary factors in determining hinge-moment characteristics, and it is believed that two-dimensional studies similar to the present tests can furnish a reasonably accurate insight into three-dimensional flap characteristics.

Slope values of the zero-balanced flap on a circular-arc wing (ref. 11) also show reasonably good correlation with the two- and three-dimensional balanced configurations.

Effect of Wing-Flap Gap Size

Figures 8 and 9 show the effect of wing-flap gap size on the variation of the aerodynamic coefficients with flap deflection of the blunt and beveled wings equipped with a flap having a small ($0.38c_f$) and large ($0.82c_f$) overhang balance, respectively, at $\alpha = 2^\circ$ and $\alpha = 8^\circ$.

Blunt wing.- The hinge-moment characteristics of the 38-percent-balanced blunt-wing—flap configurations (configurations 1a, 4a, and 5a) at $\alpha = 2^\circ$ (fig. 8(a)) appear to be independent of gap size until the largest gap size (0.333c) is obtained. (See configuration 5a.) The hinge-moment variation with flap deflection of this configuration does not have the breaks or regions of discontinuity evident for the configurations of lesser gap sizes (configurations 1a and 4a). The effect of gap size on aerodynamic balance is negligible, however, because of the small ($0.38c_f$) overhang balance.

In figure 9(a) is shown the hinge-moment variation with flap deflection of a flap having a large flap nose overhang ($0.82c_f$) attached to the blunt-base wing, as a function of wing-flap gap size (configurations 9a and 11a). It is readily seen that it is possible to obtain good balancing characteristics (low values of c_{h_δ}) through the judicious combination of wing-flap gap size and amount of flap nose overhang. (See hinge-moment-slope parameter c_{h_δ} fig. 30.)

Normal-force, pitching-moment, and chord-force characteristics for the 38-percent-balanced flap (figs. 8(b), 8(c), and 8(d), respectively) reflect the same trends previously observed in the hinge-moment characteristics, namely, that the aerodynamic coefficients at $\alpha = 2^\circ$ appear to be independent of wing-flap gap size until the largest gap size (0.333c) is obtained. The substantial increase in flap effectiveness (fig. 8(b)) at the largest gap size is clearly seen in the pressure-distribution diagrams of figure 15(a). Also seen on the diagrams is the significant decrease in wing base pressure $\left(\text{the symbols shown plotted at } \frac{x}{c} = 0.70\right)$ with increase in gap size from 0.033c to 0.333c. This results in an increase in wing pressure drag, and partly accounts for the large chord force (fig. 8(d)) associated with the largest gap-size configuration (configuration 5a). At $\alpha = 8^\circ$ the section aerodynamic coefficients show, generally, the same trends.

For the 82-percent-balanced flap, the normal-force characteristics (fig. 9(b)) show flap effectiveness increases as expected with increase in gap size at both $\alpha = 2^\circ$ and $\alpha = 8^\circ$.

Beveled wing.- Beveling the wing ahead of the flap nose for the 38-percent-balanced flap configurations (configurations 1b, 4b, and 5b) essentially made the hinge-moment (fig. 8(a)), normal-force (fig. 8(b)), and pitching-moment (fig. 8(c)) coefficients independent of wing-flap gap size up to and including the largest (0.333c) gap size at both $\alpha = 2^\circ$ and $\alpha = 8^\circ$. The chord-force coefficients (fig. 8(d)), however, still show some variations with gap size.

An interesting feature of the pressure-distribution diagrams (fig. 16) is the retardation of flow separation from the upper surface of the wing afterbody when the wing-flap gap size is increased from 0.033c to 0.333c. (This effect is also evident on the schlieren photographs of fig. 24.)

The hinge-moment characteristics (fig. 9(a)) of the large-balance (82-percent) flap-beveled-wing configurations (configurations 9b and 11b) at $\alpha = 2^\circ$ show slope reversals (from negative to positive) as the wing-flap gap size is increased from 0.033c to 0.333c. (See hinge-moment slope parameter c_{h_δ}, fig. 30.) At $\alpha = 8^\circ$, the effect of gap size on the hinge moments is small.

The normal-force characteristics (fig. 9(b)) show slight increases in lift effectiveness c_{n_δ} as the gap is increased at both $\alpha = 2^\circ$ and $\alpha = 8^\circ$.

Effect of Fixed Transition

Figures 10(a) and 10(b) show the effects of fixed transition on the variation of the hinge-moment and normal-force characteristics with flap deflection, respectively, of basic wings 1 (blunt) and 2 (beveled) equipped with a 38-percent-balanced $\left(\frac{c_b}{c_f} = 0.38\right)$ flap, at $\alpha = 2^\circ$ and $\alpha = 8^\circ$.

Blunt wing.- The only apparent effect of fixing transition on hinge-moment characteristics (fig. 10(a)) appears to be the elimination of the discontinuity in the curves at $\alpha = 2^\circ$ and an increase in control heaviness at $\alpha = 8^\circ$.

Normal-force curves (fig. 10(b)) exhibit trends similar to the hinge-moment curves in that the "breaks" or regions of discontinuity in the force curves, at both $\alpha = 2^\circ$ and $\alpha = 8^\circ$, are eliminated when transition is fixed. An investigation (ref. 11) at $M = 1.93$ of the effects of fixed transition on the force and moment characteristics of a 9-percent-thick, circular-arc airfoil equipped with a 30-percent-chord plain trailing-edge flap yielded similar results.

Beveled wing.- The effect of fixed transition on the hinge-moment and normal-force characteristics of the beveled wing-flap configurations (configurations 1b and 2b) (figs. 10(a) and 10(b), respectively) are nearly identical to those produced on the blunt-wing—flap configurations.

The pressure-distribution diagrams of figure 18 show the powerful effect of fixed transition on curbing or eliminating completely the flow separation from the upper surface of the wing afterbody. (Also see fig. 26.)

Effect of Nose Balance Shape

Figure 11 shows the effect of nose balance shape on the variation of the section aerodynamic coefficients with flap deflection at $\alpha = 2^{\circ}$ and $\alpha = 8^{\circ}$ for both the blunt- and beveled-wing—flap configurations. The wing-flap gap size is 0.033c.

The section aerodynamic coefficients of both the blunt- and beveled-wing—flap configurations show, with exception of the chord force, practically no variance with change in flap nose shape at both $\alpha = 2^{\circ}$ and $\alpha = 8^{\circ}$ (figs. 11(a) to 11(c)).

The chord-force characteristics (fig. 11(d)) of the blunt wing-flap configurations (configurations 7a and 12a) are practically identical at $\alpha = 2^{\circ}$ and show a slight deviation in the positive flap deflection range at $\alpha = 8^{\circ}$. The beveled-wing—flap configurations (7b and 12b) show a marked dissimilarity in chord-force characteristics (fig. 11(d)) at $\alpha = 2^{\circ}$. This effect is believed to be due to the variation of the high pressures which build up on the nose of the flaps (see fig. 20(a)), the highest pressures generally occuring on the blunt-nose flap (configuration 12b) in the negative-flap-deflection region; conversely, the peak pressures occur on the sharp-nose flap (configuration 7b) in the positive-flap-deflection range. At $\alpha = 8^{\circ}$, the same trends as at $\alpha = 2^{\circ}$ are evident but on a much smaller scale.

Effect of Flap Trailing-Edge Thickness

Figure 12 shows the effect on the variation of the hinge-moment and normal-force coefficients with flap deflection and angle of attack of a blunt-wing—flap configuration of changing the ratio of the flap trailing-edge thickness t_B to flap maximum thickness t from 0 to 1. The flap has a 60-percent flap nose overhang. The force and moment results are presented at $\alpha = 2^{\circ}$ and $\alpha = 8^{\circ}$.

The results of increasing the flap trailing-edge thickness is manifested in an increase in control heaviness (decrease in balancing effectiveness) as shown by the hinge-moment curves of figure 12(a) (also see

hinge-moment slope parameter c_{h_δ}, fig. 31), and an increase in flap effectiveness shown in the normal-force curves of figure 12(b). Both effects result primarily from the increased load over the flap high-pressure surface to the rear of the hinge line when the flap trailing edge was made blunt. (See pressure-distribution diagrams of fig. 21.)

Figures 12(c) and 12(d) show, respectively, the hinge-moment and normal-force variation with angle of attack at constant flap deflections of the pointed- and blunt-trailing-edge flap configurations (configurations 7a and 15). The hinge-moment variations (fig. 12(c)) of the blunt-trailing-edge-flap configuration (configuration 15) show a slightly more underbalanced condition (more negative c_{h_α}, see fig. 31) than that of the sharp-trailing-edge-flap configuration (configuration 7a). The normal-force variations with α (fig. 12(d)) show that the normal-force-curve slopes c_{n_α} are approximately equal at all flap deflections shown. The displacement between the curves of configurations 7a and 15 at $\delta = 12^\circ$ is indicative of the superior lifting ability of the blunt-trailing-edge flap configuration (configuration 15).

Experimental and Calculated Control Surface Loading

A method for estimating the loads on flap-type controls with overhang nose balances based on shock-expansion theory and subject to several assumptions was found to give good results (figs. 32 and 33). The assumed flow patterns over the wing-flap configurations upon which the calculations of the local pressures are based are indicated by the small arrows on the diagrammatic sketches shown at the top of the figures.

Figure 32 shows the experimental and calculated loading over basic wing 1, at $\alpha = 8^\circ$, equipped with flaps having 38- and 82-percent flap-chord overhang nose balances at $\delta = 8^\circ$ and $\delta = 16^\circ$. The flow over the upper surface of the wing is assumed to follow the contour of the wing surface until it intersects the flap. The flow after leaving the lower surface of the basic wings is assumed to expand to free-stream direction. This assumption is reasonably correct as is borne out by calculations made by using the experimentally determined base pressures as measured in the present tests. It is also assumed that the flow velocity remains supersonic over the configurations, a prerequisite for the application of the shock-expansion theory. It is seen that the method gives a good approximation of the magnitudes of the loading over the control surfaces, particularly in those regions forward of the hinge lines where large peak pressures are experienced. The loading over the basic wing, which can be predicted quite accurately by using shock-expansion theory in the absence of flow separation, is seen to be good except in those regions where flow separation is prevalent.

Figure 33 shows the experimental and calculated loadings over basic wings 1 and 2 at $\alpha = 8^{\circ}$ equipped with control surfaces having 82-percent-flap-chord overhang nose balances at $\delta = 8^{\circ}$. The loadings are shown for two wing-flap gap sizes. For the basic wing 2 case, it is assumed that the nose of the flap overhang when unported acts in a manner similar to that of a spoiler and the flow moves in a straight line from the wing shoulder to the flap nose. In figure 33(a), which shows the loadings for the configurations with the smallest gap sizes, the method overestimates the loading over the flap surfaces; nevertheless, fairly good approximations of the loadings are achieved. The loadings over the basic wings are good except in the separated flow regions.

Figure 33(b) is for the large wing-flap gap size configurations and the flap is assumed to be operating as an independent airfoil under free-stream conditions. The flow leaves the trailing edges of the basic wings in the free-stream direction as shown in the sketches above the figures. Good approximations of the loadings over the control surfaces are again obtained. A substantial decrease in separation effects on the basic wings resulted in much better agreement between theory and experiment.

CONCLUSIONS

An investigation has been made at Mach number of 2.40 and a Reynolds number of 0.78×10^6 of some of the factors affecting the two-dimensional characteristics of flap-type controls equipped with overhang nose balances. An analysis of the results indicated the following conclusions:

1. The hinge-moment characteristics of flaps with 0.38 flap chord (c_f) overhang nose balances on blunt-base wings for a wing-flap gap size of 0.033 model chord exhibited a statically stable, or underbalanced, variation with flap deflection. Increasing the overhang balance chord from $0.38c_f$ to $0.82c_f$ decreased the unbalanced hinge moments due to flap deflections c_{h_δ} from approximately -0.006 to -0.002, and resulted in a value of the rate of change of hinge moment with angle of attack c_{h_α} of approximately zero.

2. Beveling the afterbody of the basic wing forward of the flap nose caused the overhang balance to become more effective, and at a moderate angle of attack $(\alpha = 8^{\circ})$ resulted in unstable variations of hinge-moment coefficients with control deflection c_{h_δ} for the 60- and 82-percent-balanced flaps.

3. Increasing wing-flap gap size from 0.033 model chord to 0.333 model chord on the blunt-wing—flap configurations favorably altered the

hinge-moment parameters c_{h_δ} and c_{h_α} when the flap overhang balance was about 0.60 flap chord (c_f), increased the lift and pitching effectiveness, and caused a substantial chord-force rise. The aerodynamic characteristics of the beveled-wing—flap configurations were affected, in general, to a much less extent with change in wing-flap gap size.

4. The lifting effectiveness of the flap was not appreciably changed by overhang balance.

5. The effects of fixed transition to simulate high Reynolds numbers on the flap balancing characteristics were small; however, the flow separation from the basic wings was greatly reduced.

6. The effect of changing the shape of the flap overhang nose balance from a sharp double wedge to elliptical was negligible.

7. Increasing the trailing-edge thickness of the control from $\frac{t_B}{t} = 0$ to $\frac{t_B}{t} = 1.00$ $\left(t_B/t \text{ is the ratio of the flap trailing-edge thickness to the maximum thickness of the model}\right)$ resulted in increased control heaviness with the change in c_{h_α} being about twice as much as the change in c_{h_δ}.

8. The loading over trailing-edge flap-type controls with overhang nose balances can be calculated by using an approximate method based on shock-expansion theory.

Langley Aeronautical Laboratory,
National Advisory Committee for Aeronautics,
Langley Field, Va., September 1, 1953.

REFERENCES

1. Hammond, Alexander D.: The Effect of Various Aerodynamic Balances on the Low-Speed Lateral-Control and Hinge-Moment Characteristics of a 0.20-Chord Partial-Span Outboard Aileron on a Wing With Leading Edge Swept Back 51.3°. NACA RM L52G03, 1952.

2. Thompson, Robert F., and Moseley, William C., Jr.: Hinge-Moment and Control-Effectiveness Characteristics of an Outboard Flap With an Overhang Nose Balance on a Tapered 35° Sweptback Wing of Aspect Ratio 4. NACA RM L52G08, 1952.

3. Wiley, Harleth G., and Zontek, Leon: Aerodynamic Characteristics at Transonic Speeds of a 60° Delta Wing Equipped With a Constant-Chord Flap-Type Control With and Without an Unshielded Horn Balance. NACA RM L51H22, 1952.

4. Wiley, Harleth G.: Aerodynamic Characteristics at Transonic Speeds of a 60° Delta Wing Equipped With a Triangular Plan-Form Control Having a Skewed Hinge Axis and an Overhang Balance. Transonic-Bump Method. NACA RM L50L01, 1951.

5. Lockwood, Vernard E., and Hagerman, John R.: Aerodynamic Characteristics at Transonic Speeds of a Tapered 45° Sweptback Wing of Aspect Ratio 3 Having a Full-Span Flap Type of Control With Overhang Balance. Transonic-Bump Method. NACA RM L51L11, 1952.

6. Lowry, John G., and Fikes, Joseph E.: Preliminary Investigation of Control Characteristics at Transonic Speeds of a Tapered 45° Sweptback Wing of Aspect Ratio 3 Having a Horn-Balanced Full-Span Control. NACA RM L52A11, 1952.

7. Mason, Maxwell, and Miller, Robert C.: Wind-Tunnel Test of 11 Per Cent Scale Semispan Models of the Douglas Nike 484 Missile. Rep. No. SWT 12-8, Jet Propulsion Lab., C.I.T., 1950.

8. Thomas, G. B.: Analysis of Supersonic Wind Tunnel Tests of Balanced Aileron Configurations for the Nike Guided Missile. Rep. No. SM-13796, Douglas Aircraft Co., Inc., Sept 29, 1950.

9. Mueller, James N., and Czarnecki, K. R.: Preliminary Data at a Mach Number of 2.40 of the Characteristics of Flap-Type Controls Equipped With Plain Overhang Balances. NACA RM L52F10, 1952.

10. Ivey, H. Reese, Stickle, George W., and Schuettler, Alberta: Charts for Determining the Characteristics of Sharp-Nose Airfoils in Two-Dimensional Flow at Supersonic Speeds. NACA TN 1143, 1947.

11. Czarnecki, K. R., and Mueller, James N.: Investigation at Supersonic Speeds of Some of the Factors Affecting the Flow Over a Rectangular Wing With Symmetrical Circular-Arc Section and 30-Percent-Chord Trailing-Edge Flap. NACA RM L50J18, 1951.

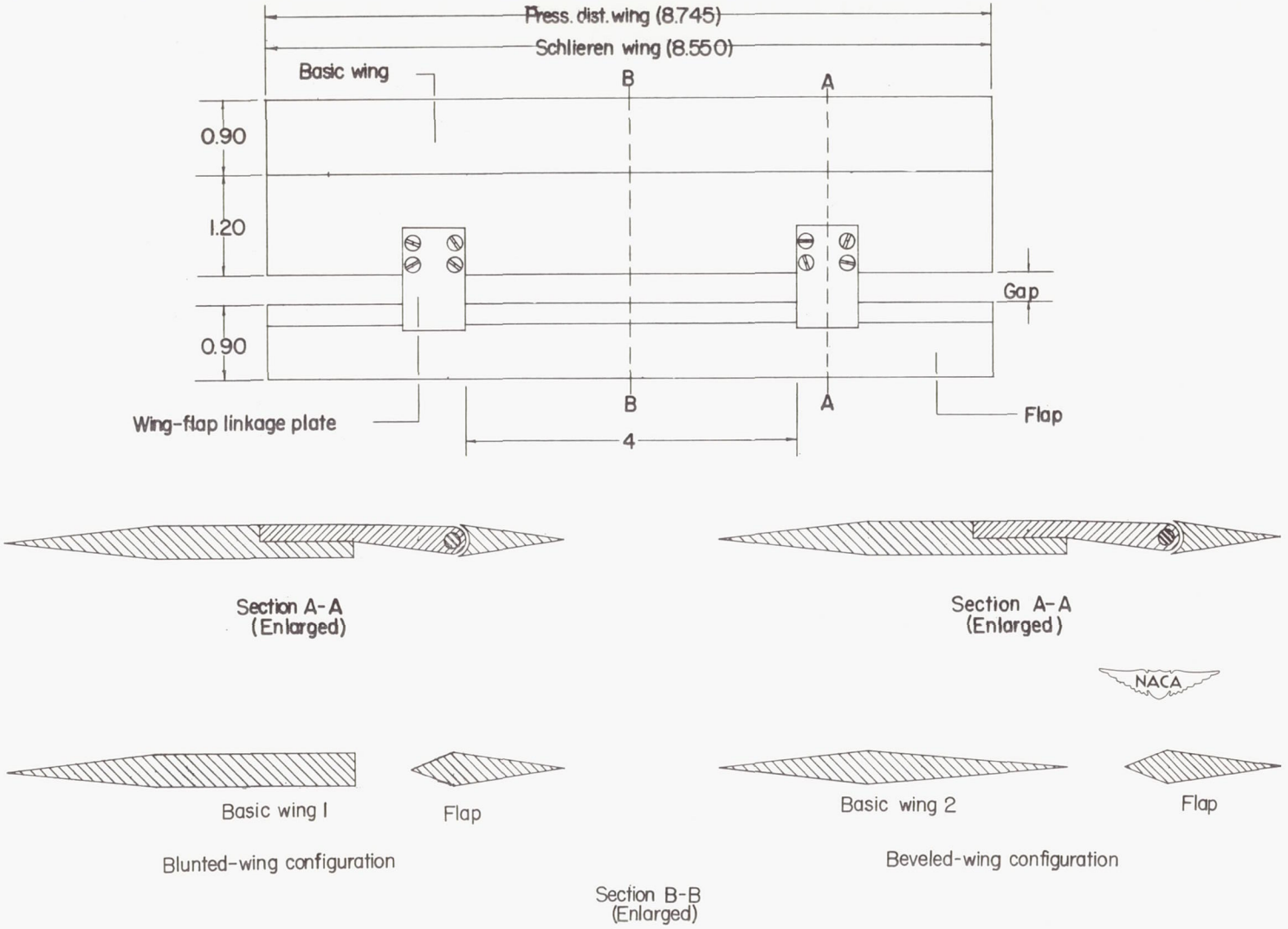


Figure 2.- General arrangements and basic dimensions of the pressure distribution and schlieren models. All dimensions are in inches.

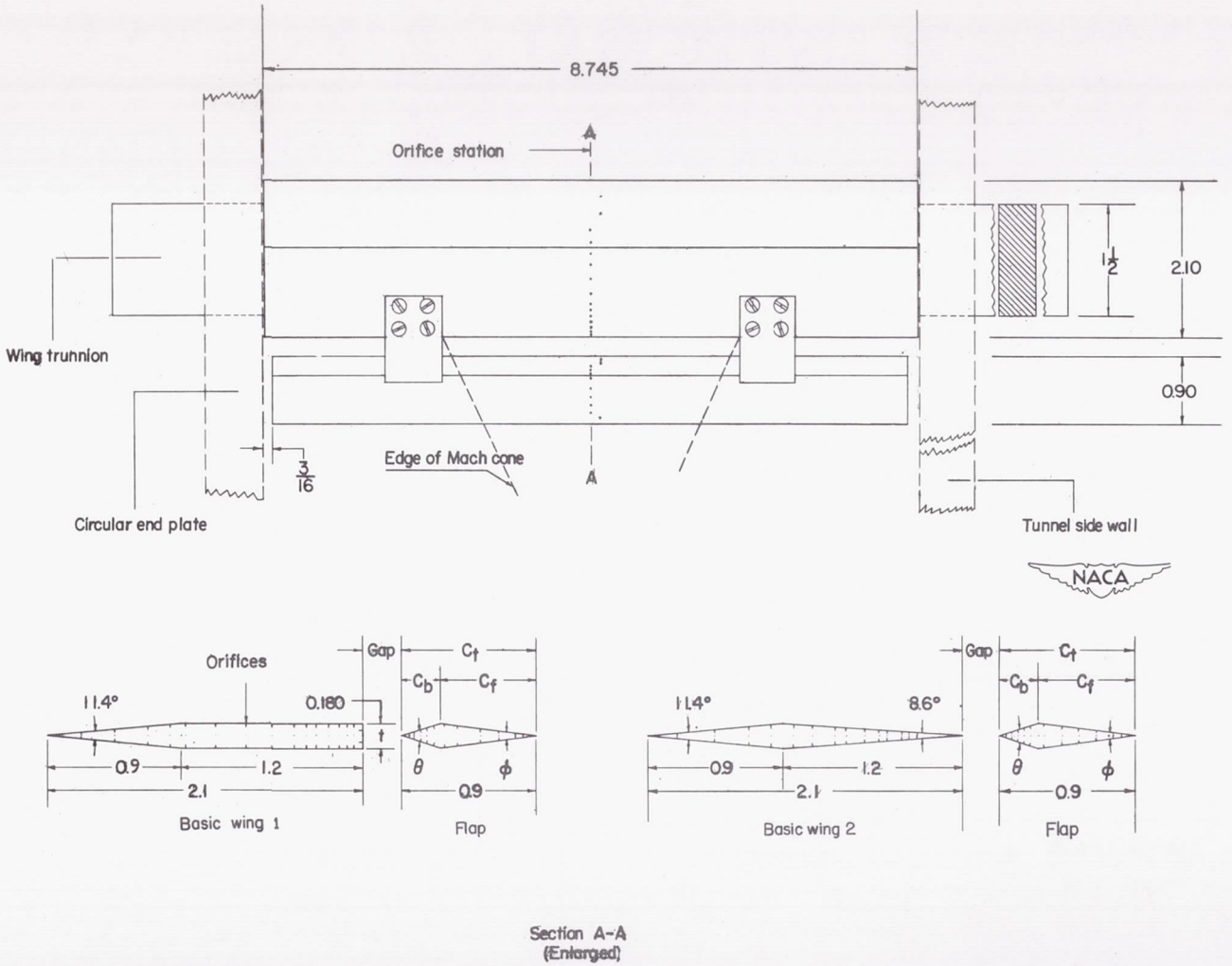


Figure 3.- Dimensional sketch of pressure-distribution model illustrating manner of mounting model in tunnel for testing. All dimensions shown are in inches.

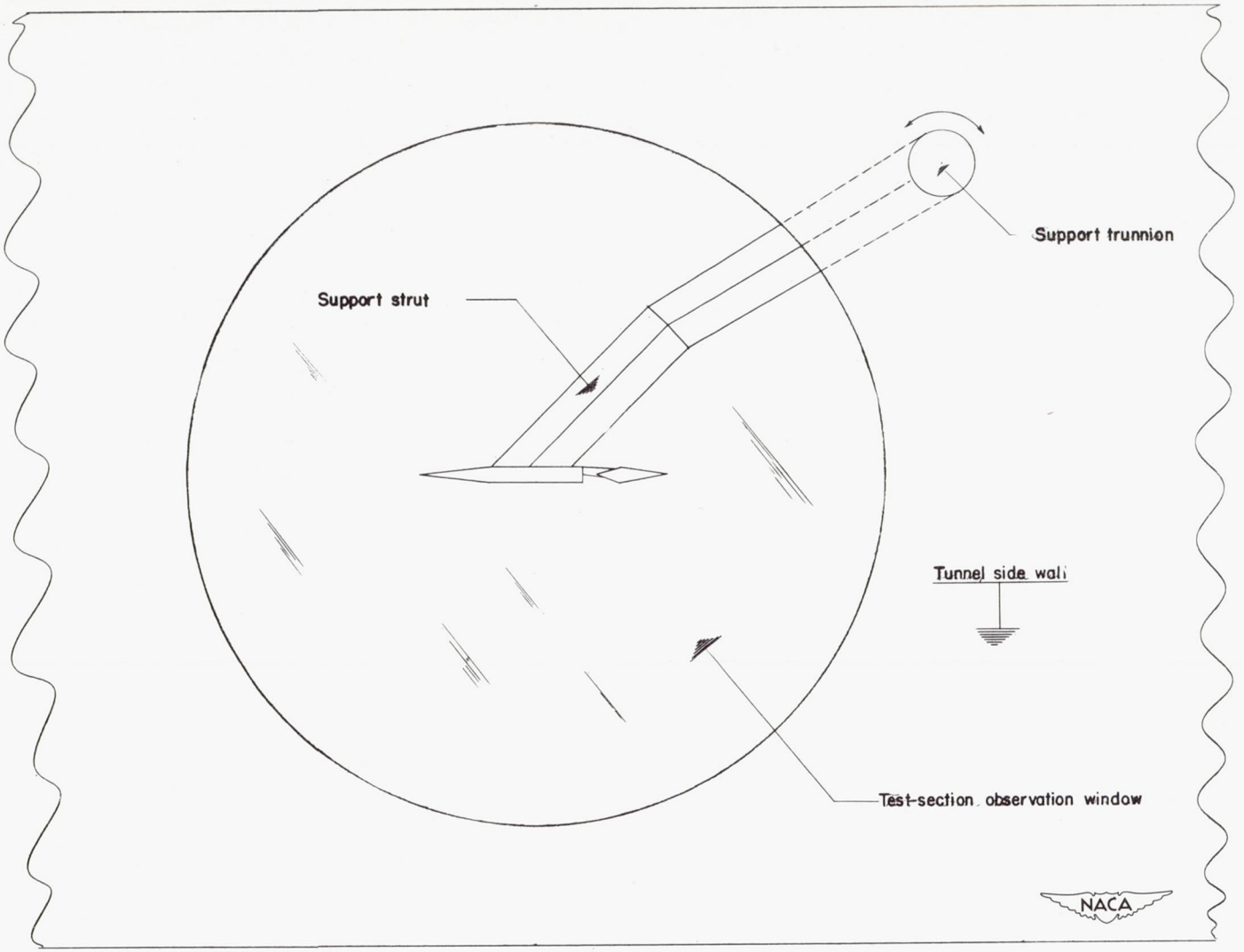
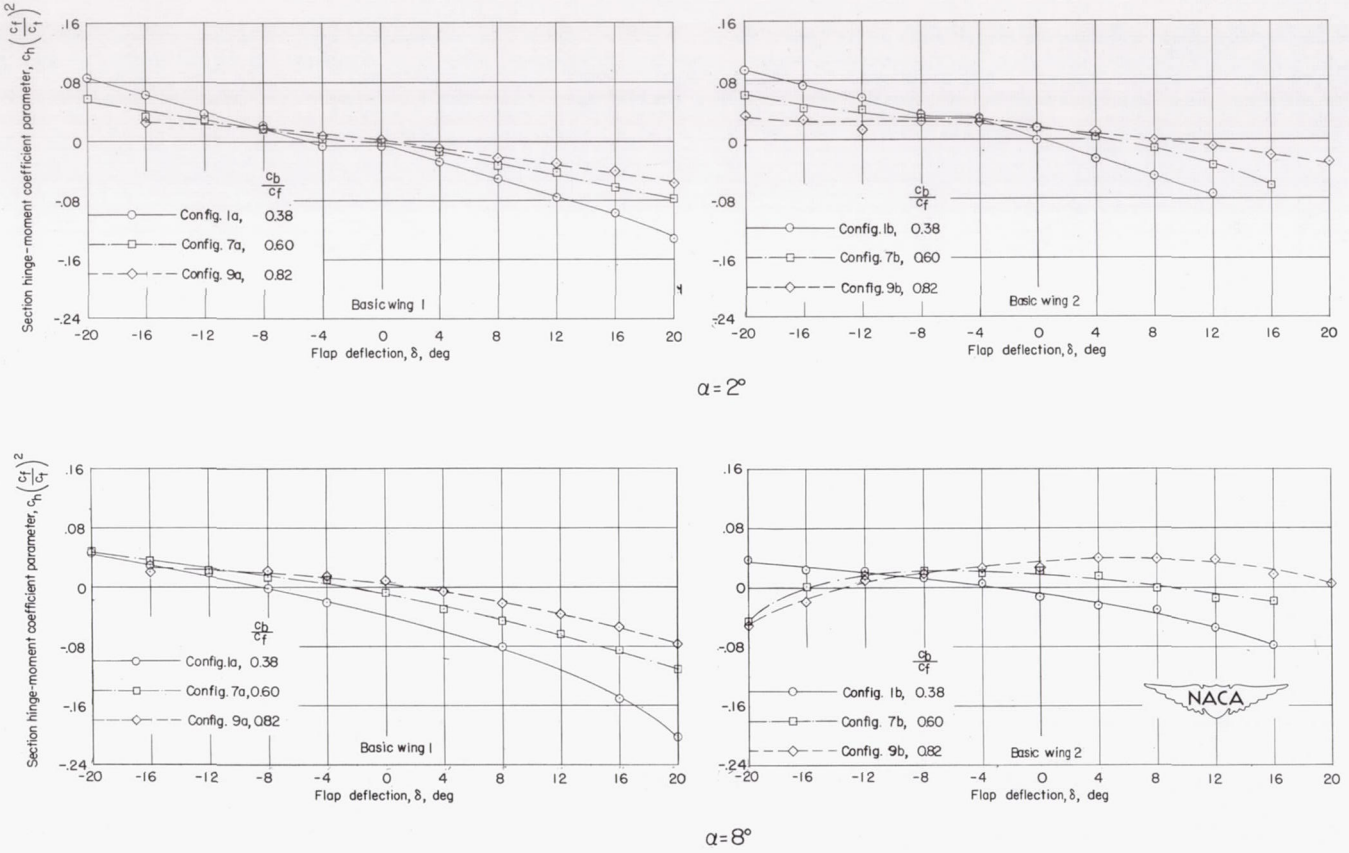
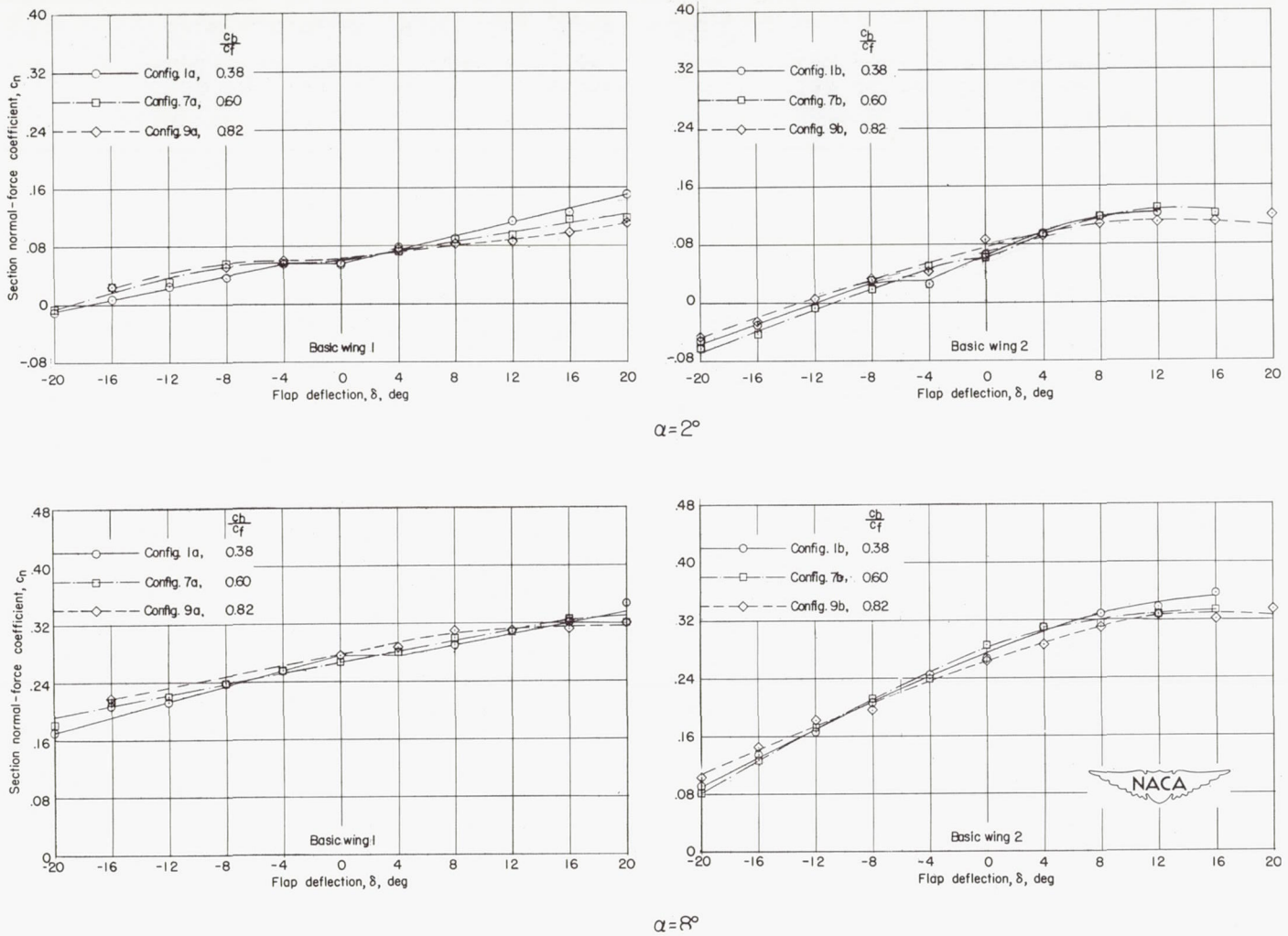


Figure 4.- Sketch showing method of mounting schlieren model for visual-flow observations.



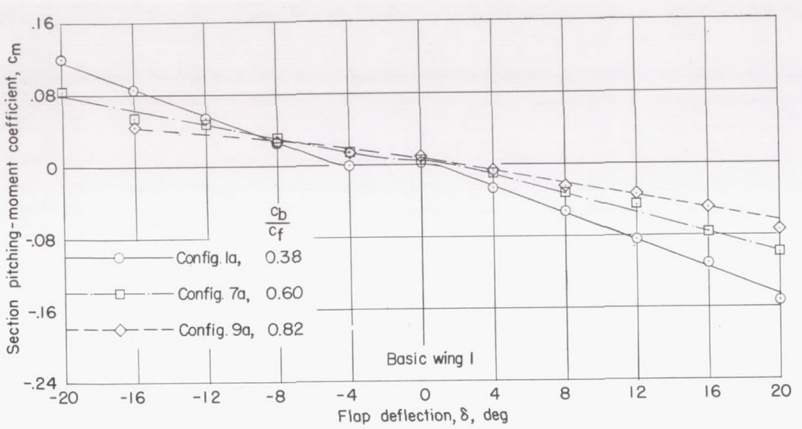
(a) $c_h\left(\frac{c_f}{c_t}\right)^2$.

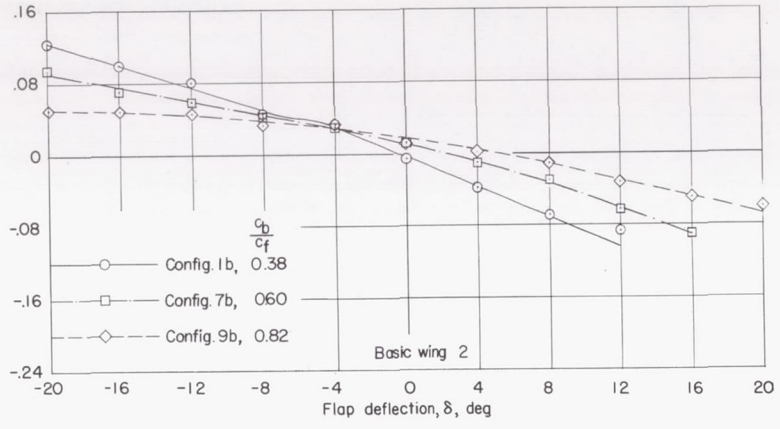
Figure 5.- Effect of percent overhang nose balance on the variation of the section aerodynamic coefficients with flap deflection of a 6-percent-thick symmetrical wing equipped with trailing-edge flap-type controls. Wing-flap gap size, 0.033c.



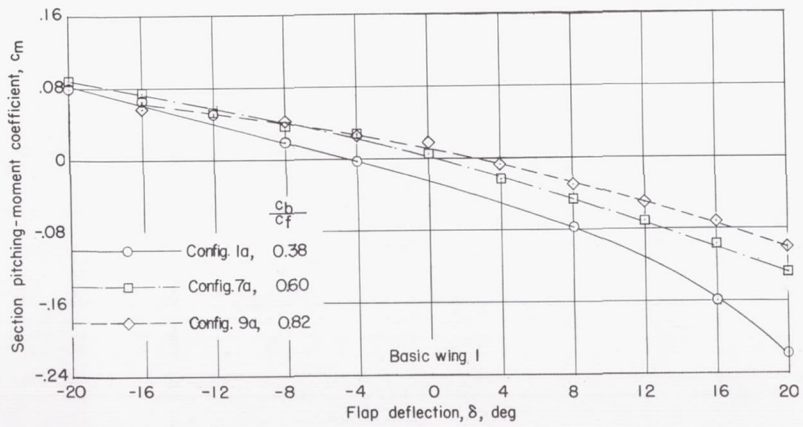
(b) c_n.

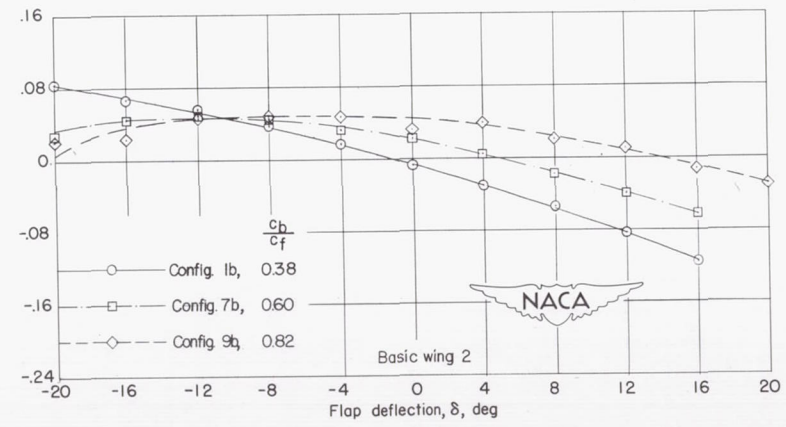
Figure 5.- Continued.





$\alpha = 2°$

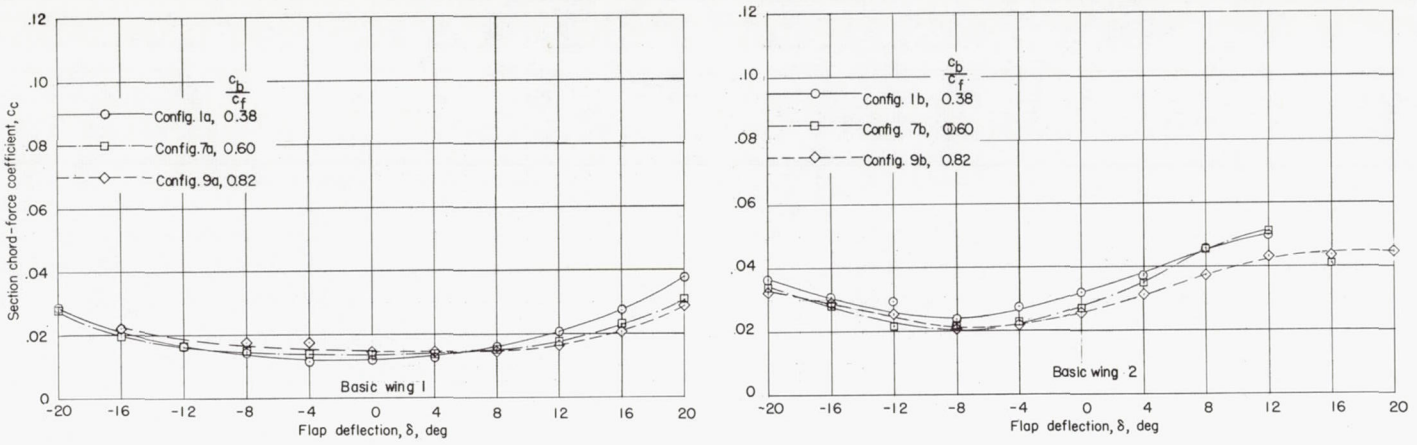




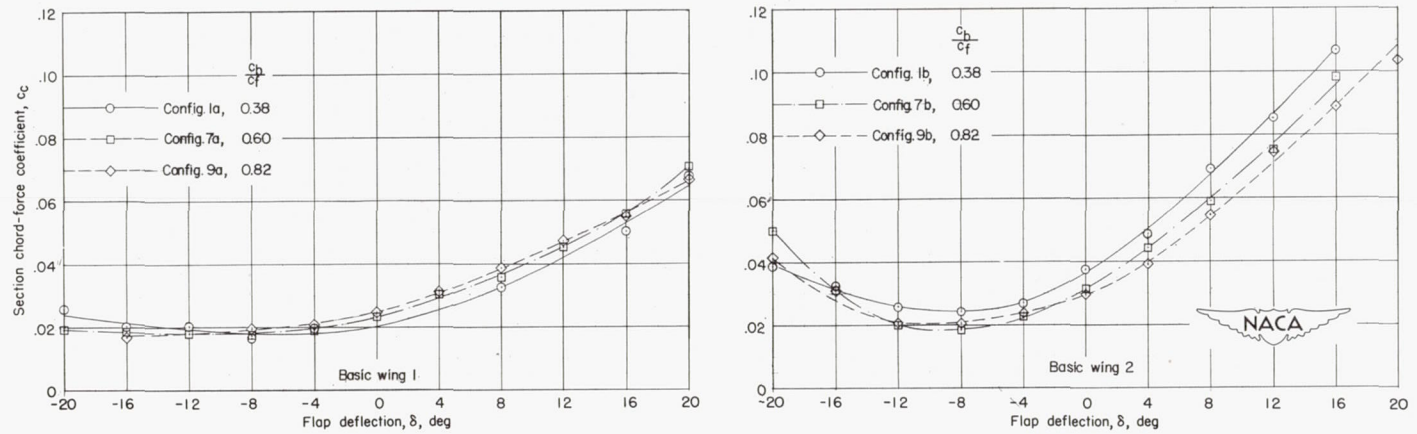
$\alpha = 8°$

(c) c_m.

Figure 5.- Continued.



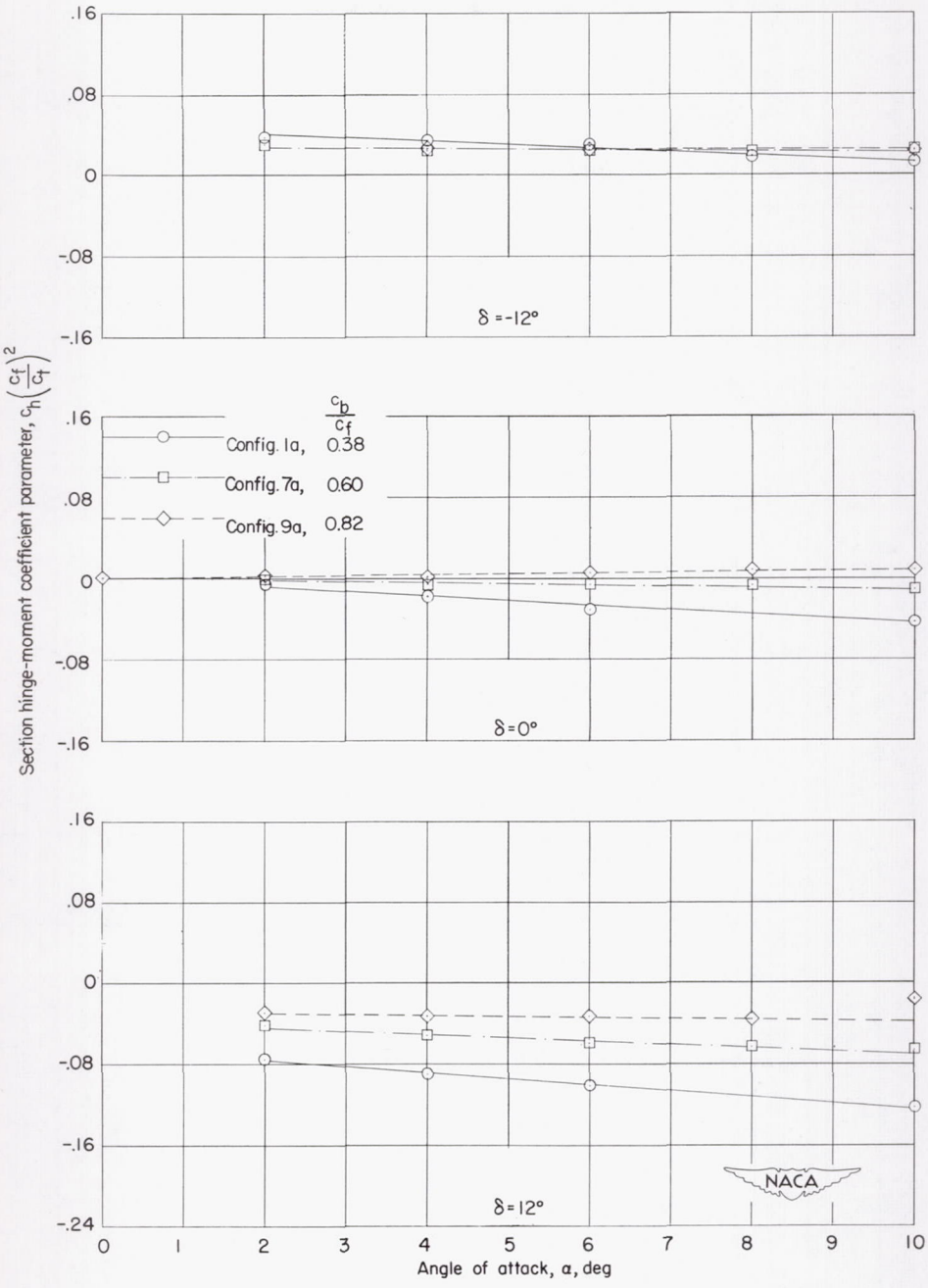
$\alpha = 2°$



$\alpha = 8°$

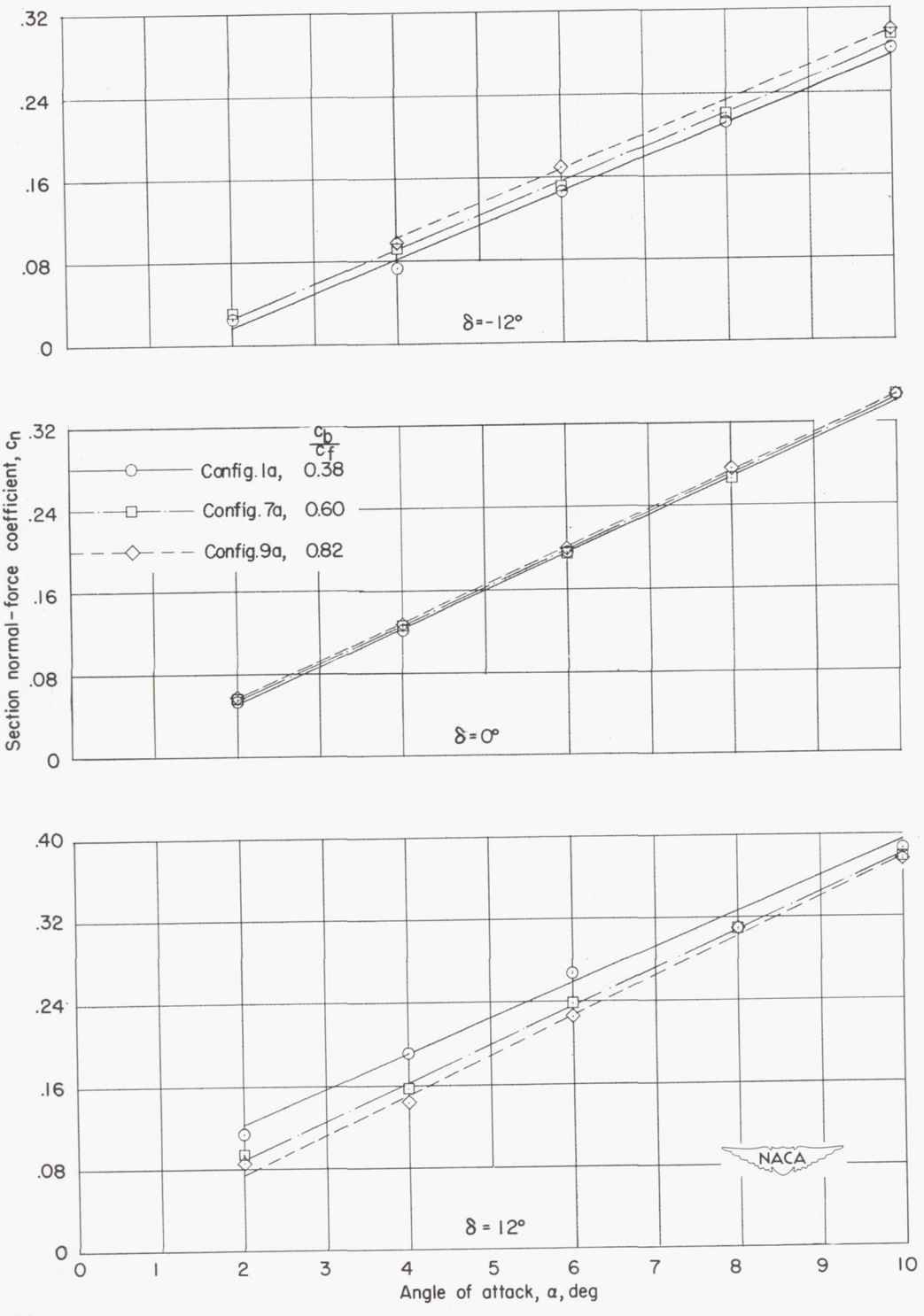
(d) c_c.

Figure 5.- Concluded.



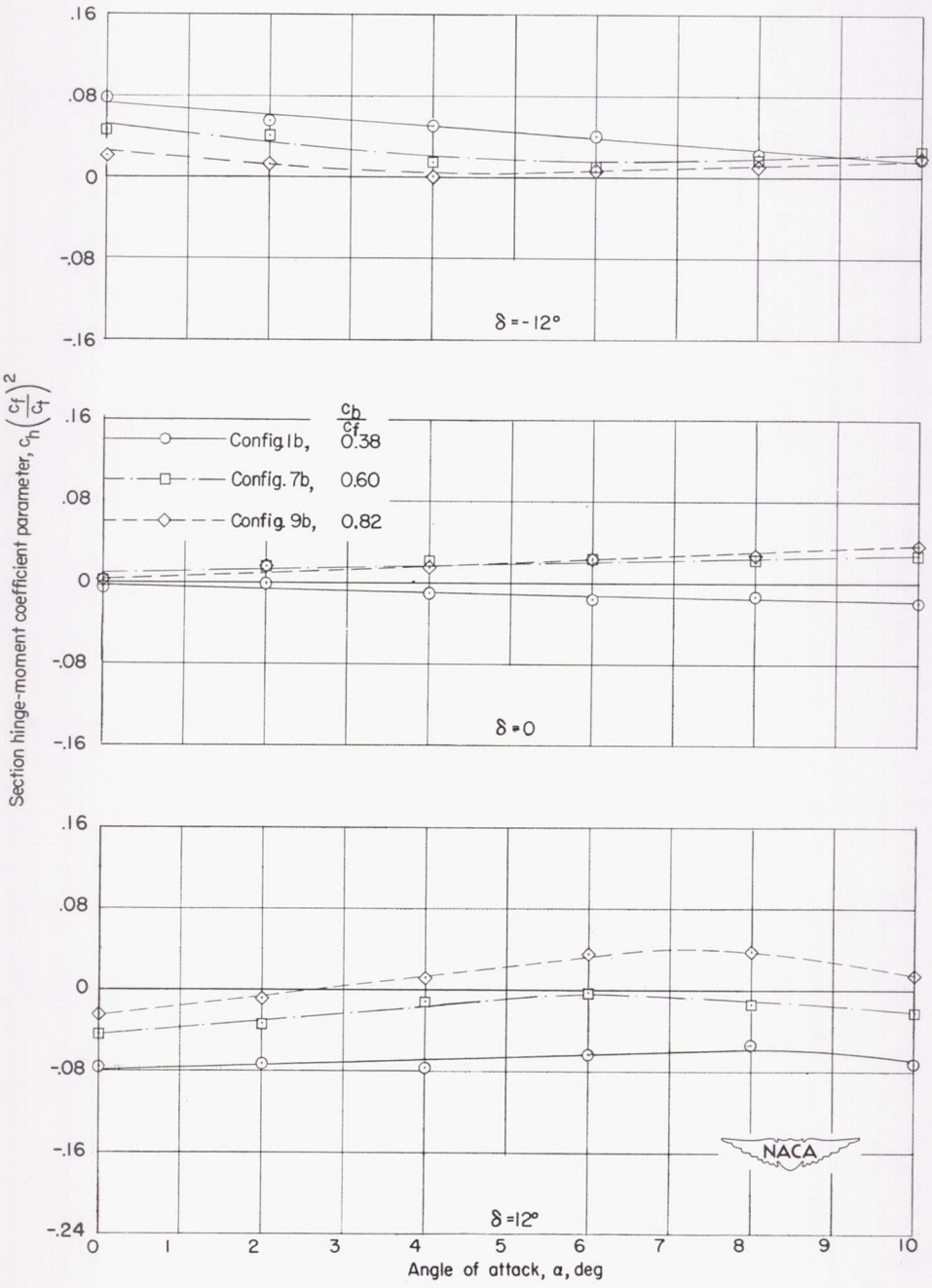
(a) $c_h\left(\frac{c_f}{c_t}\right)^2$.

Figure 6.- Effect of percent overhang nose balance on the variation of the section hinge-moment and normal-force coefficient, with angle of attack of a 6-percent-thick symmetrical wing equipped with trailing-edge flap-type controls. Wing-flap gap size, 0.033c; basic wing 1.



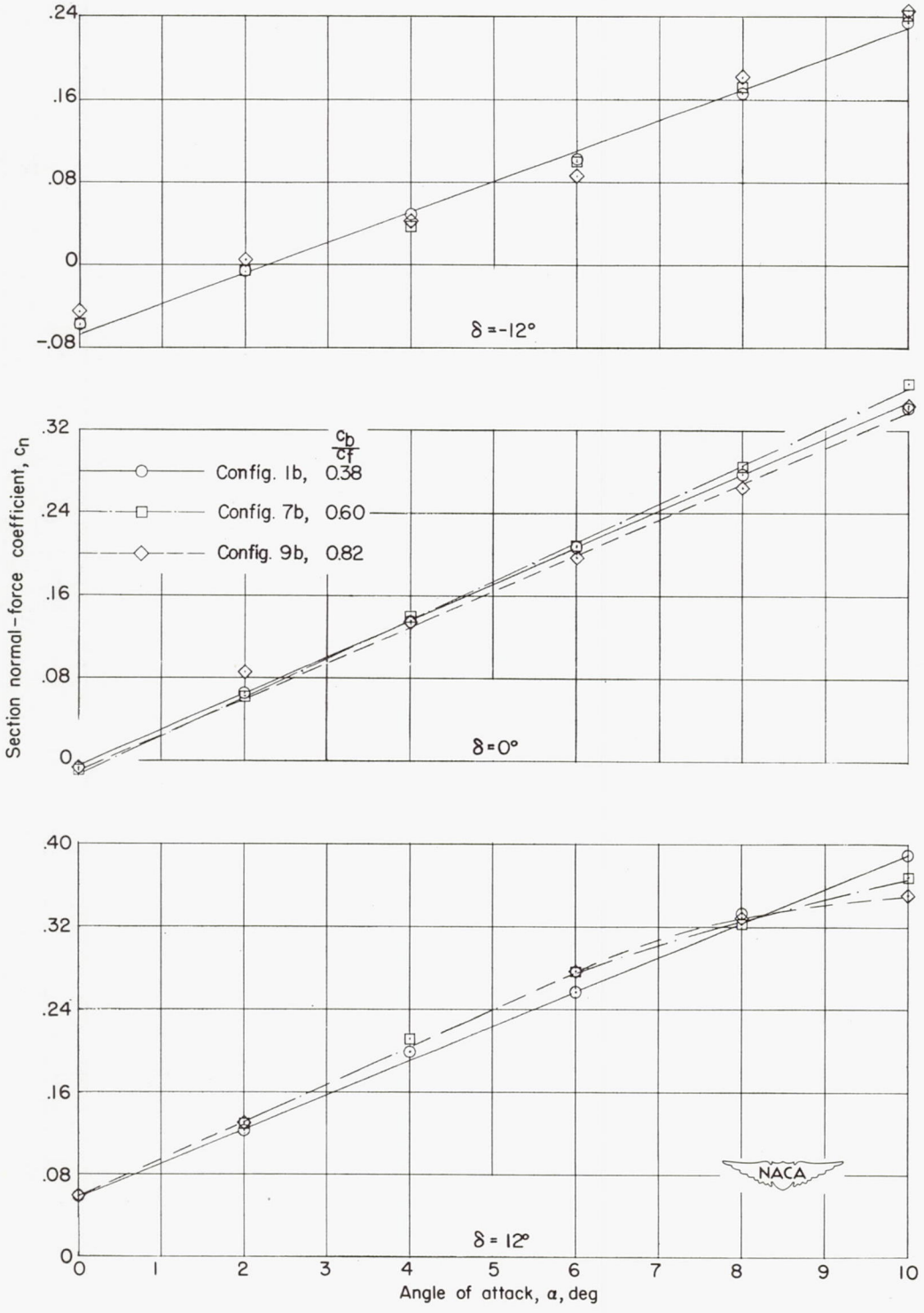
(b) c_n.

Figure 6.- Concluded.



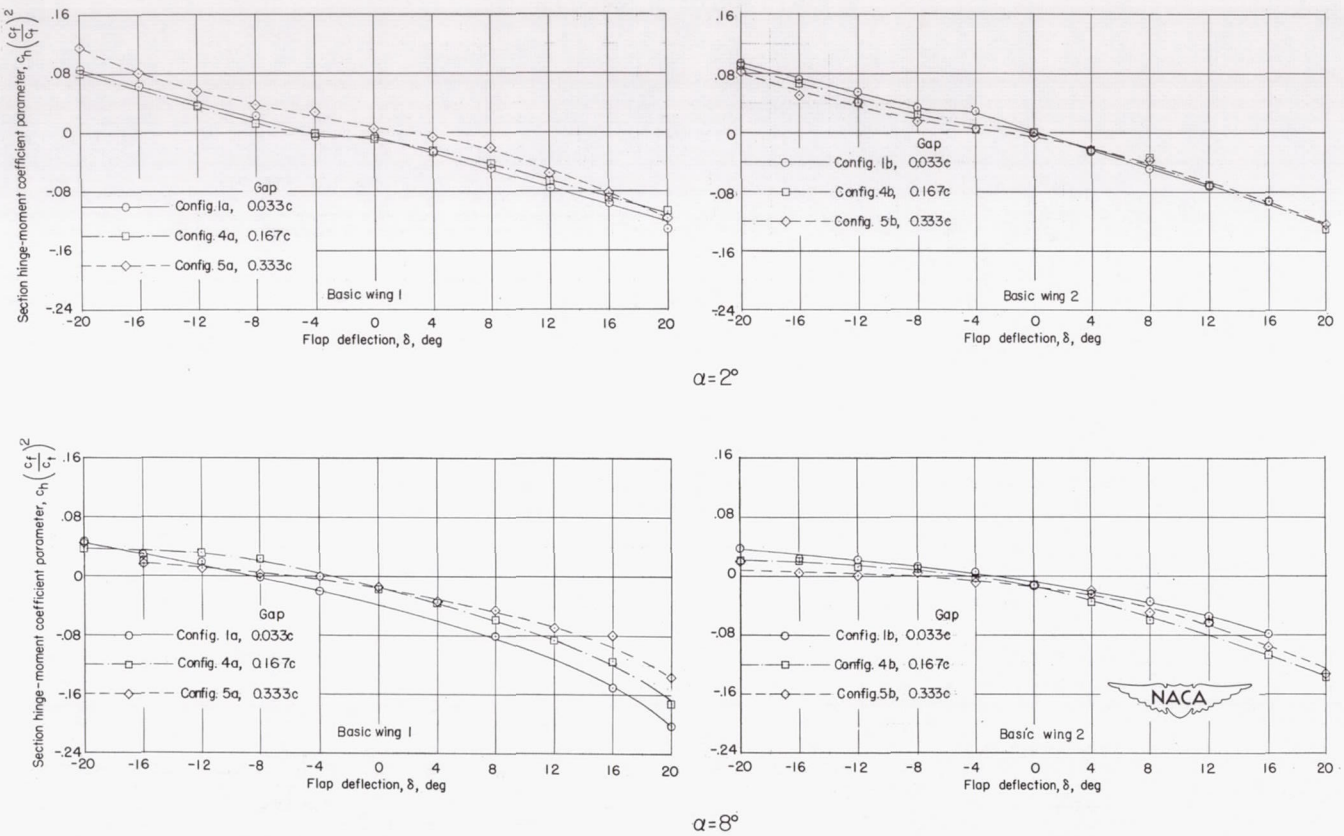
(a) $c_h\left(\frac{c_f}{c_t}\right)^2$.

Figure 7.- Effect of percent overhang nose balance on the variation of the section hinge-moment and normal-force coefficients with angle of attack of a 6-percent-thick symmetrical wing equipped with trailing-edge flap-type controls. Wing-flap gap size, 0.033c; basic wing 2.



(b) c_n.

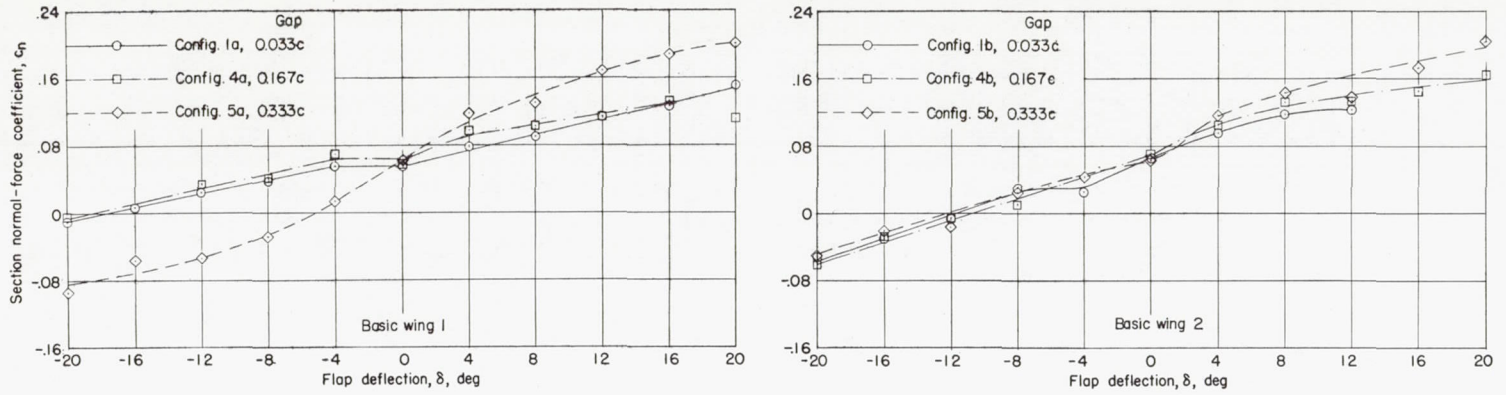
Figure 7.- Concluded.



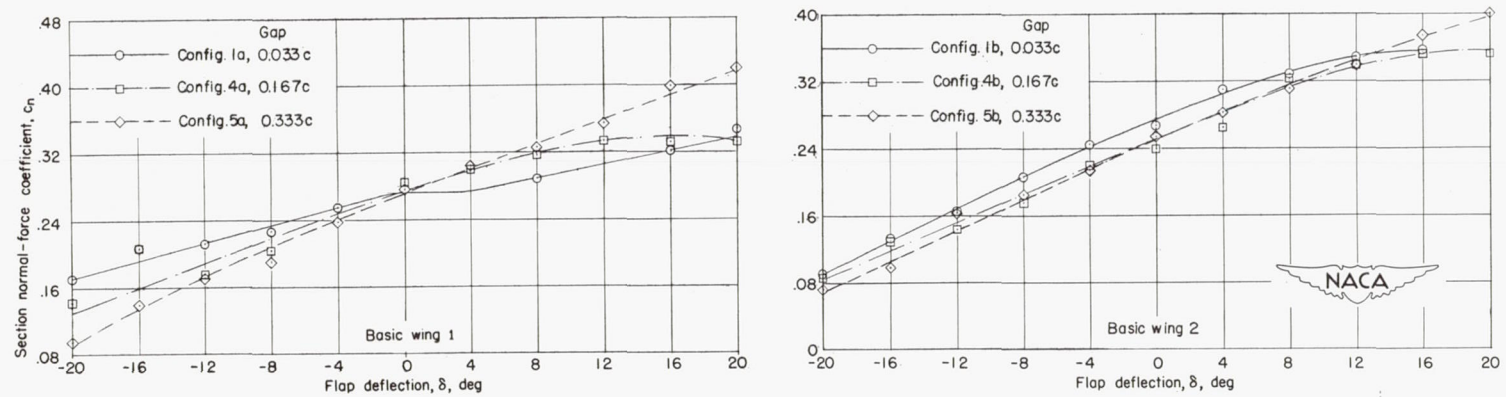
(a) $c_h\left(\frac{c_f}{c_t}\right)^2$.

Figure 8.- Effect of wing-flap gap size on the variation of the section aerodynamic coefficients with flap deflection of a 6-percent-thick symmetrical wing equipped with trailing-edge flap-type controls.

$\frac{c_b}{c_f} = 0.38$.



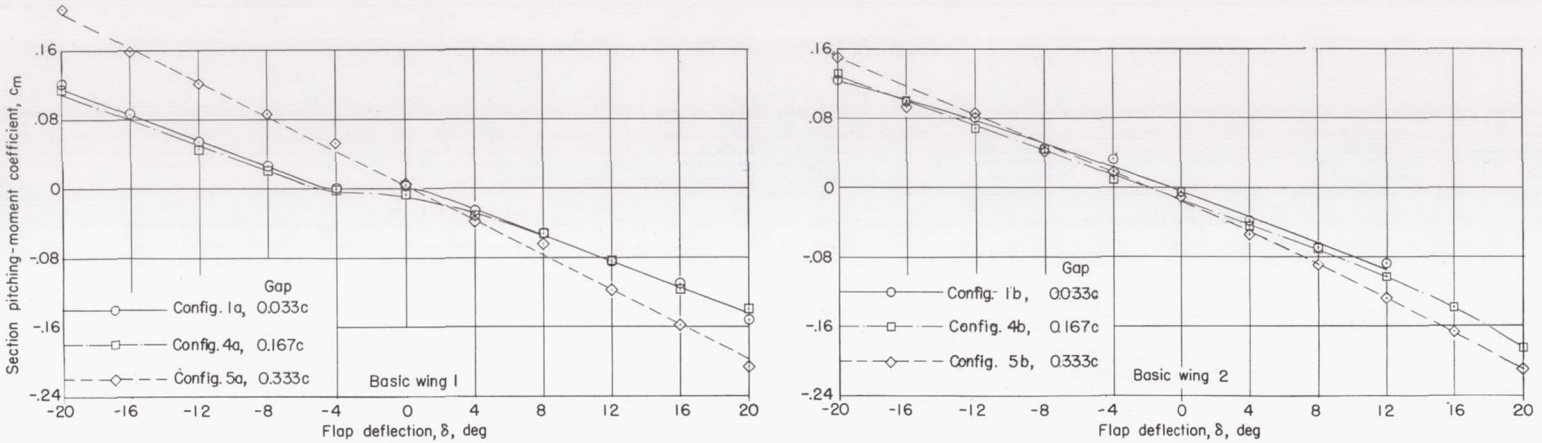
$\alpha = 2°$



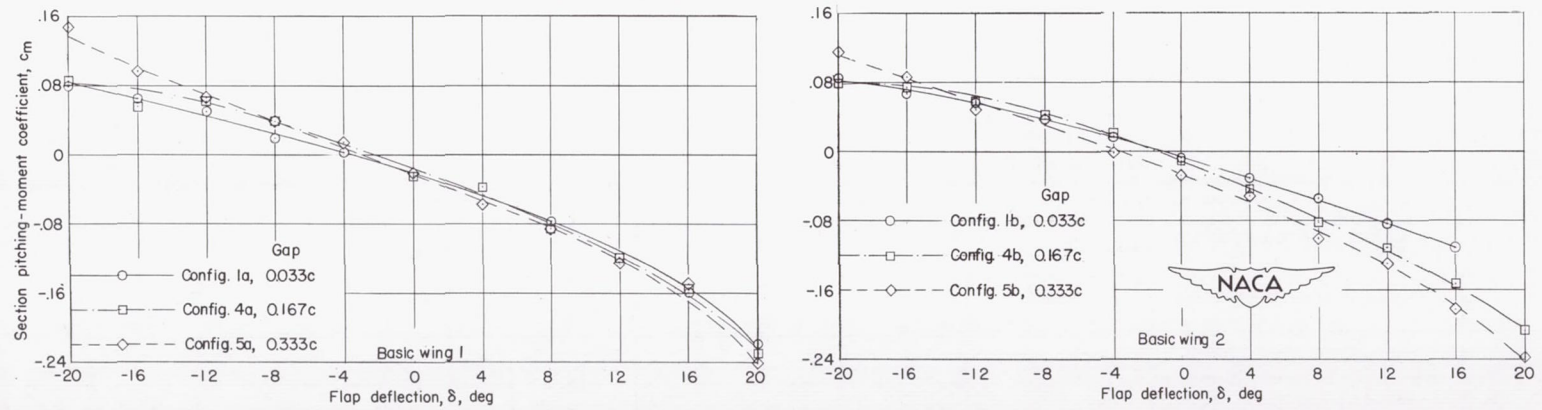
$\alpha = 8°$

(b) c_n.

Figure 8.- Continued.



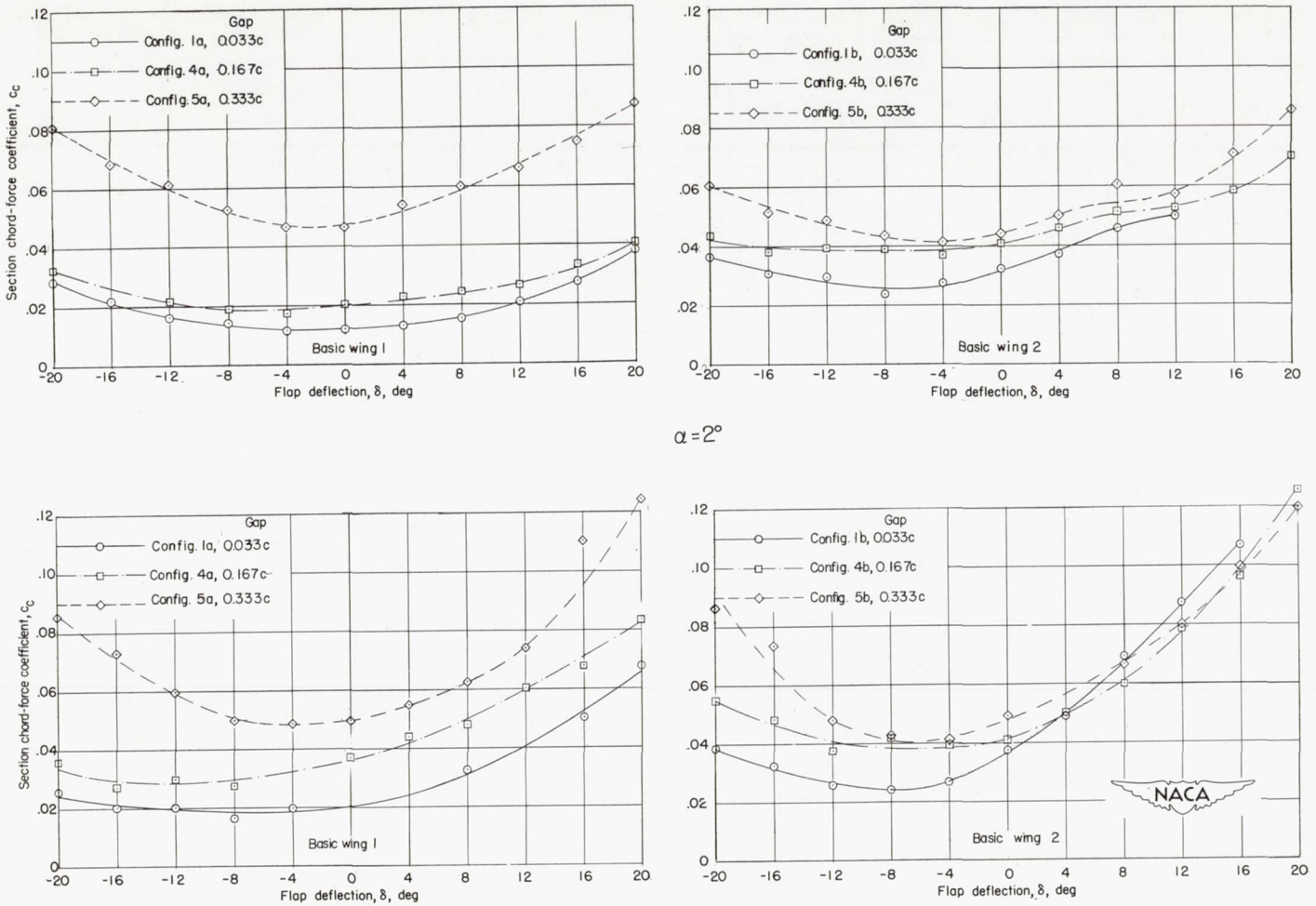
$\alpha = 2°$



$\alpha = 8°$

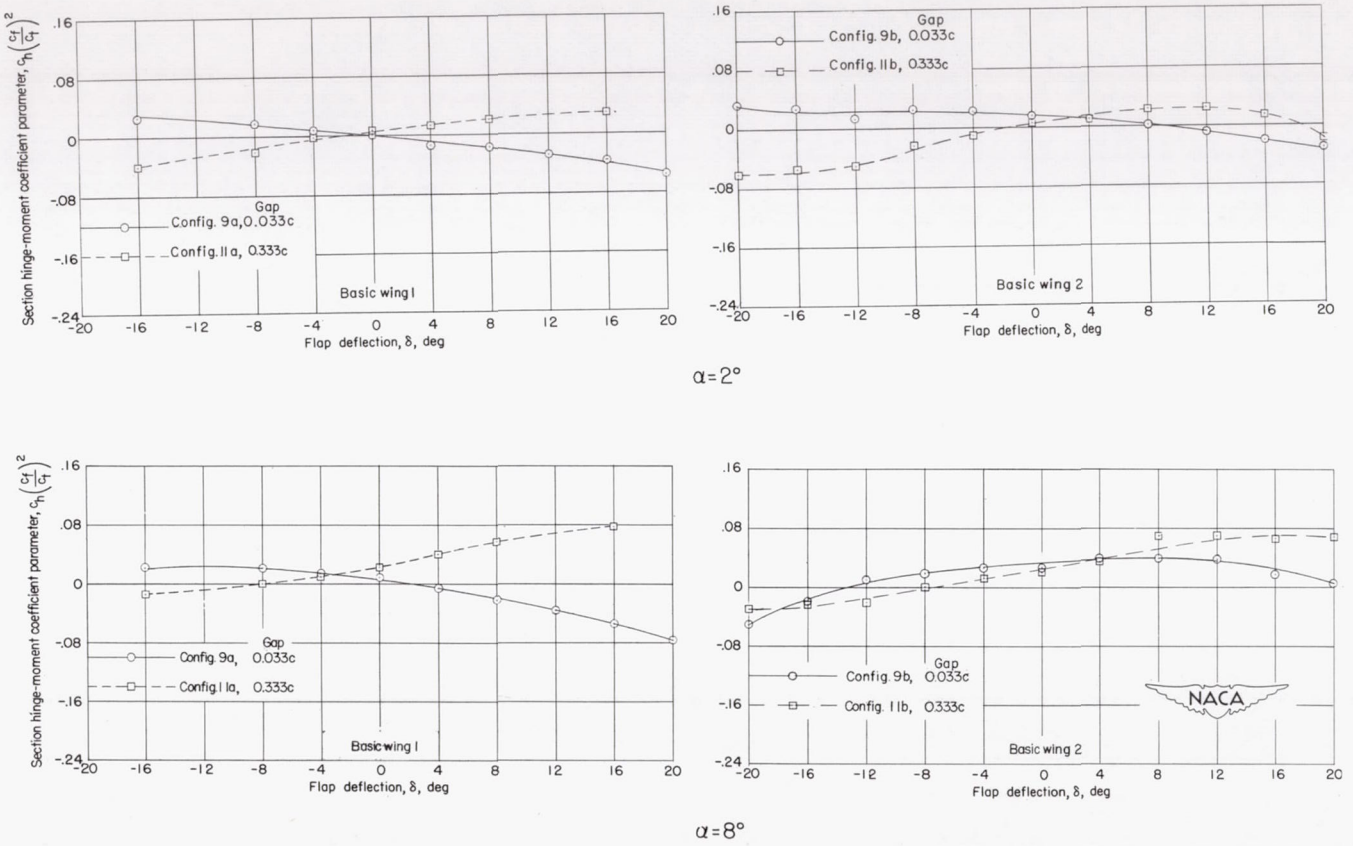
(c) c_m.

Figure 8.- Continued.



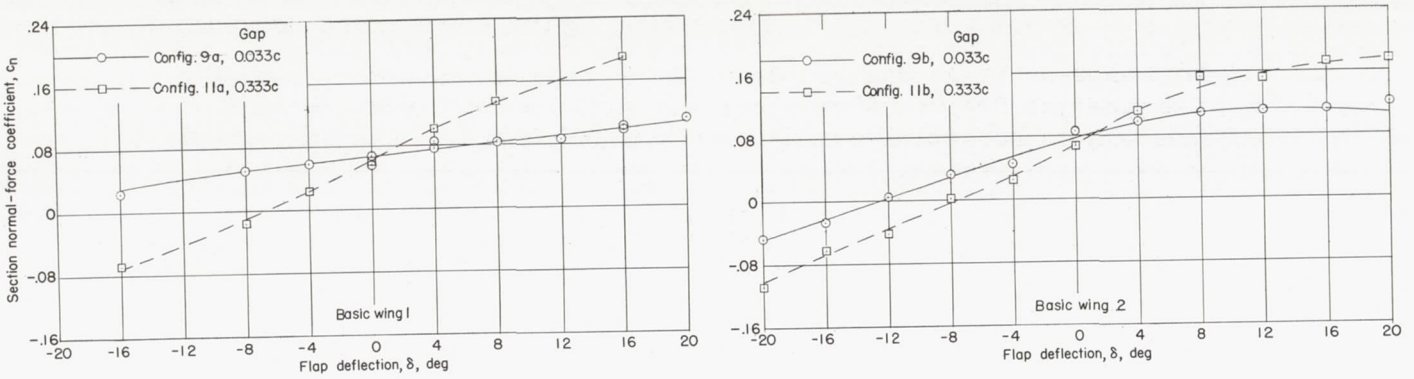
(d) c_c.

Figure 8.- Concluded.

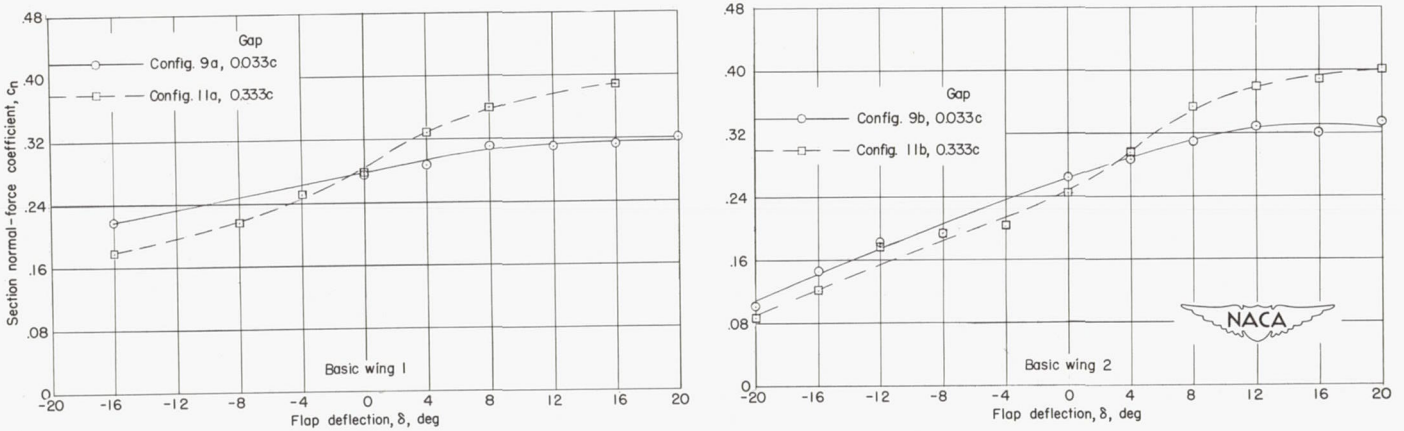


(a) $c_h\left(\frac{c_f}{c_t}\right)^2$.

Figure 9.- Effect of wing-flap gap size on the variation of the section hinge-moment and normal-force coefficients with flap deflection of a 6-percent-thick symmetrical wing equipped with trailing-edge flap-type controls. $\frac{c_b}{c_f} = 0.82$.



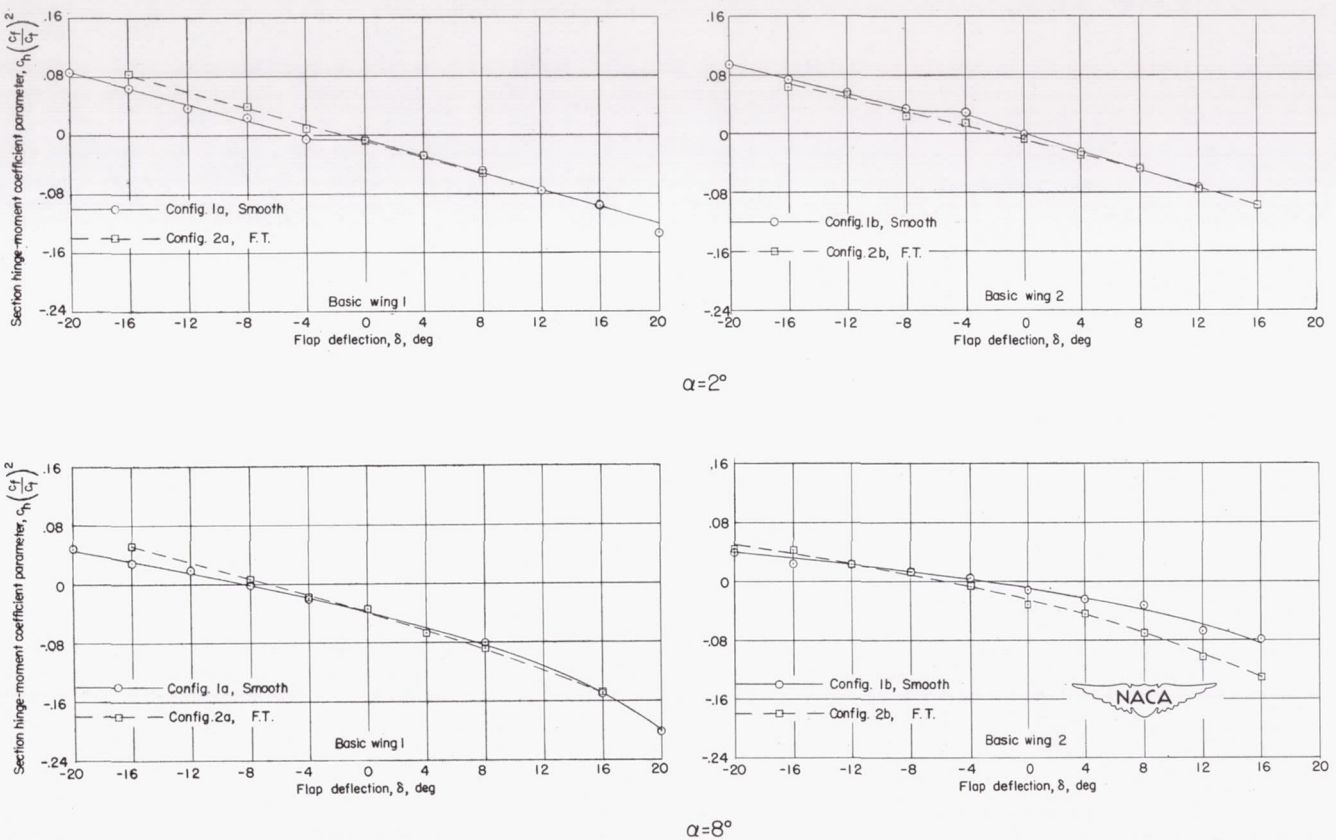
$\alpha = 2°$



$\alpha = 8°$

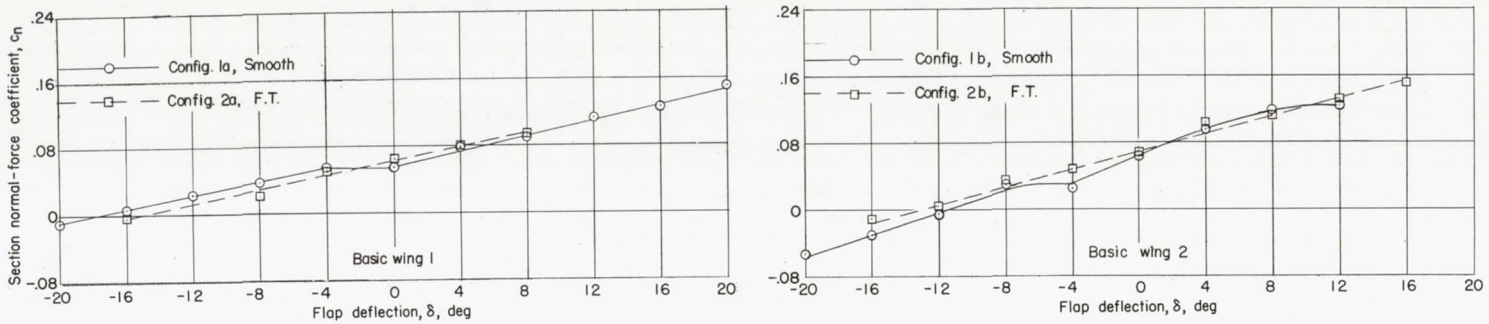
(b) c_n.

Figure 9.- Concluded.

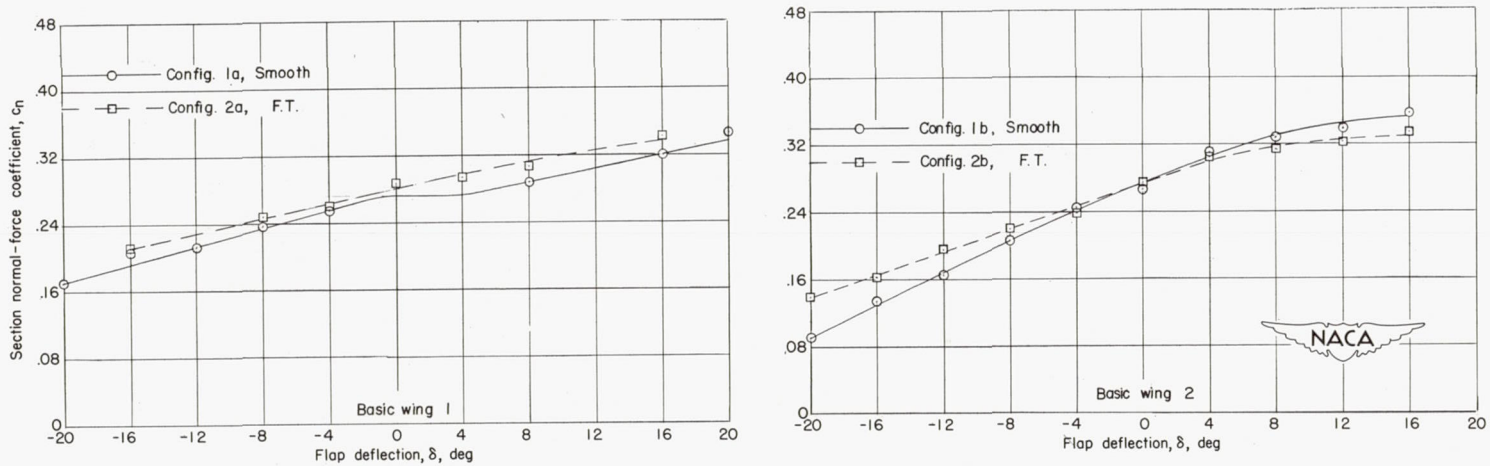


(a) $c_h\left(\frac{c_f}{c_t}\right)^2$.

Figure 10.- Effect of fixed transition on the variation of the section hinge-moment and normal-force coefficients with flap deflection of a 6-percent-thick symmetrical wing equipped with trailing-edge flap-type controls. $\frac{c_b}{c_f}$ = 0.38; wing-flap gap size, 0.033c.



$\alpha = 2°$

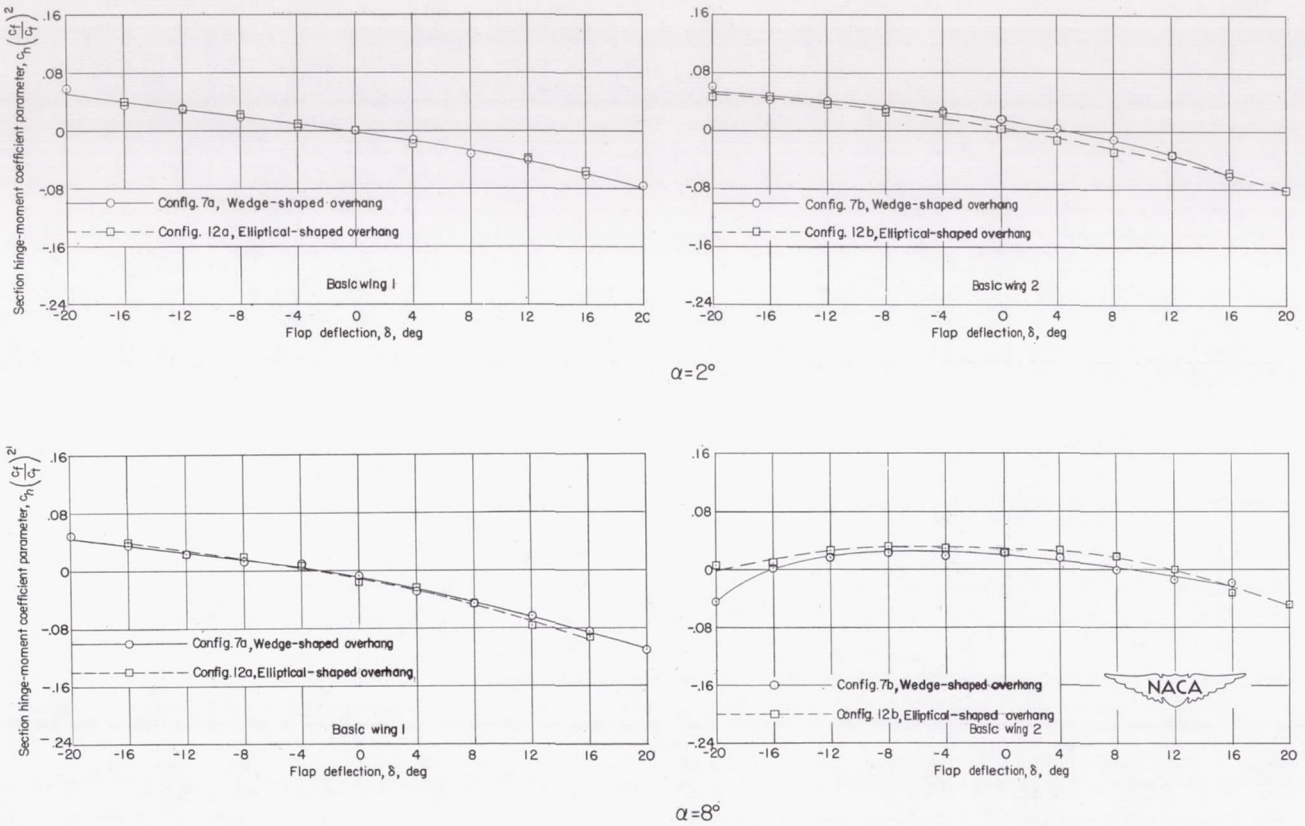


$\alpha = 8°$

(b) c_n.

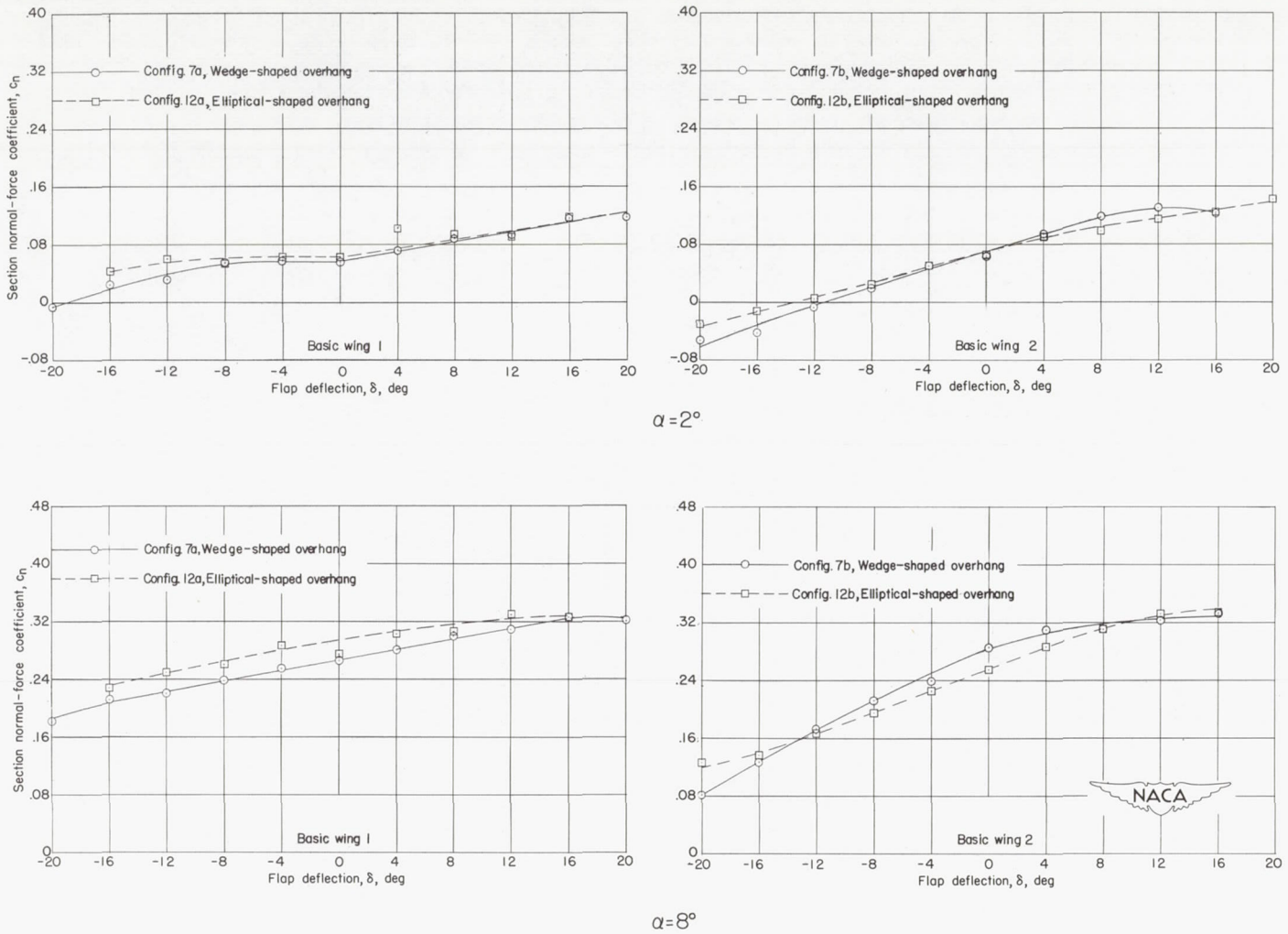
Figure 10.- Concluded.

CONFIDENTIAL



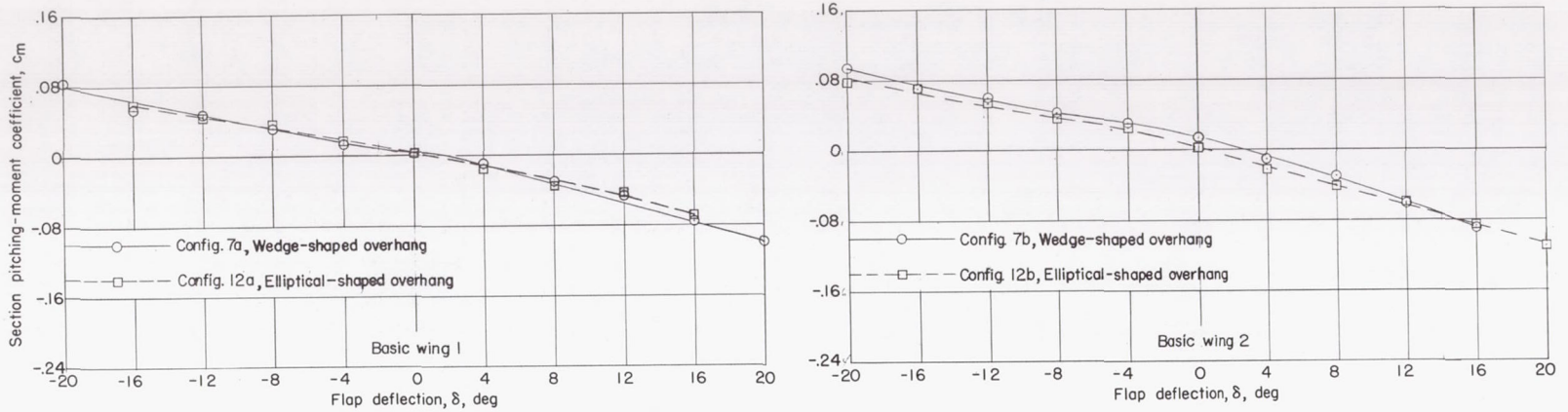
(a) $c_h\left(\frac{c_f}{c_t}\right)^2$.

Figure 11.- Effect of overhang-nose balance shape on the variation of the section aerodynamic coefficients with flap deflection of a 6-percent-thick symmetrical wing equipped with trailing-edge flap-type controls. $\frac{c_b}{c_f}$ = 0.60; wing-flap gap size, 0.033c.

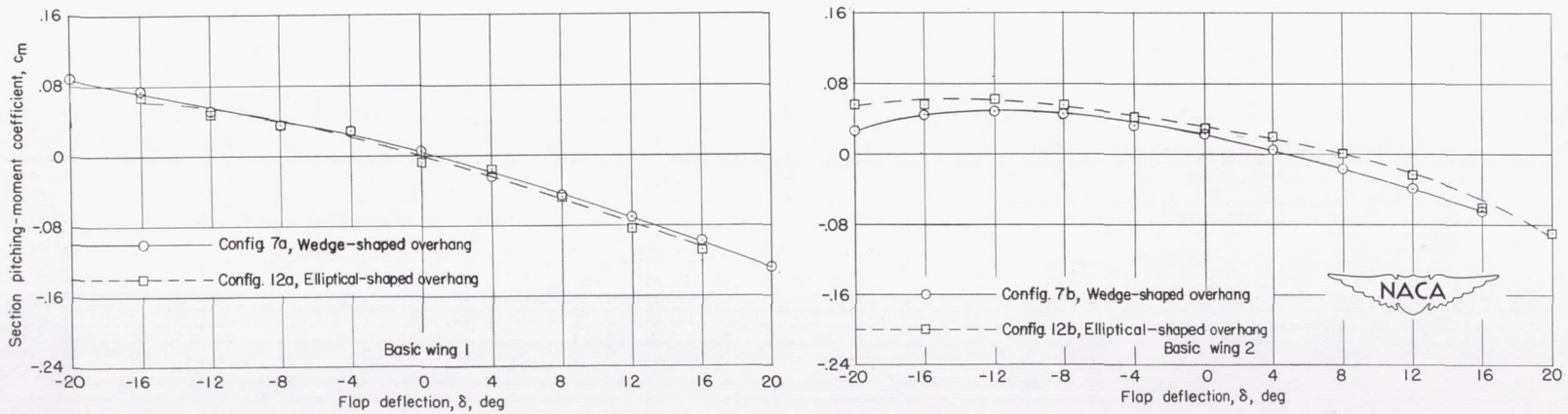


(b) c_n.

Figure 11.- Continued.



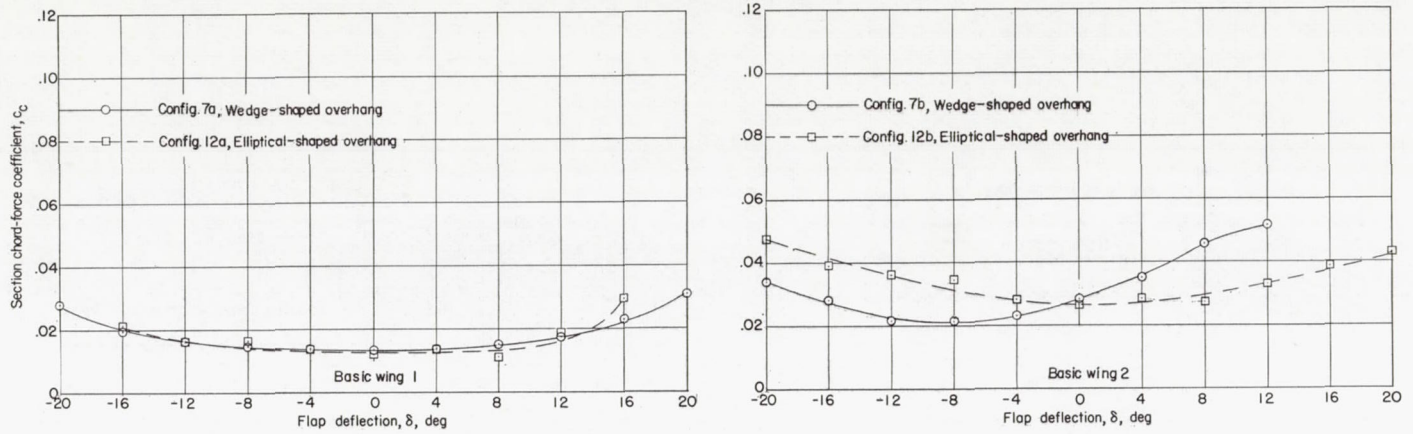
$\alpha = 2°$



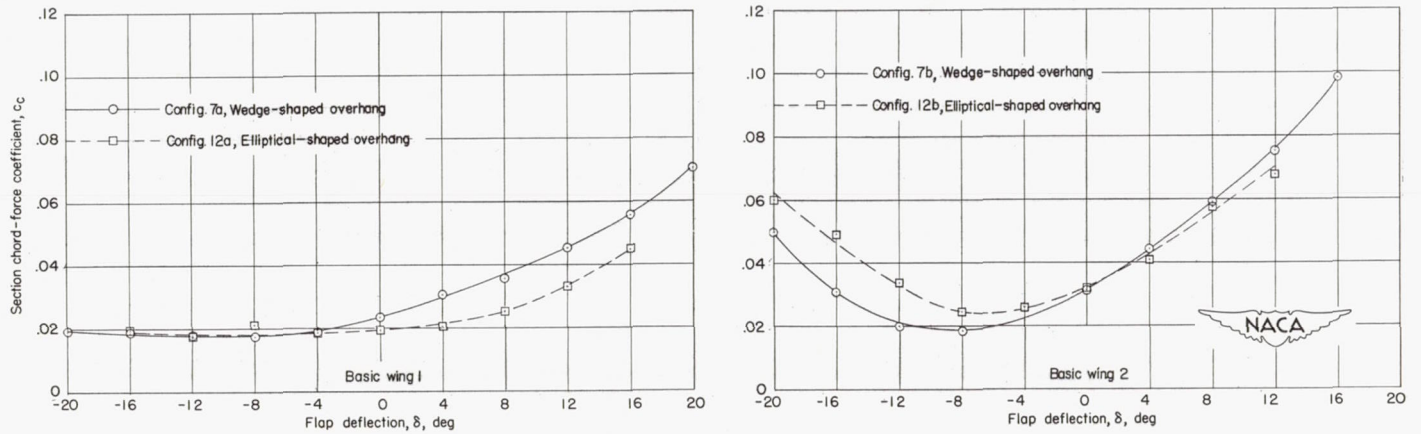
$\alpha = 8°$

(c) c_m.

Figure 11.- Continued.



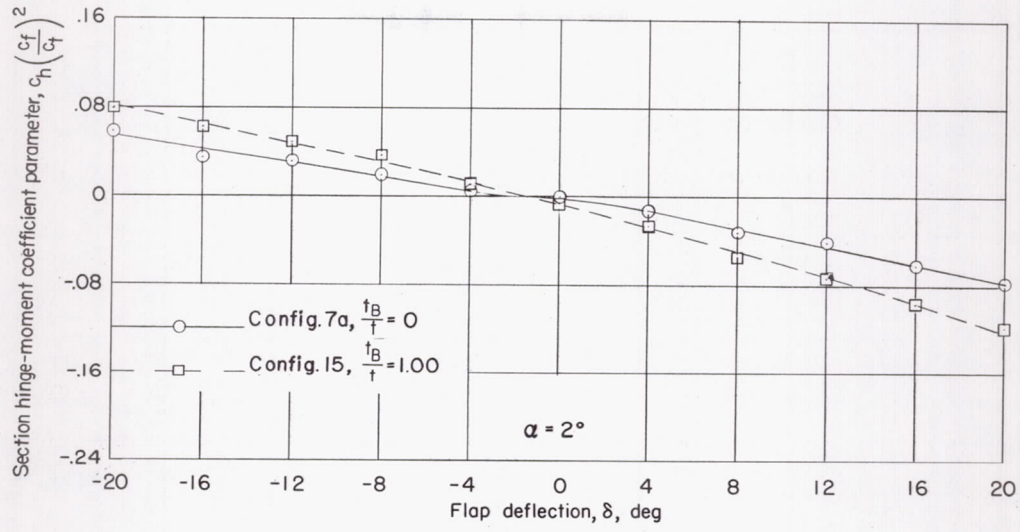
$\alpha = 2°$

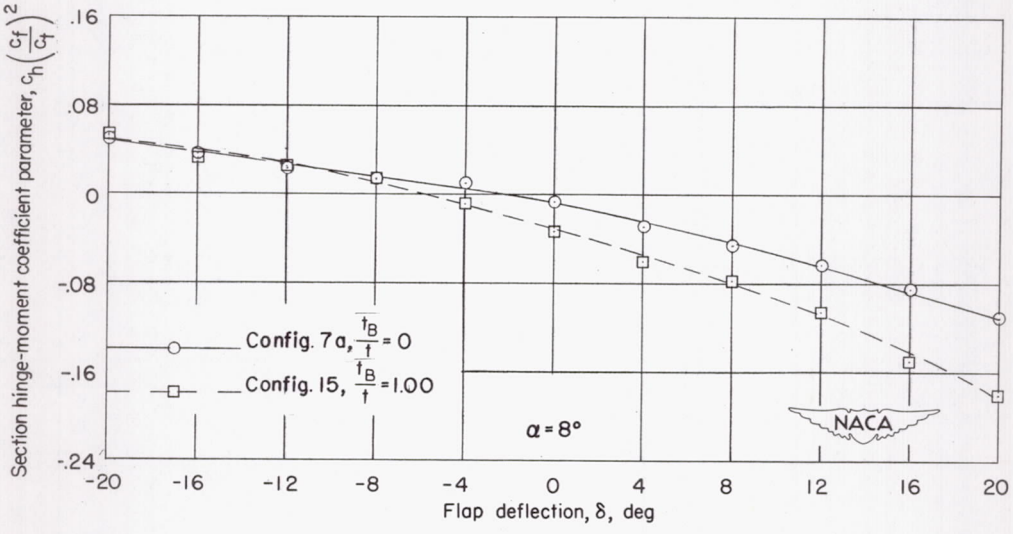


$\alpha = 8°$

(d) c_c.

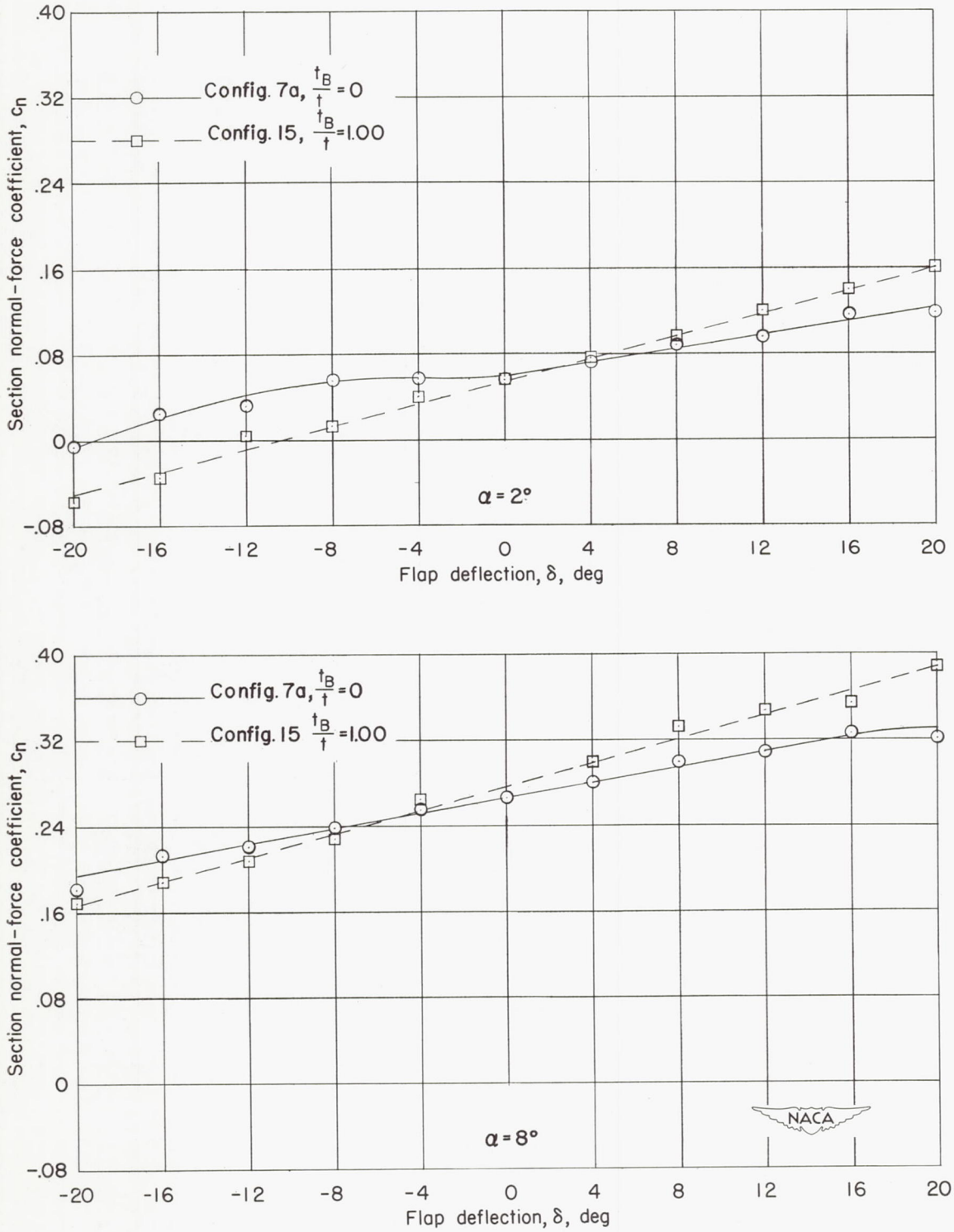
Figure 11.- Concluded.





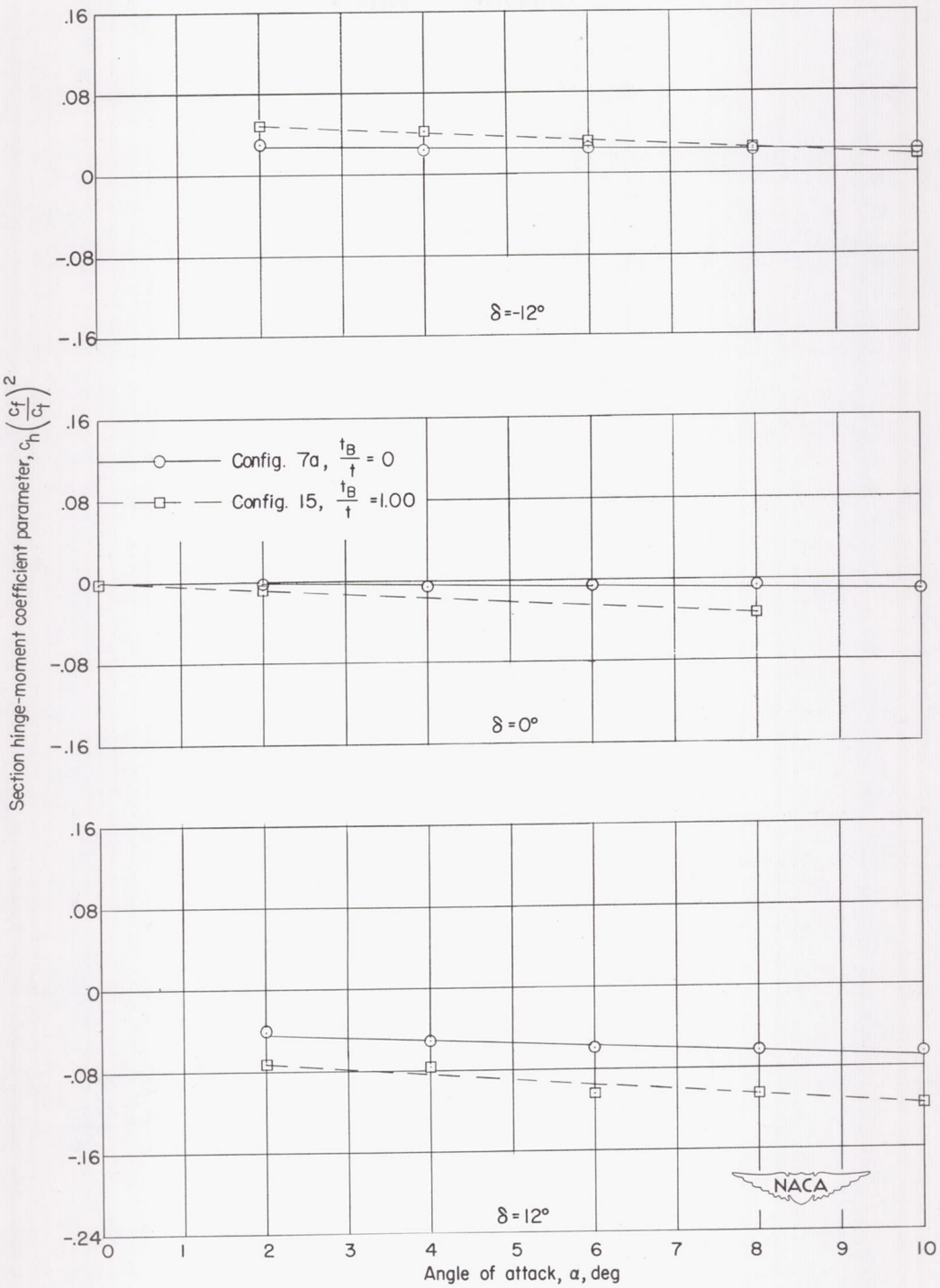
(a) $c_h\left(\frac{c_f}{c_t}\right)^2$ against δ.

Figure 12.- Effect of flap trailing-edge thickness on the variation of the section hinge-moment and normal-force coefficients with flap deflection and angle of attack of a 6-percent-thick symmetrical wing equipped with trailing-edge flap-type controls. $\frac{c_b}{c_f}$ = 0.60; wing-flap gap size, 0.033c; basic wing 1.



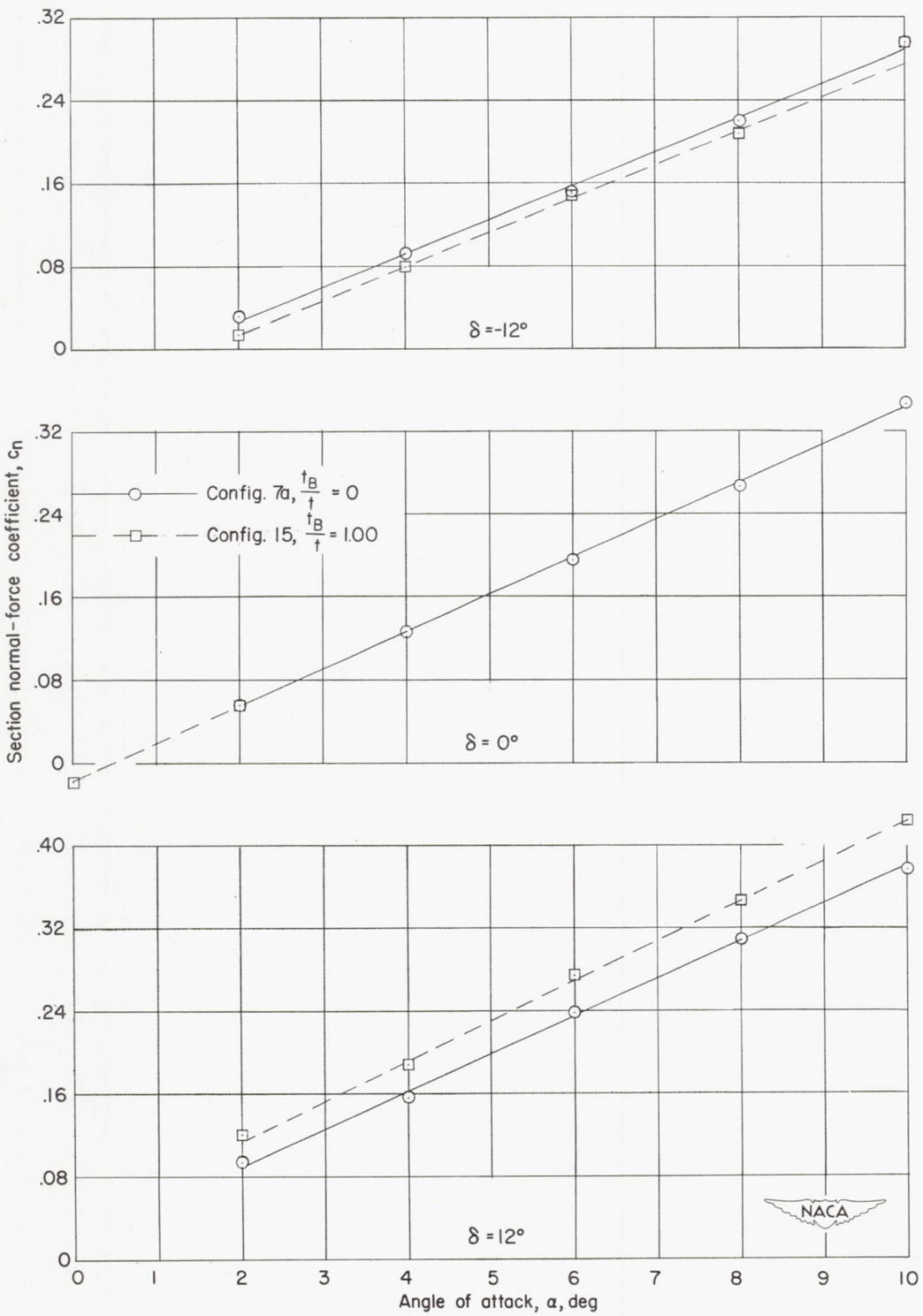
(b) c_n against δ.

Figure 12.- Continued.



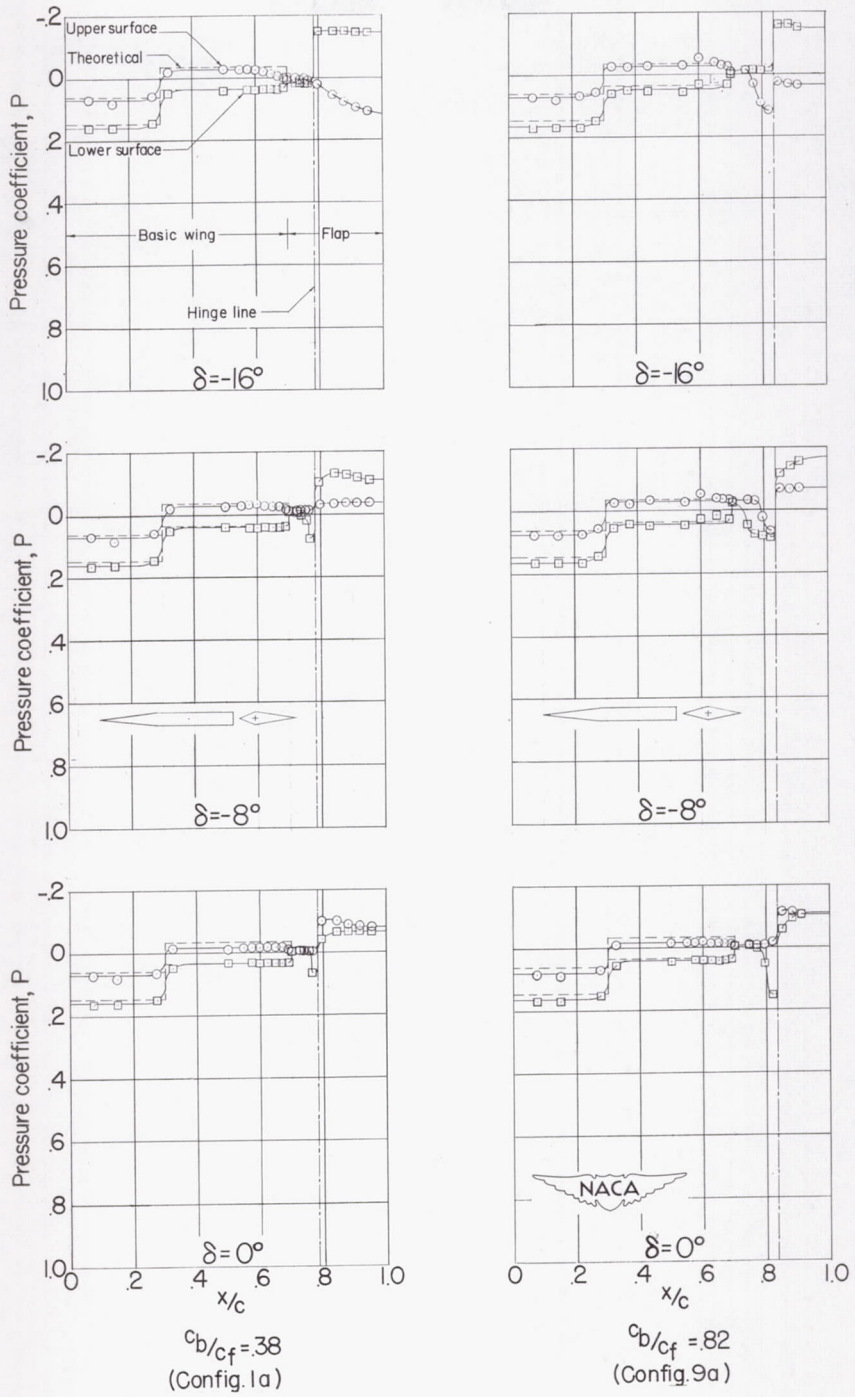
(c) $c_h\left(\frac{c_f}{c_t}\right)^2$ against α.

Figure 12.- Continued.



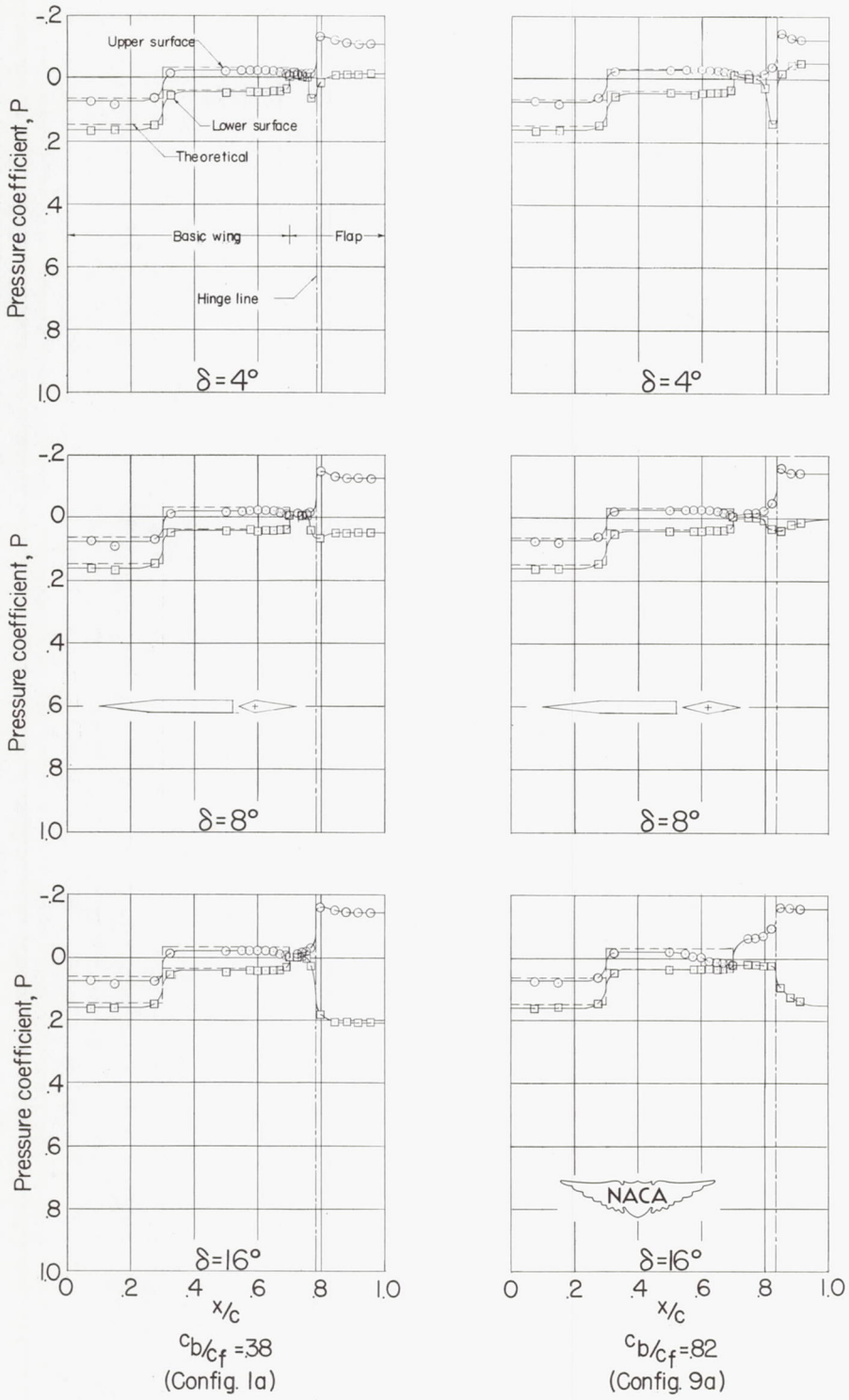
(d) c_n against α.

Figure 12.- Concluded.



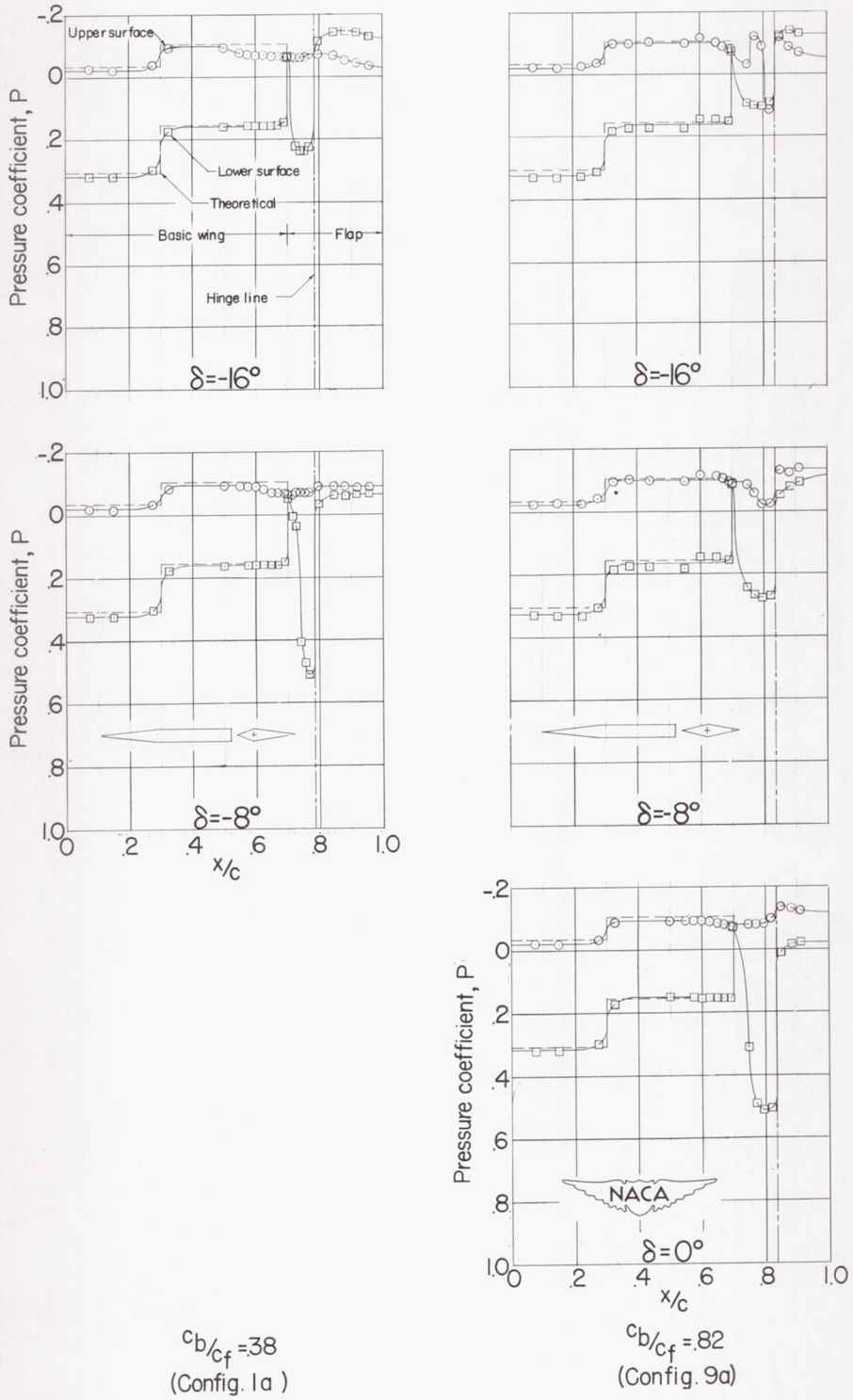
(a) $\alpha = 2^{\circ}$.

Figure 13.- Typical pressure distributions over a 6-percent-thick symmetrical wing equipped with flap-type controls showing some effects of varying percent overhang nose balance. Wing-flap gap size, 0.033c; basic wing 1.



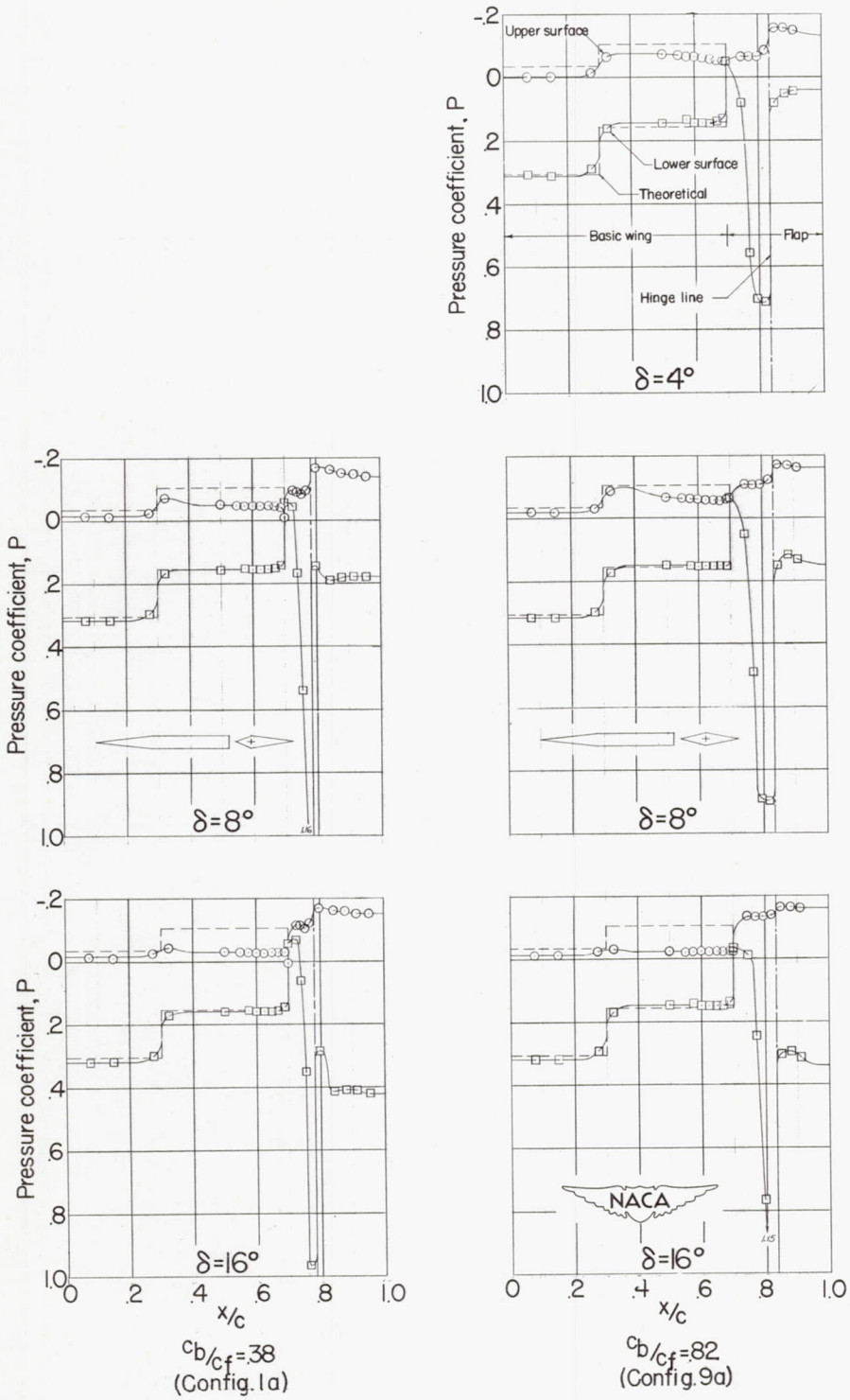
(a) Concluded.

Figure 13.- Continued.



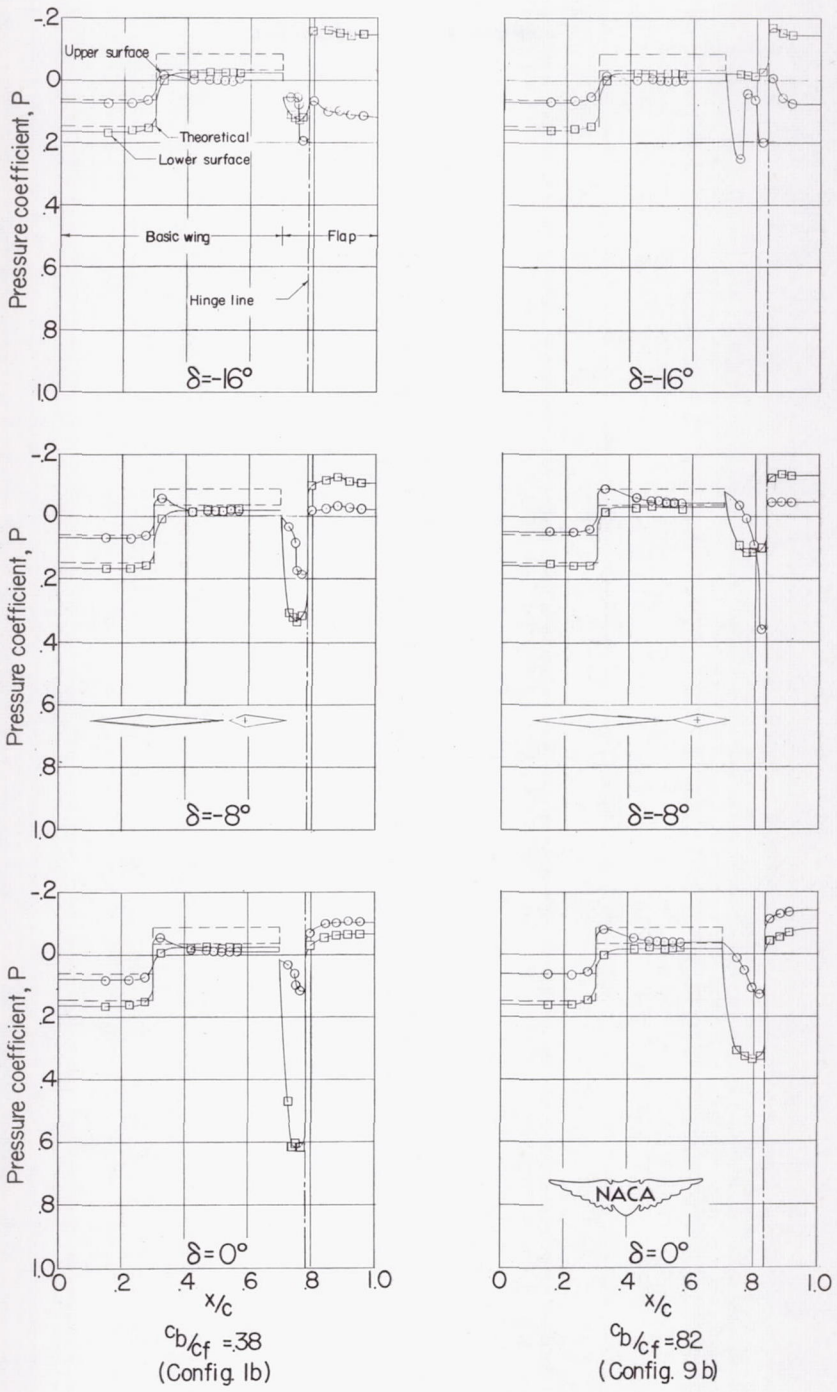
(b) $\alpha = 8^{\circ}$.

Figure 13.- Continued.



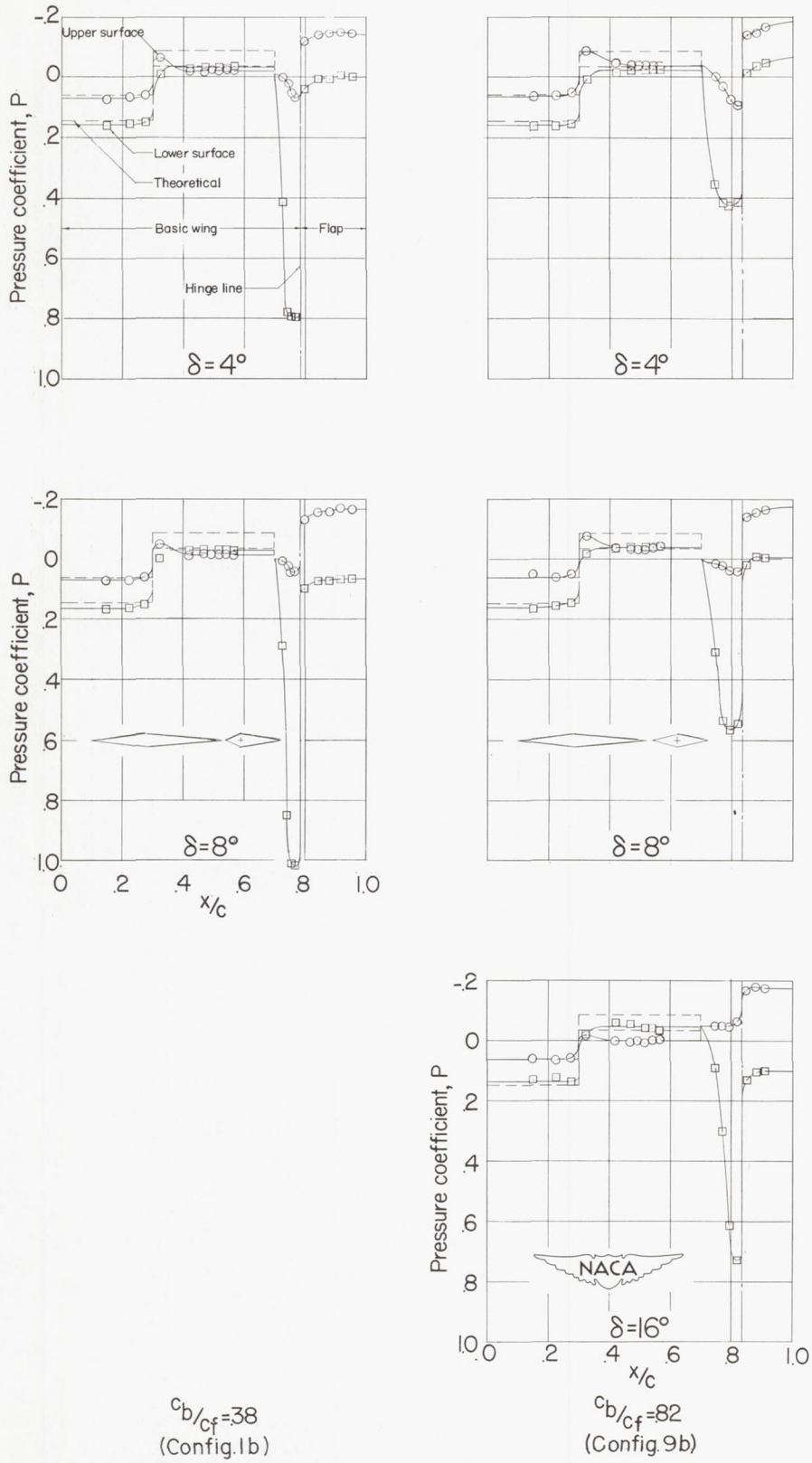
(b) Concluded.

Figure 13.- Concluded.



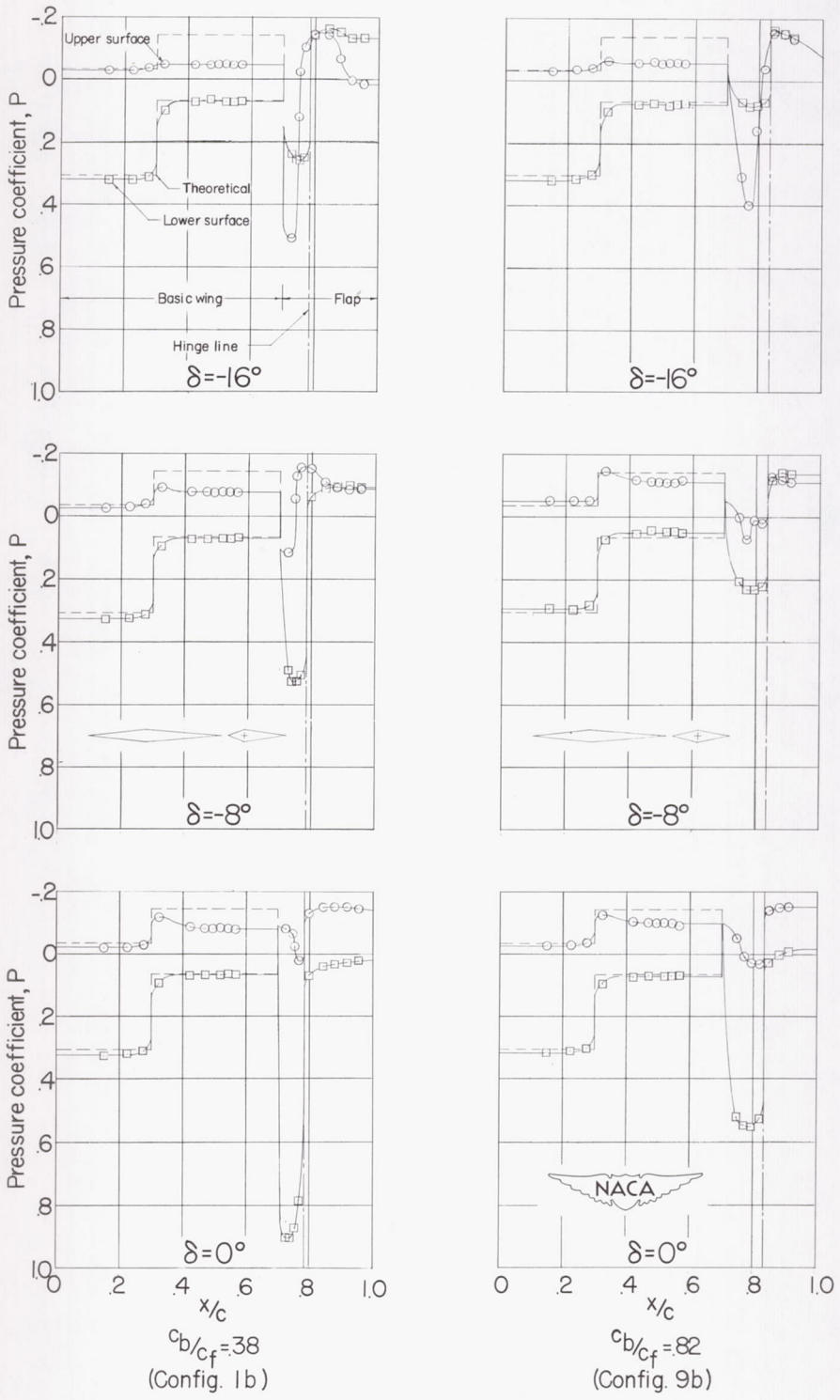
(a) $\alpha = 2^{\circ}$.

Figure 14.- Typical pressure distributions over a 6-percent-thick symmetrical wing equipped with flap-type controls showing some effects of varying percent overhang nose balance. Wing-flap gap size, 0.033c; basic wing 2.



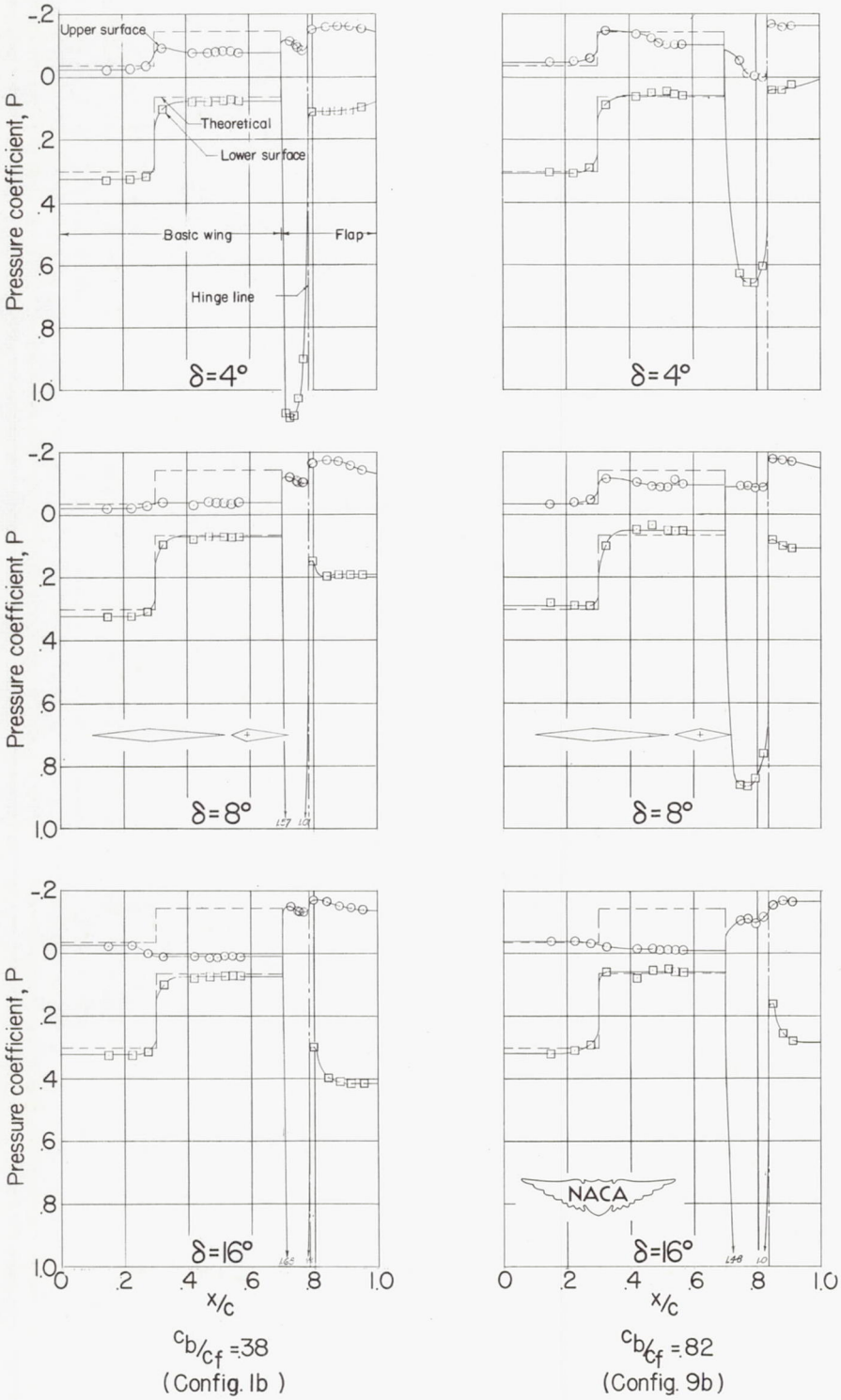
(a) Concluded.

Figure 14.- Continued.



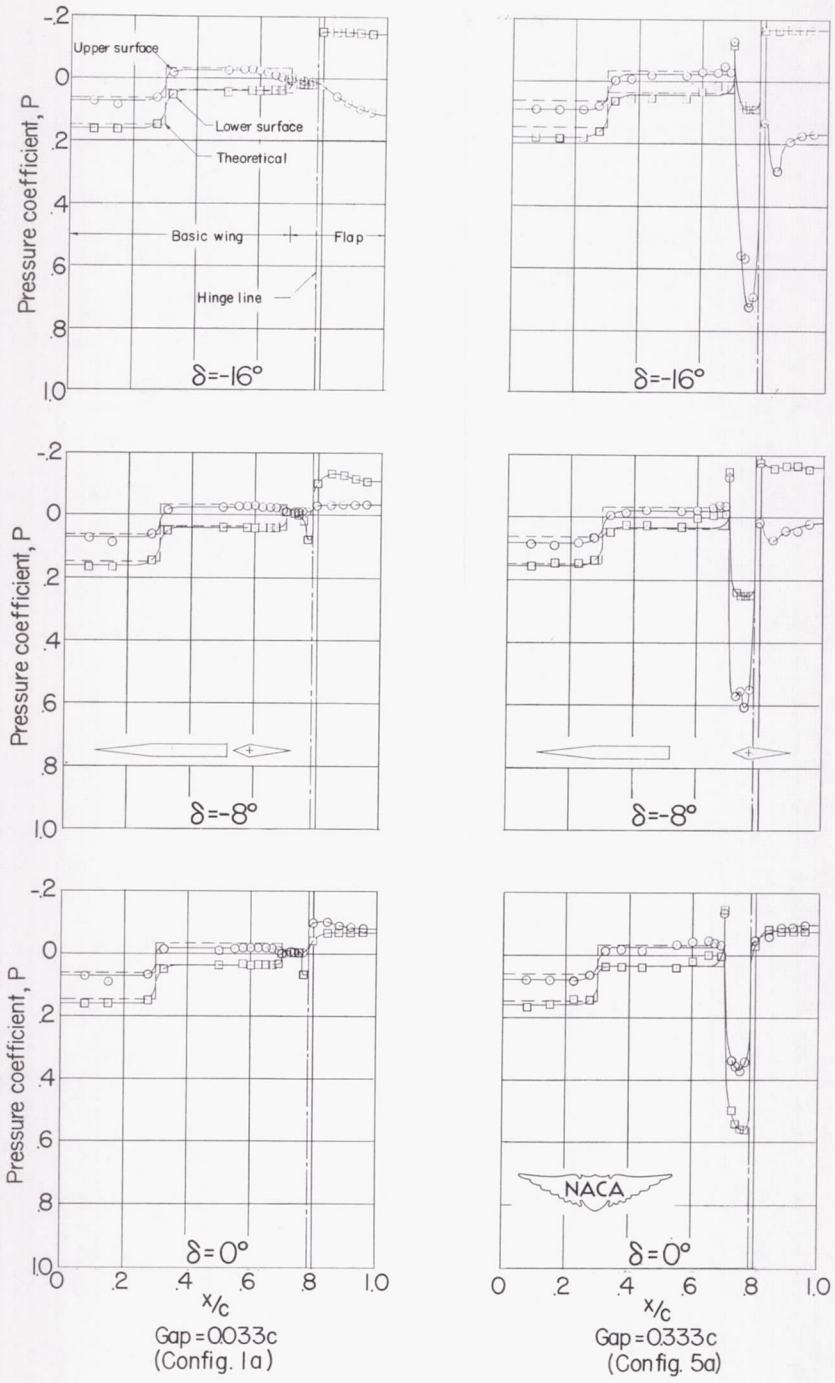
(b) $\alpha = 8^{\circ}$.

Figure 14.- Continued.



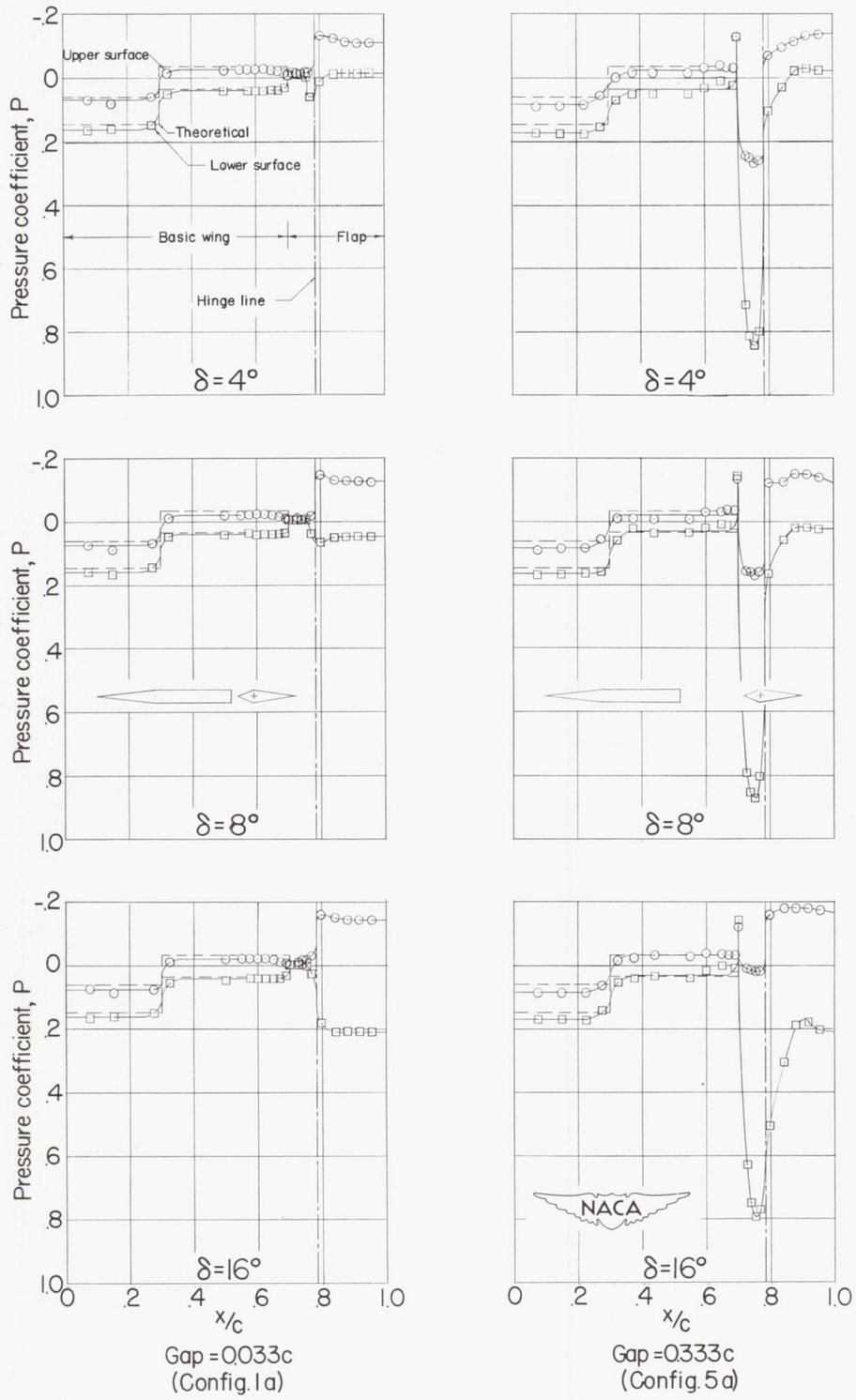
(b) Concluded.

Figure 14.- Concluded.



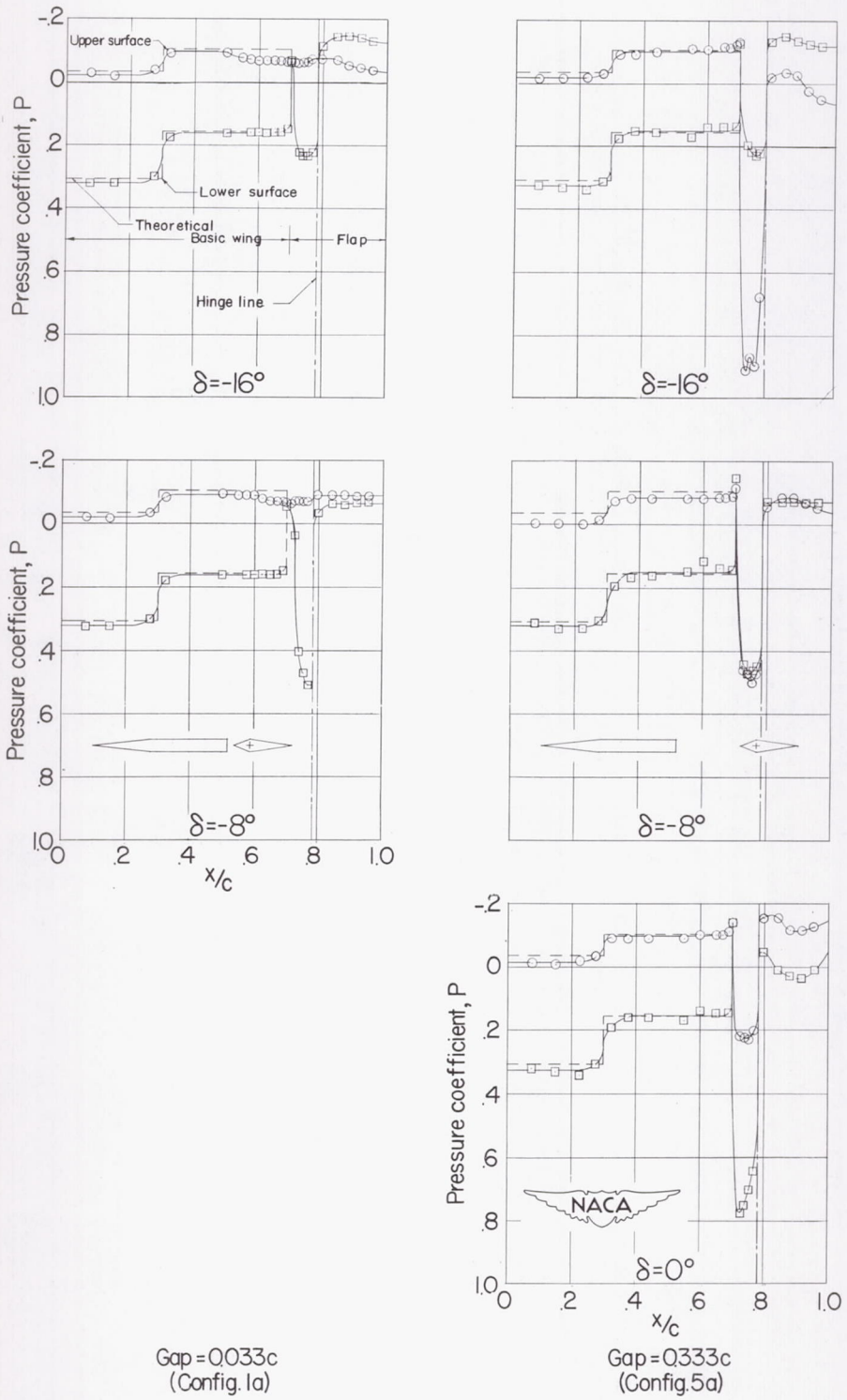
(a) $\alpha = 2^{\circ}$.

Figure 15.- Typical pressure distributions over a 6-percent-thick symmetrical wing equipped with flap-type controls showing some effects of varying wing-flap gap size. $\frac{c_b}{c_f} = 0.38$; basic wing 1.



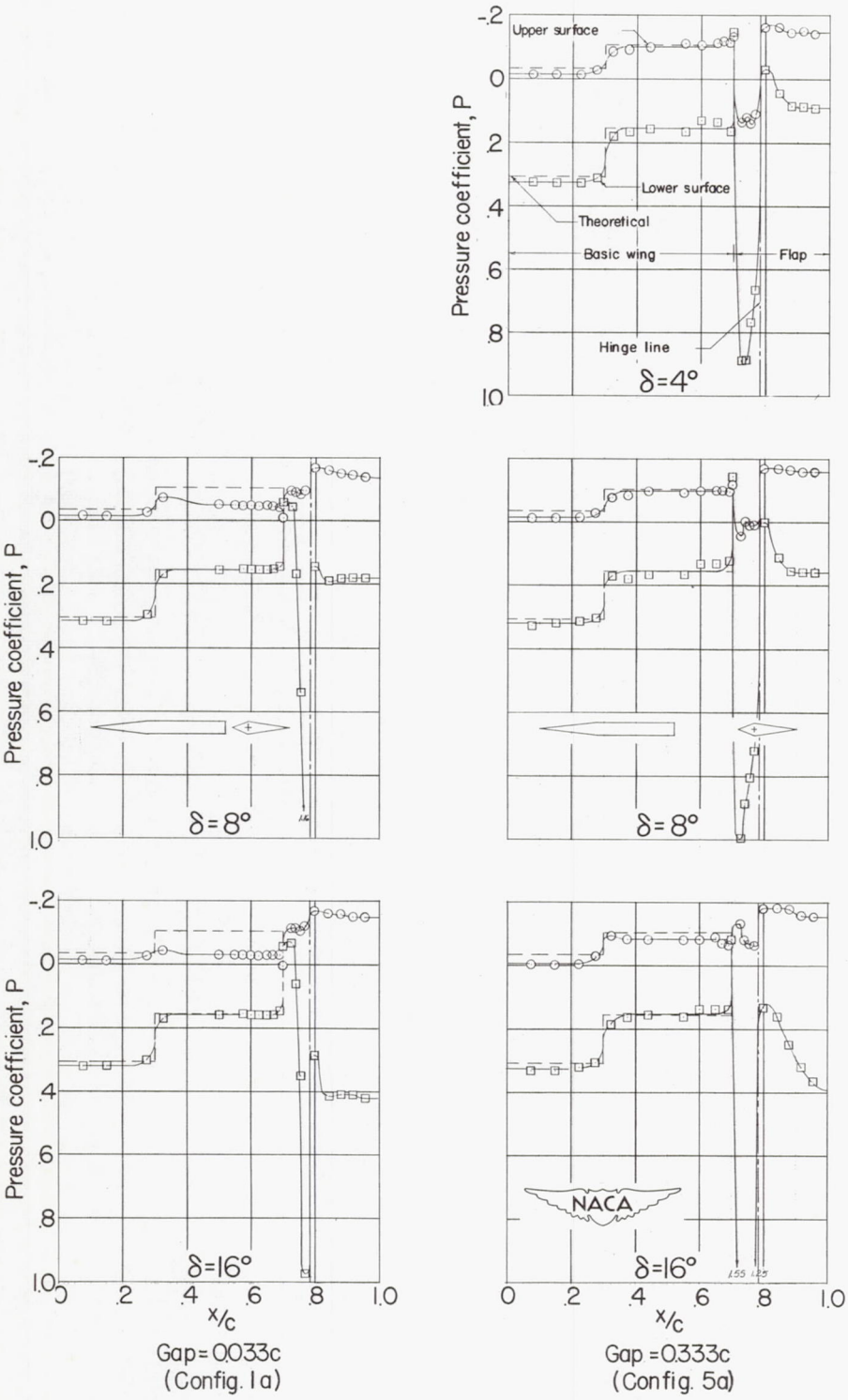
(a) Concluded.

Figure 15.- Continued.



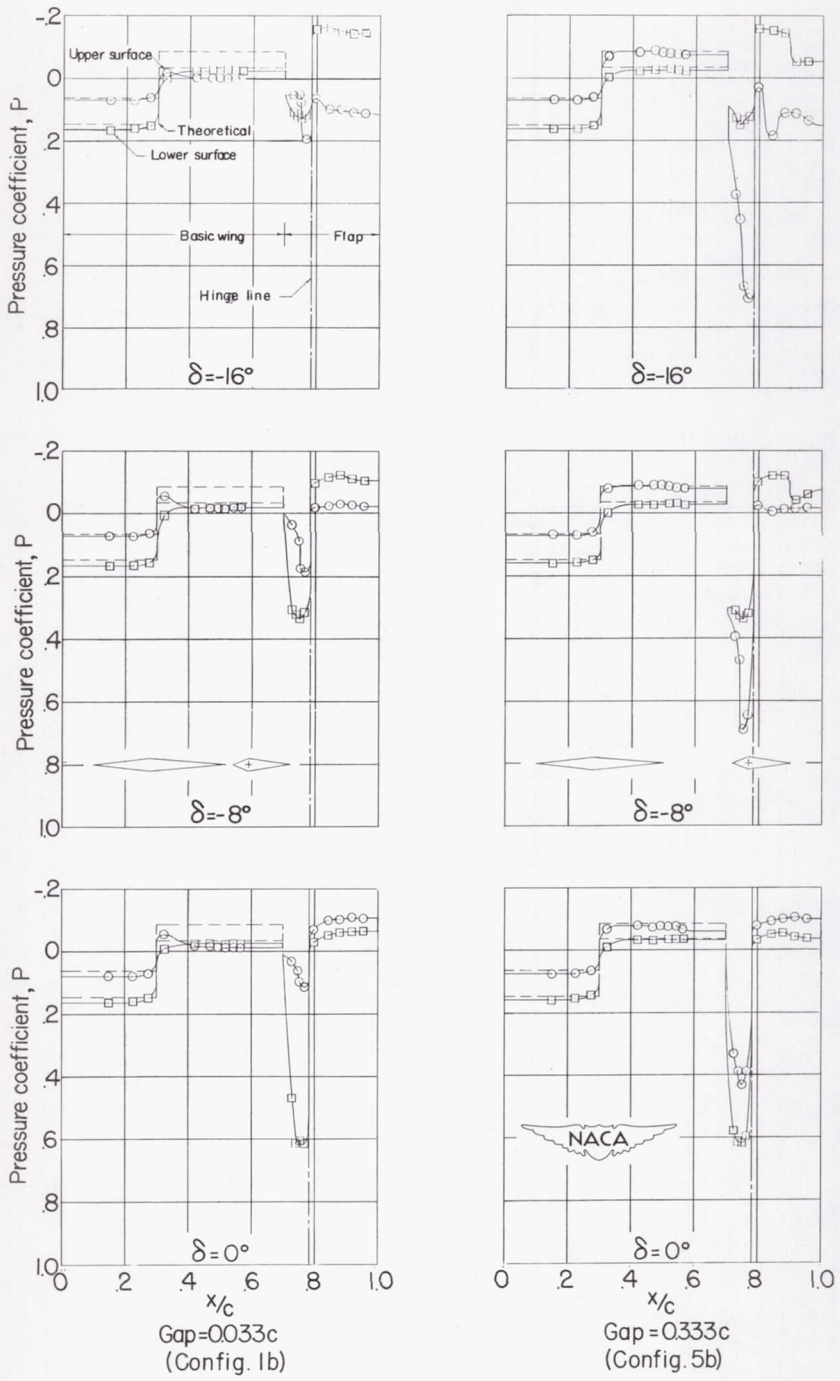
(b) $\alpha = 8^{\circ}$.

Figure 15.- Continued.



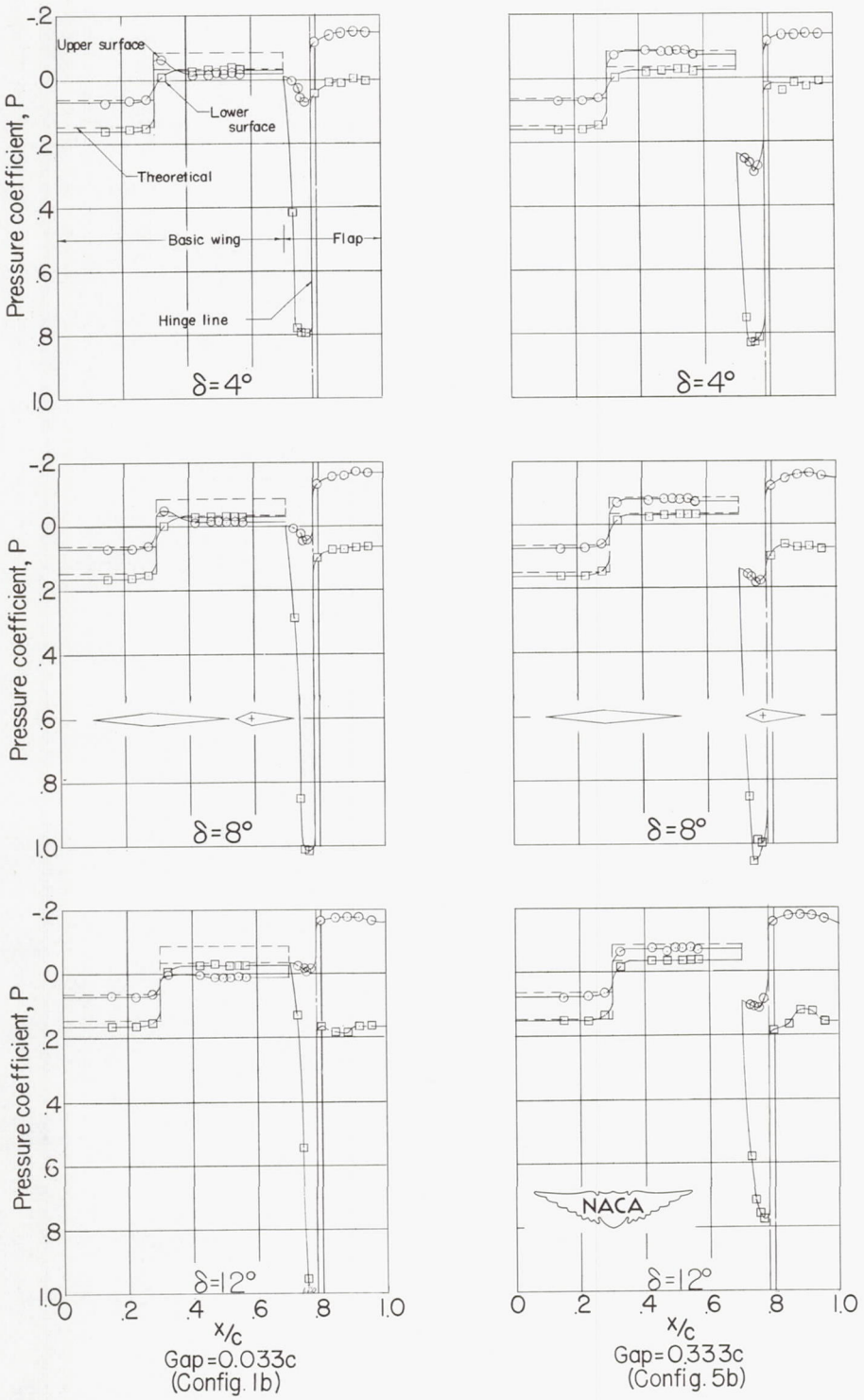
(b) Concluded.

Figure 15.- Concluded.



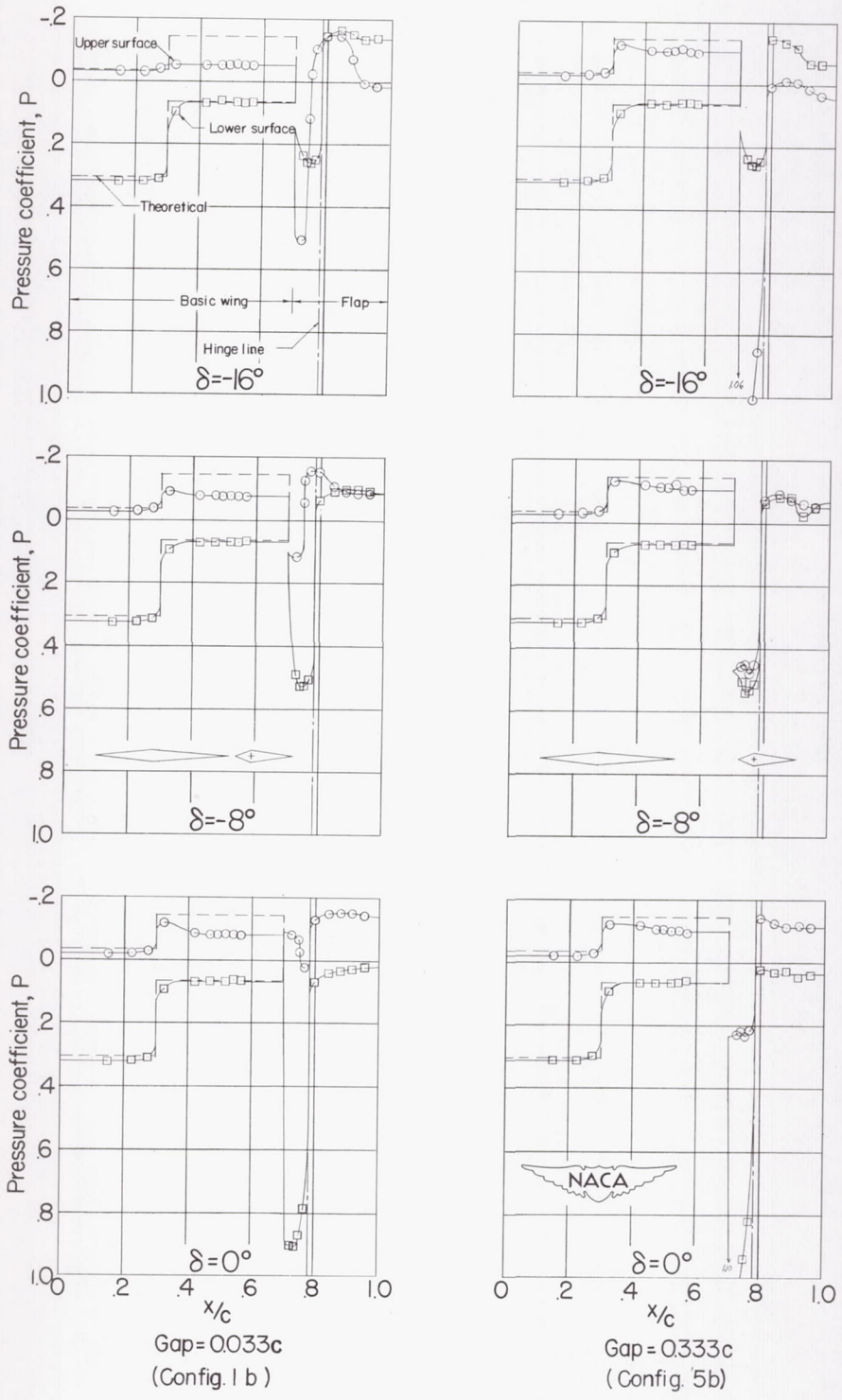
(a) $\alpha = 2^{\circ}$.

Figure 16.- Typical pressure distributions over a 6-percent-thick symmetrical wing equipped with flap-type controls showing some effects of varying wing-flap gap size. $\frac{c_b}{c_f} = 0.38$; basic wing 2.



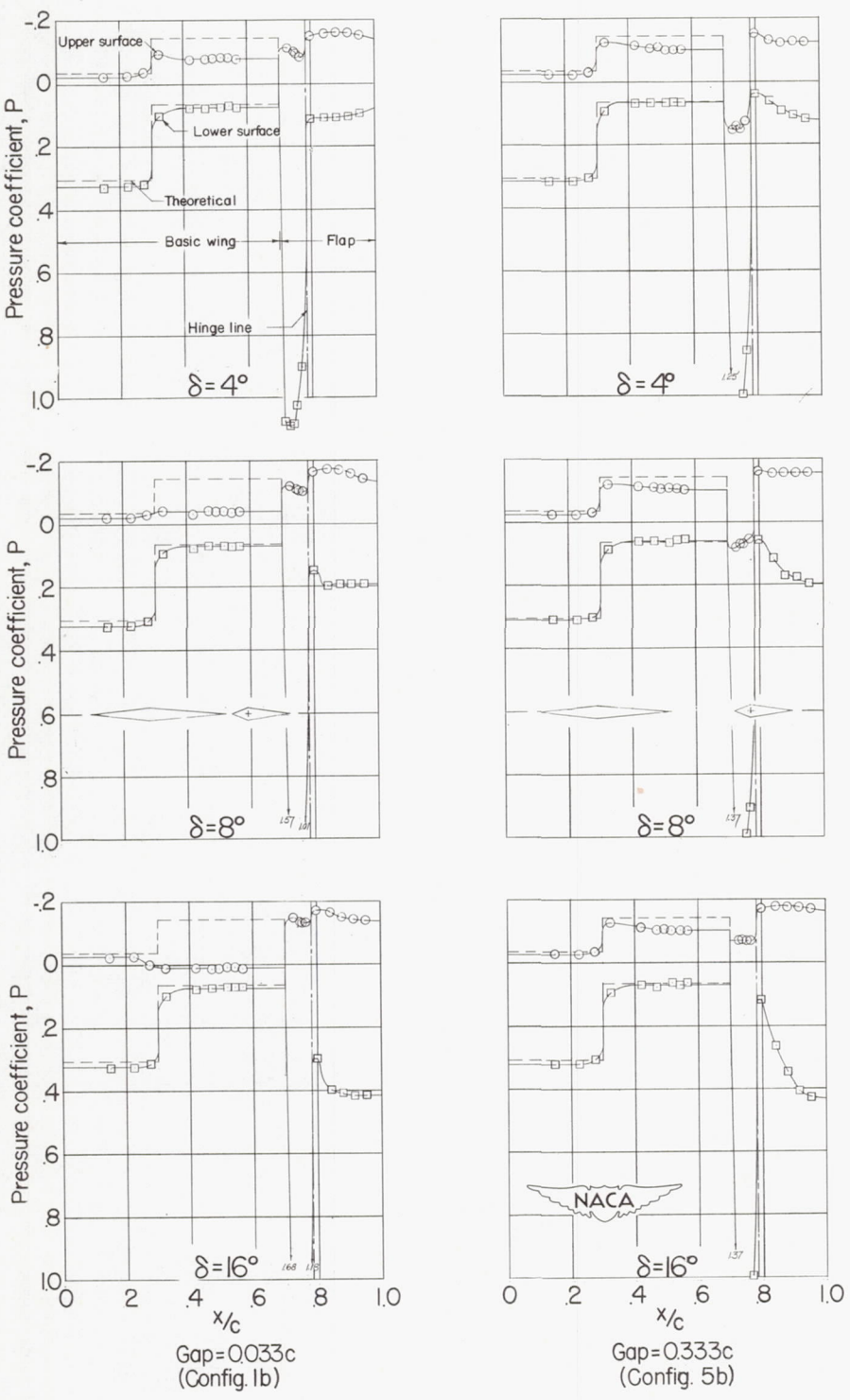
(a) Concluded.

Figure 16.- Continued.



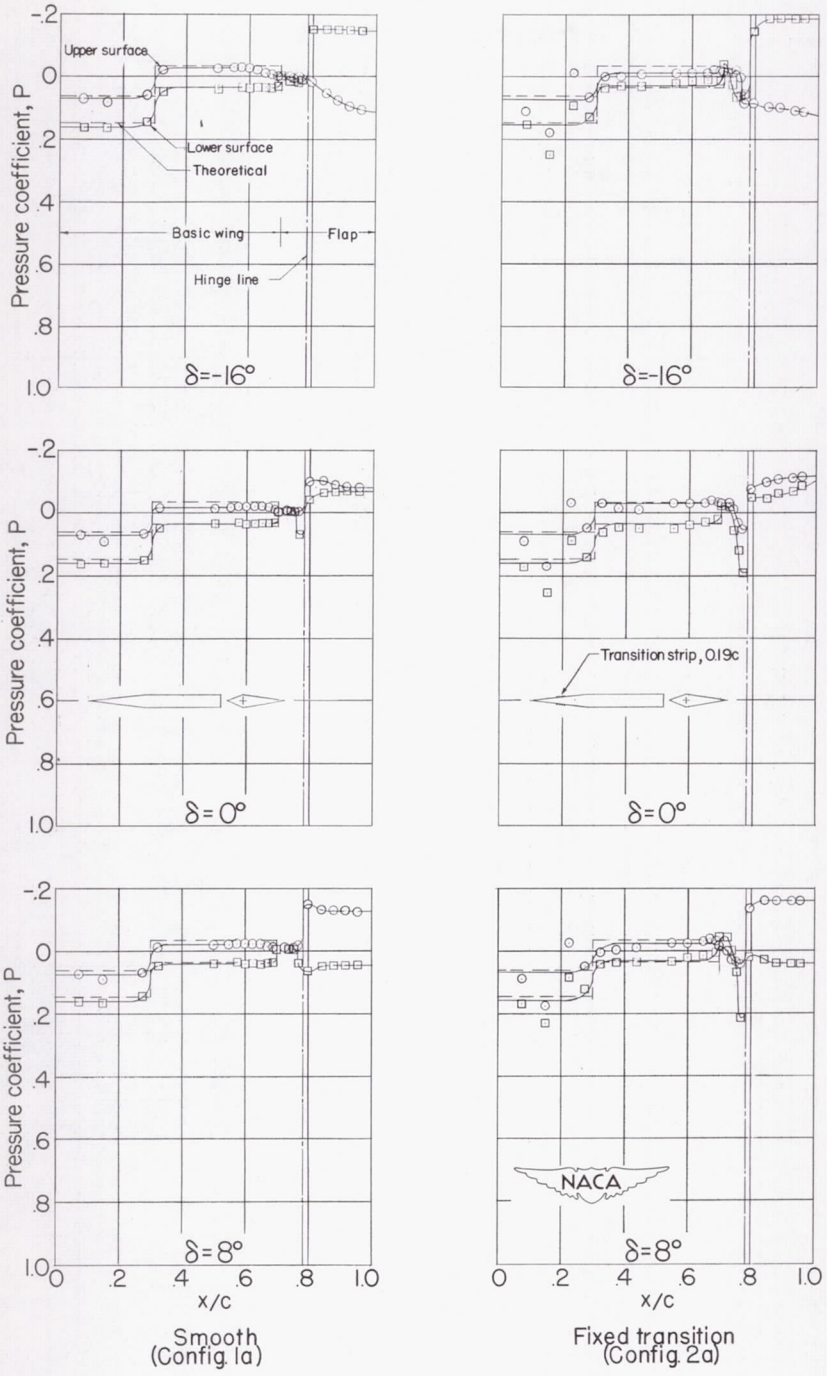
(b) $\alpha = 8^{\circ}$.

Figure 16.- Continued.



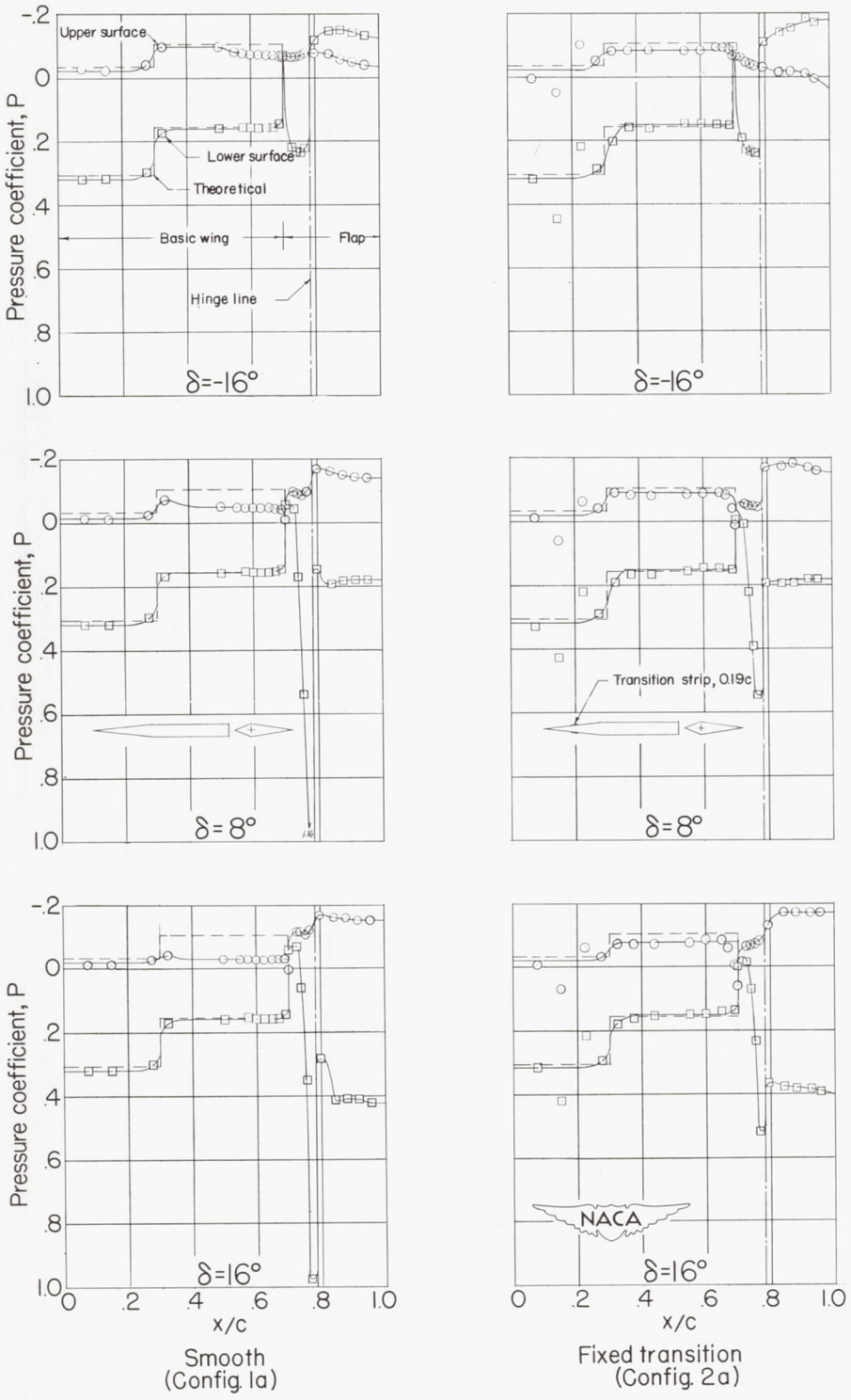
(b) Concluded.

Figure 16.- Concluded.



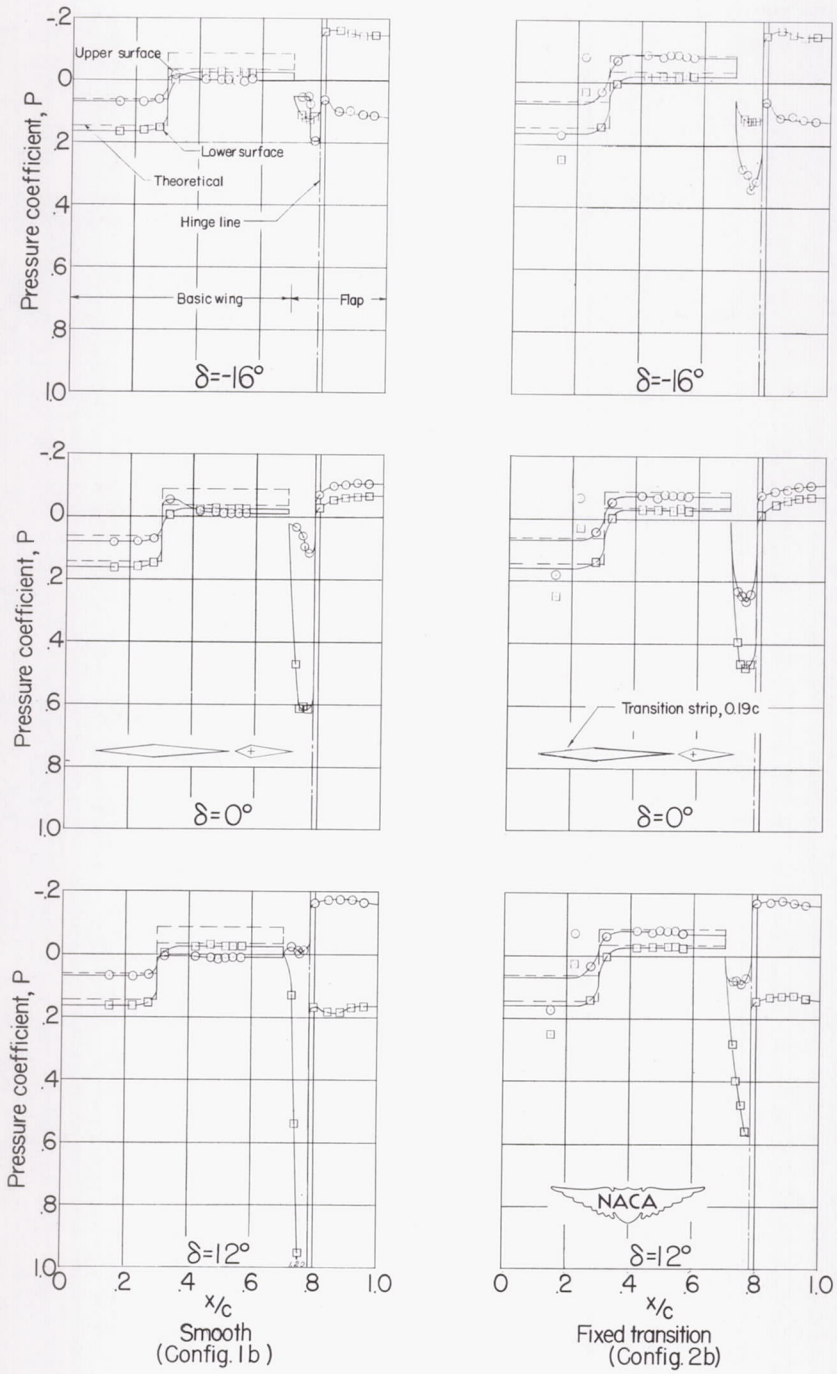
(a) $\alpha = 2^{\circ}$.

Figure 17.- Typical pressure distributions over a 6-percent-thick symmetrical wing equipped with flap-type controls showing some effects of fixed transition. $\frac{c_b}{c_f} = 0.38$; wing-flap gap size, 0.033c; basic wing 1.



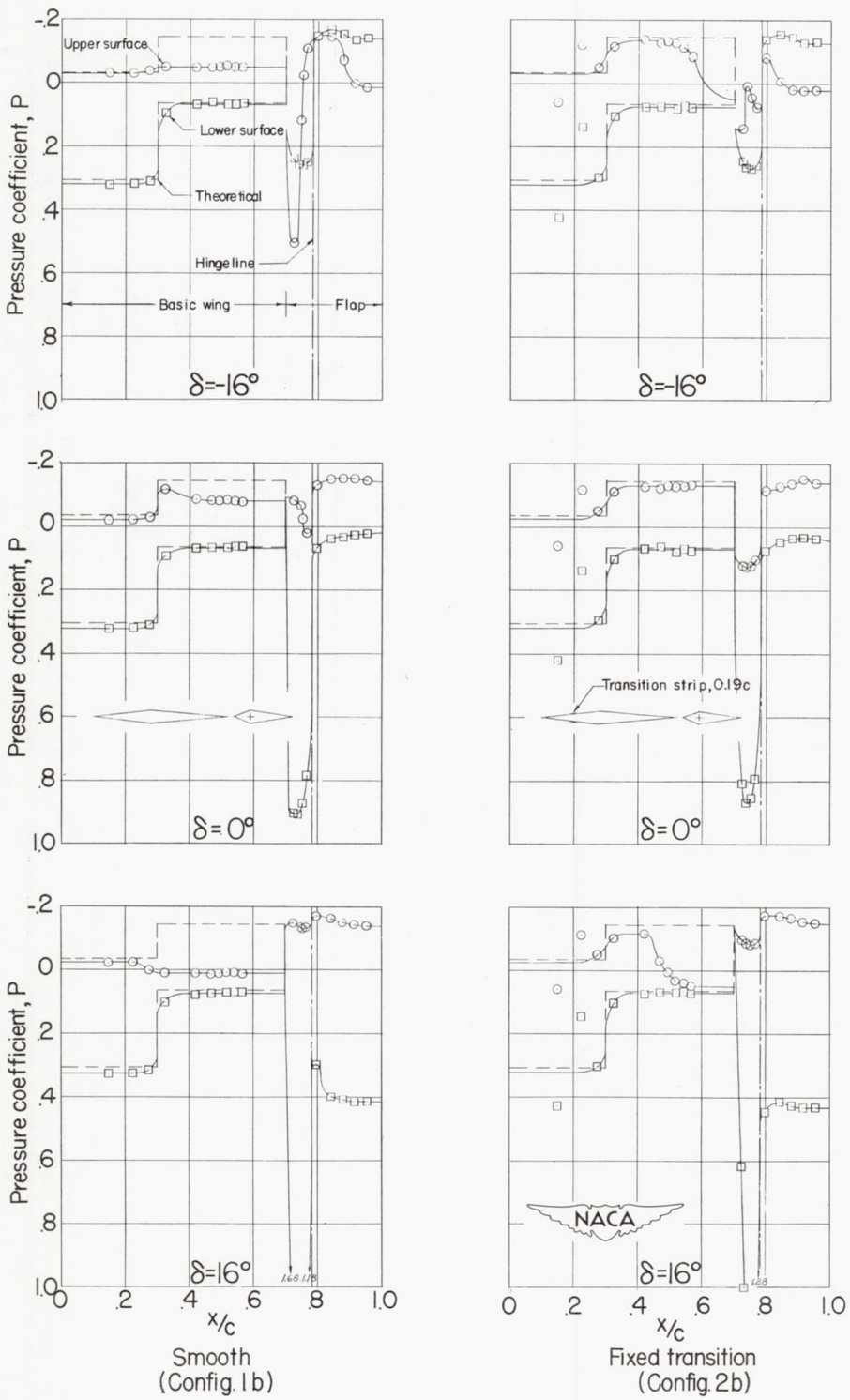
(b) $\alpha = 8^{\circ}$.

Figure 17.- Concluded.



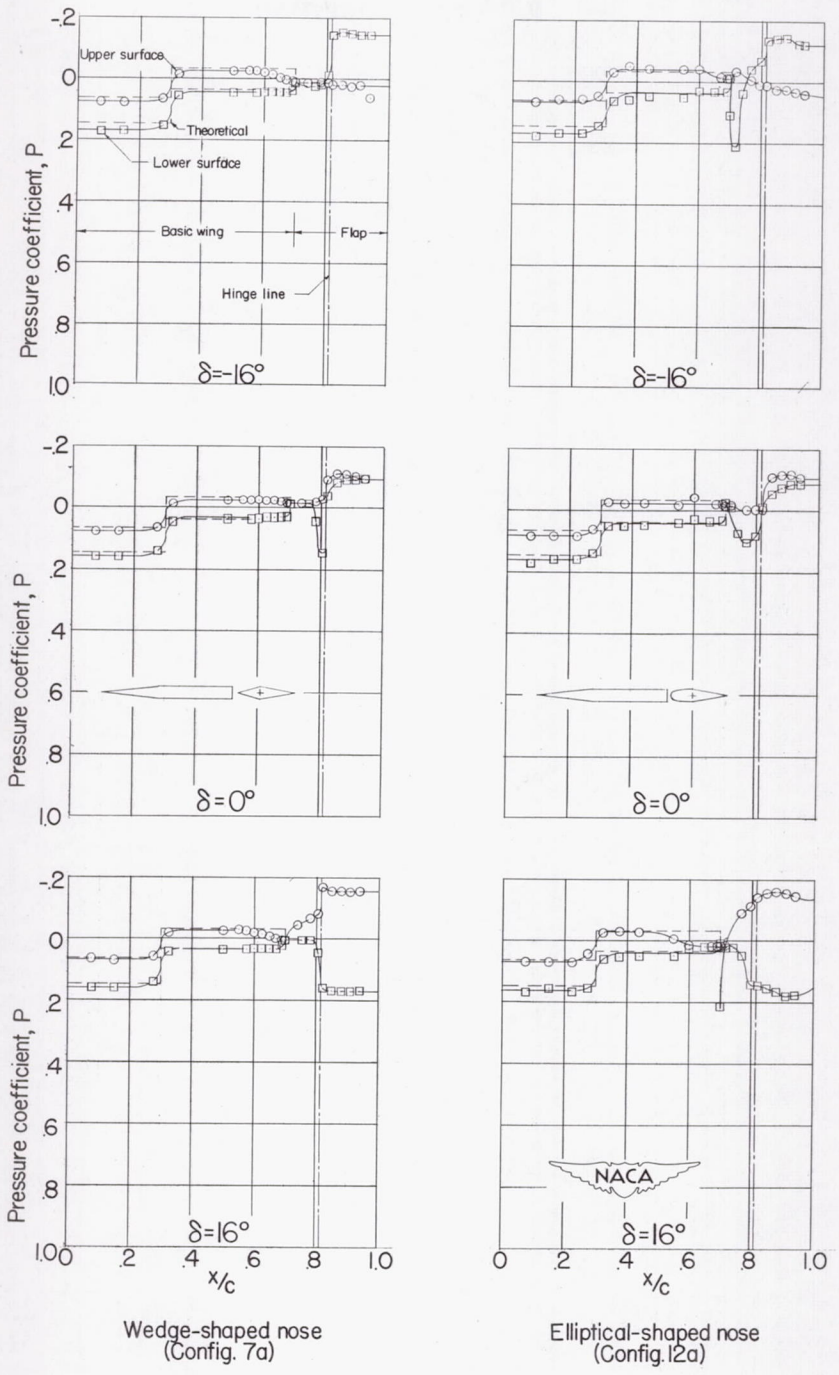
(a) $\alpha = 2^{\circ}$.

Figure 18.- Typical pressure distributions over a 6-percent-thick symmetrical wing equipped with flap-type controls showing some effects of fixed transition. $\frac{c_b}{c_f} = 0.38$; wing-flap gap size, 0.033c; basic wing 2.



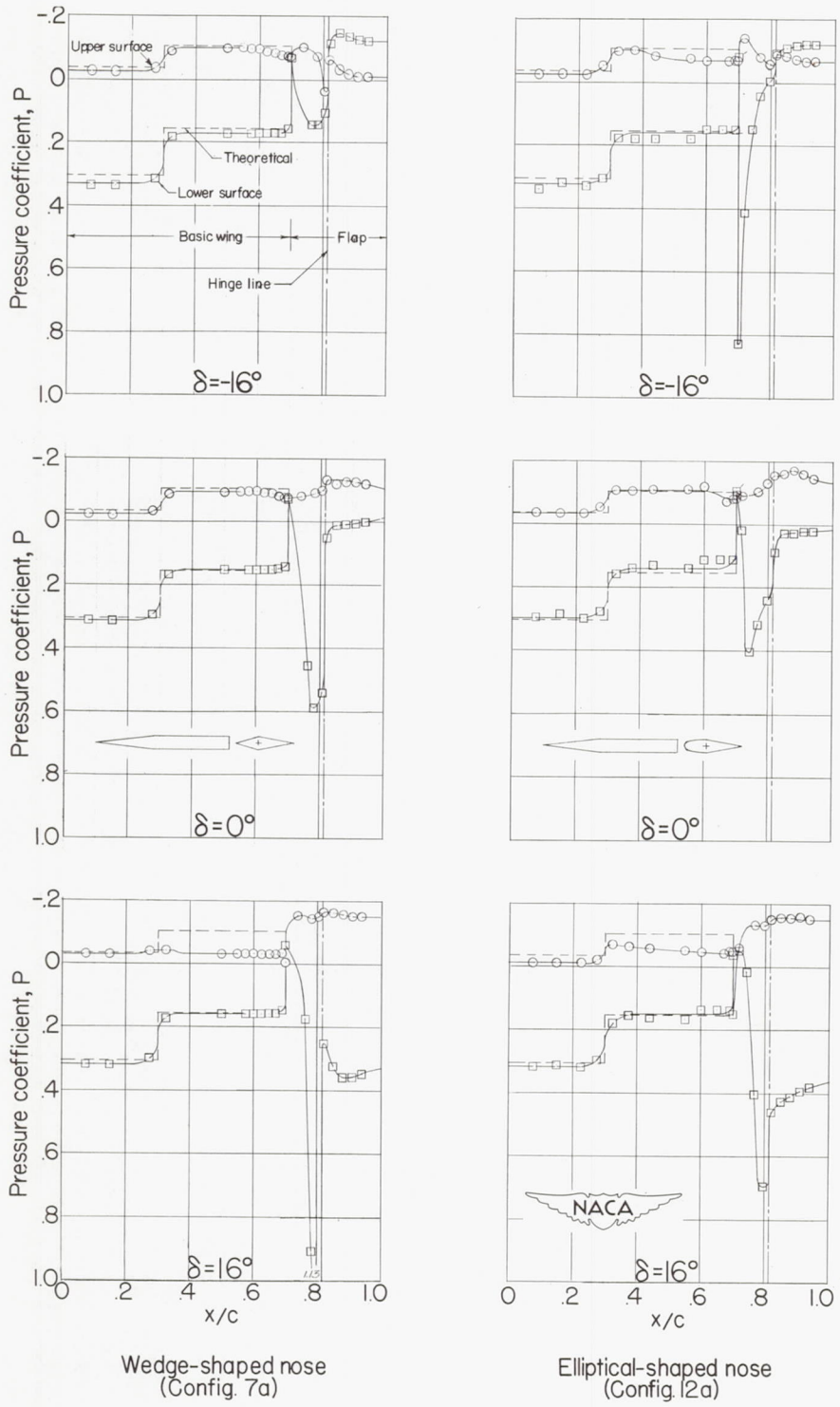
(b) $\alpha = 8^{\circ}$.

Figure 18.- Concluded.



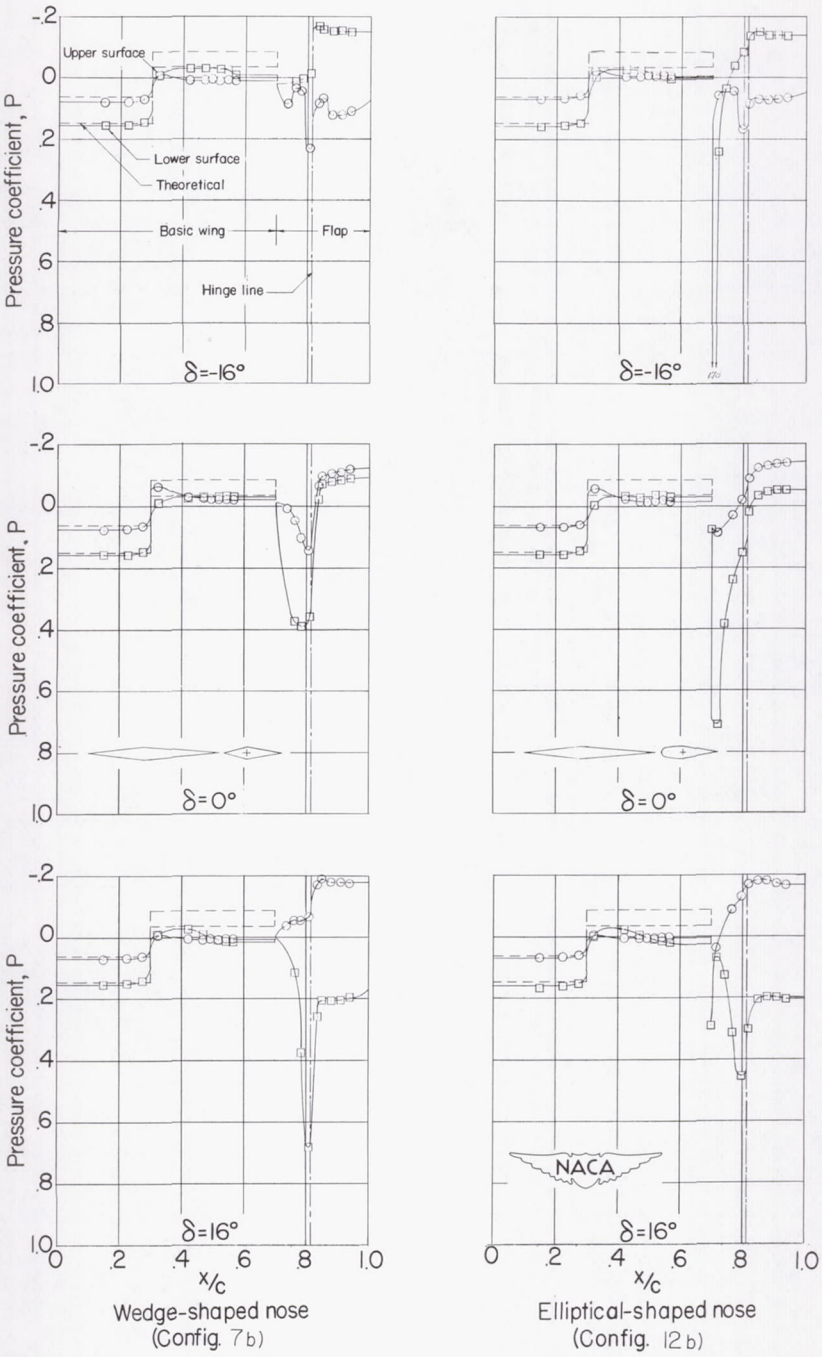
(a) $\alpha = 2^{\circ}$.

Figure 19.- Typical pressure distributions over a 6-percent-thick symmetrical wing equipped with flap-type controls showing some effects of altering the shape of the nose overhang balance. $\frac{c_b}{c_f} = 0.60$; wing-flap gap size, 0.033c; basic wing 1.



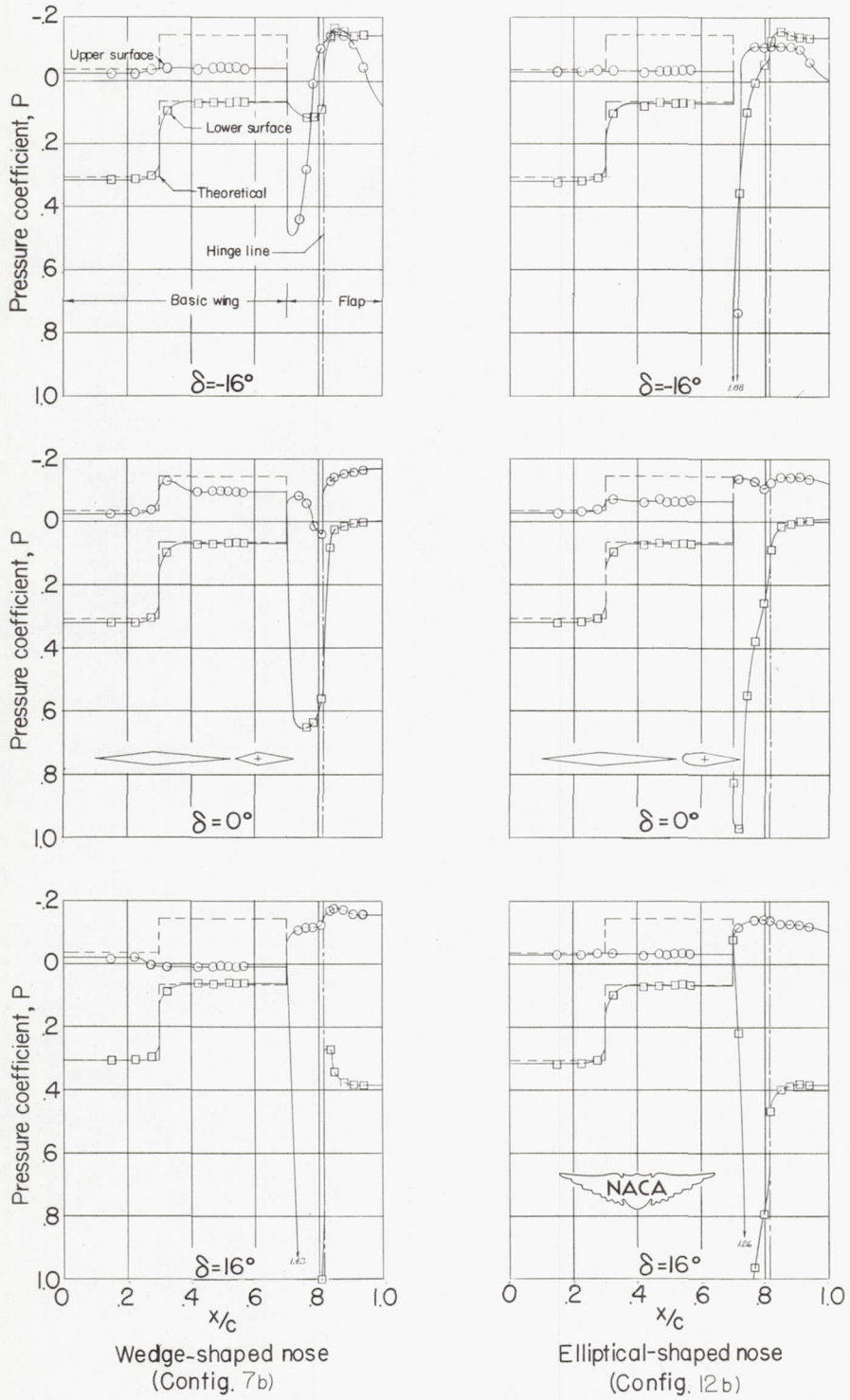
(b) $\alpha = 8°$.

Figure 19.- Concluded.



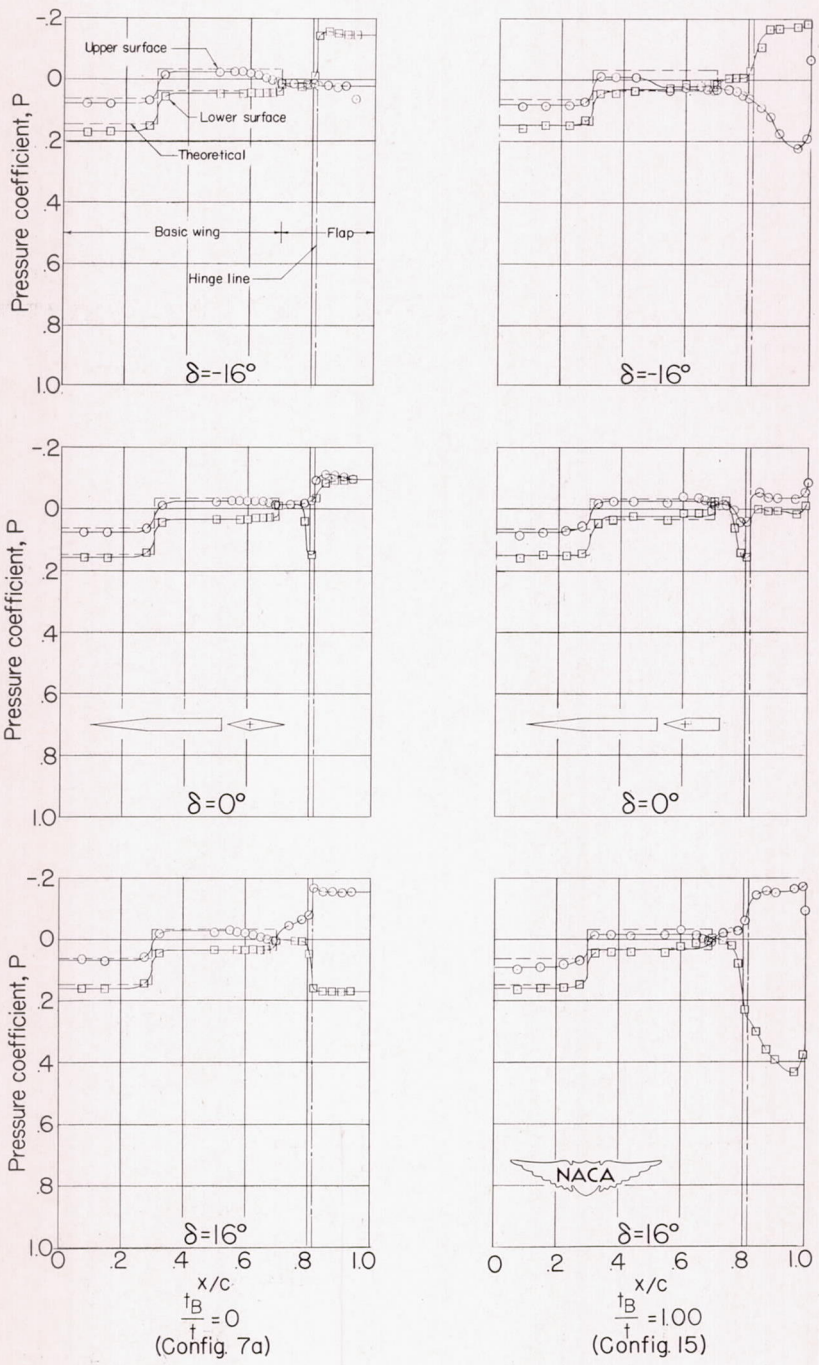
(a) $\alpha = 2^{\circ}$.

Figure 20.- Typical pressure distributions over a 6-percent-thick symmetrical wing equipped with flap-type controls showing some effects of altering the shape of the nose overhang balance. $\frac{c_b}{c_f} = 0.60$; wing-flap gap size, 0.033c; basic wing 2.



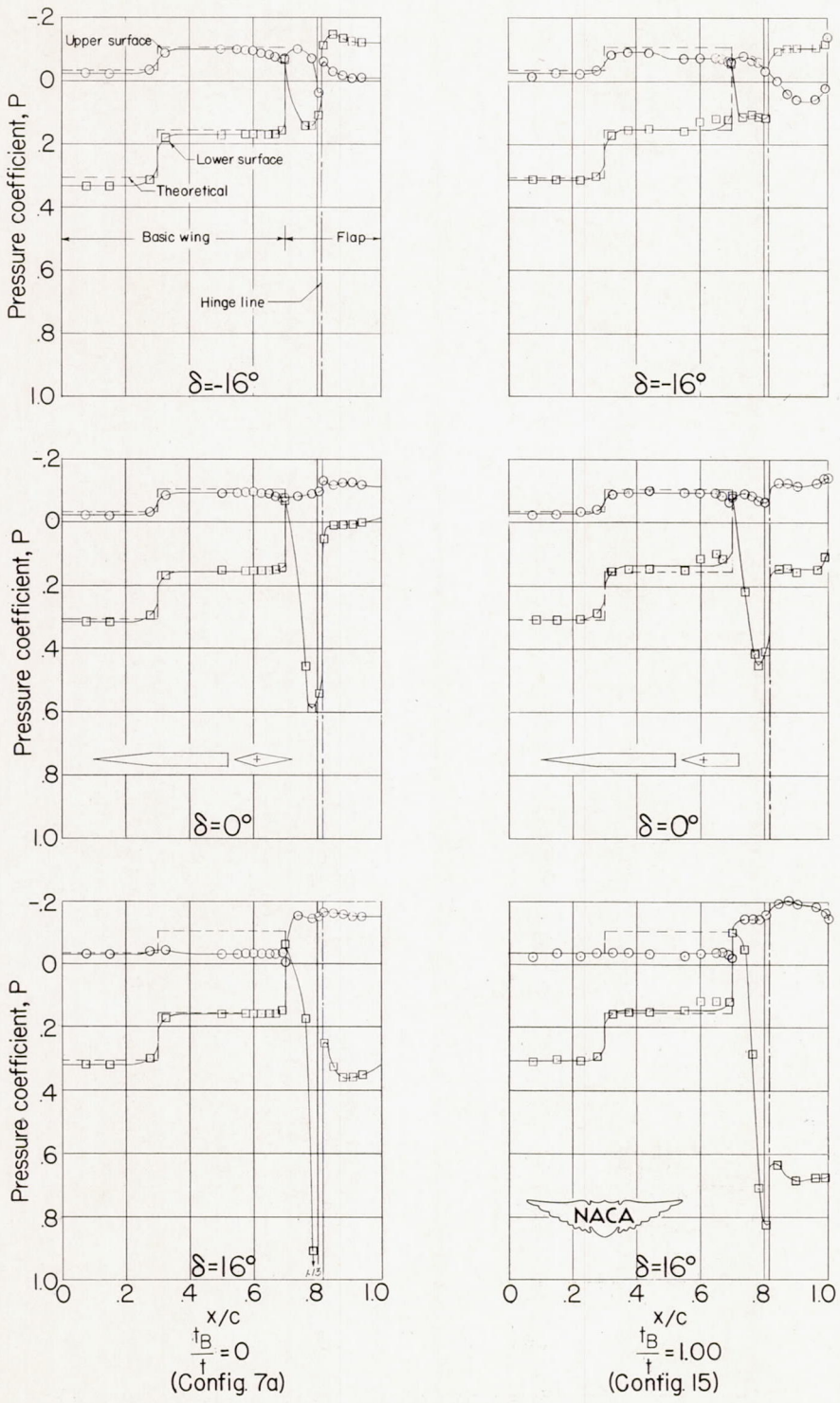
(b) $\alpha = 8^{\circ}$.

Figure 20.- Concluded.



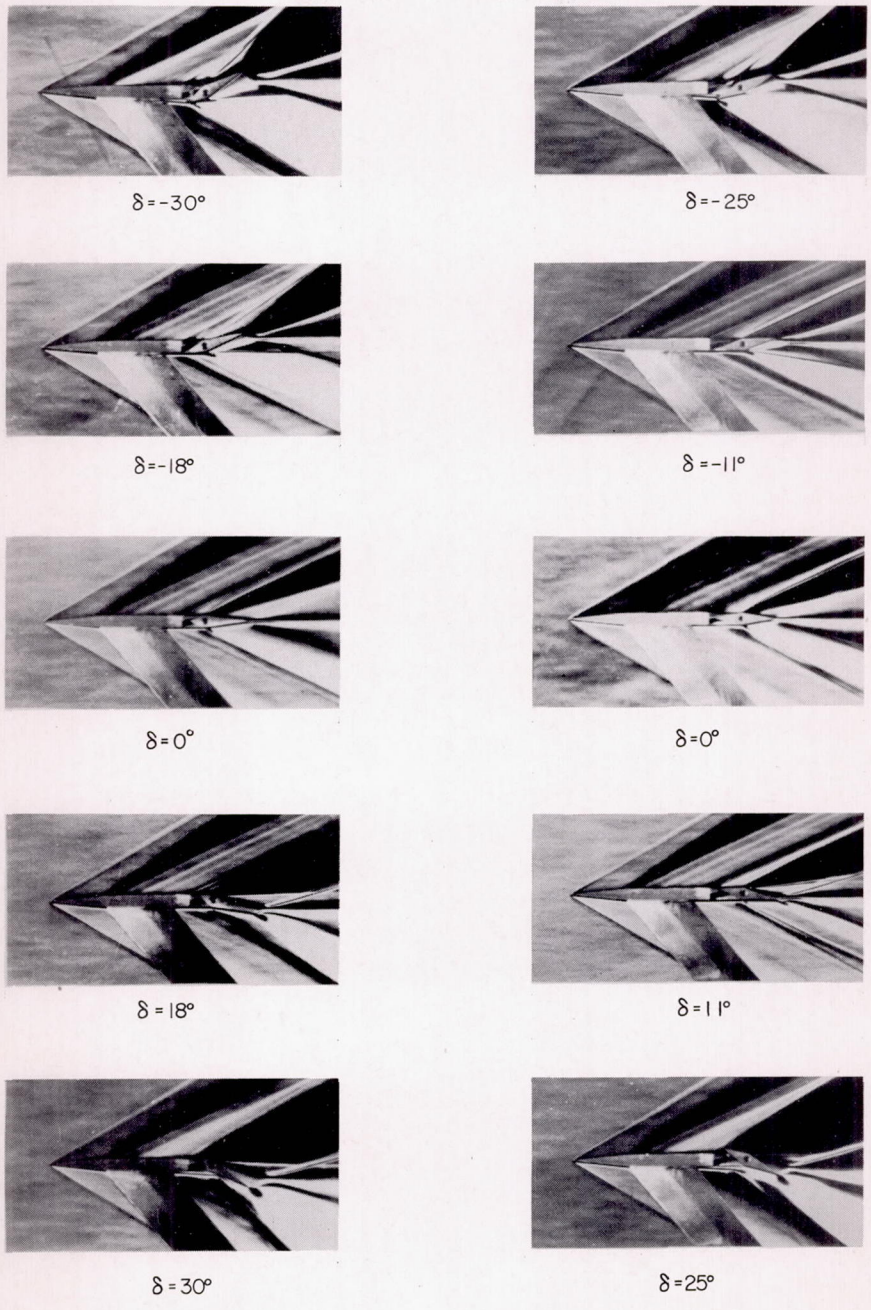
(a) $\alpha = 2^{\circ}$.

Figure 21.- Typical pressure distributions over a 6-percent-thick symmetrical wing equipped with flap-type controls showing some effects of flap trailing-edge thickness. $\frac{c_b}{c_f} = 0.60$; wing-flap gap, 0.033c; basic wing 1.



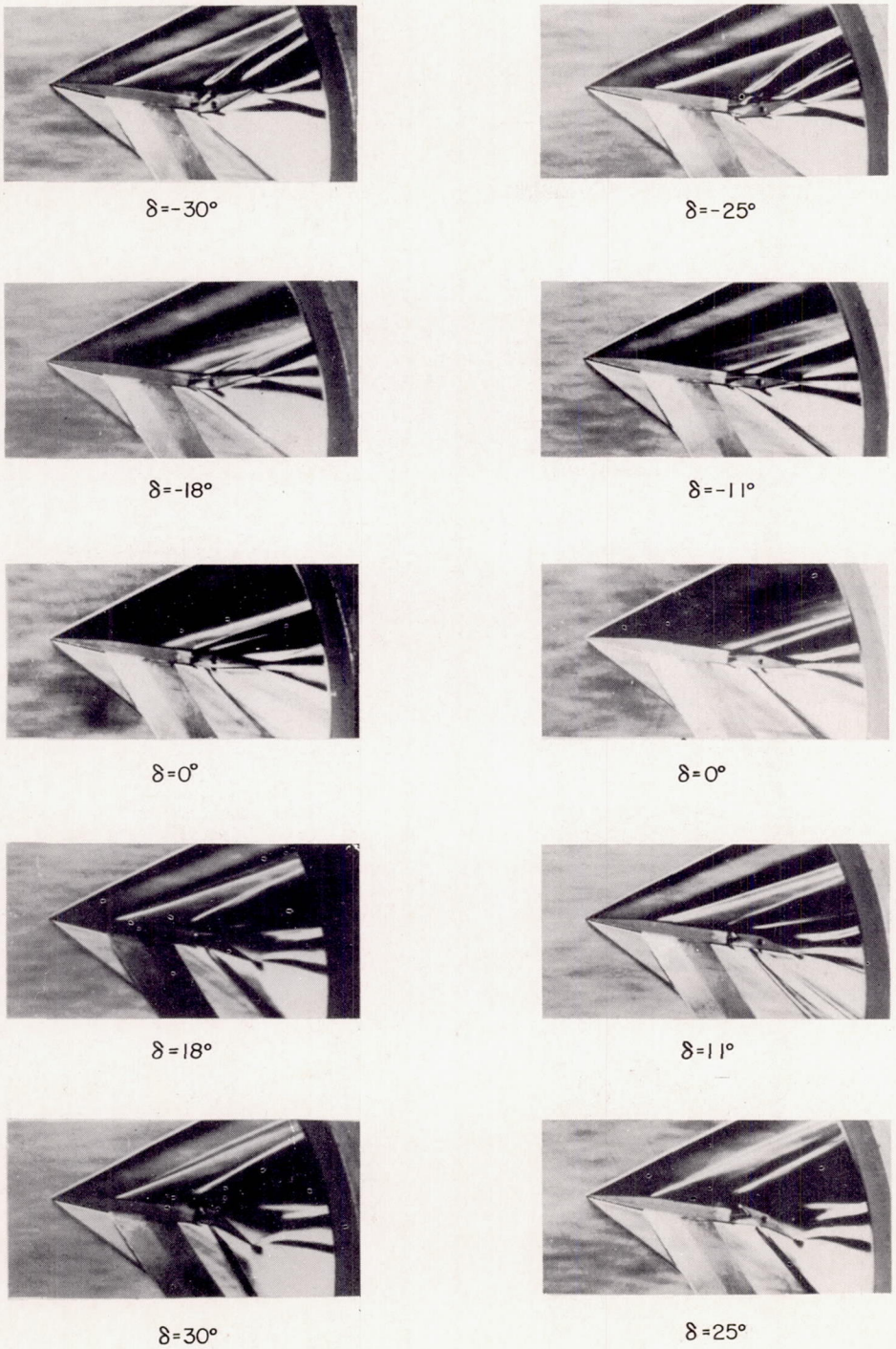
(b) $\alpha = 8^{\circ}$.

Figure 21.- Concluded.



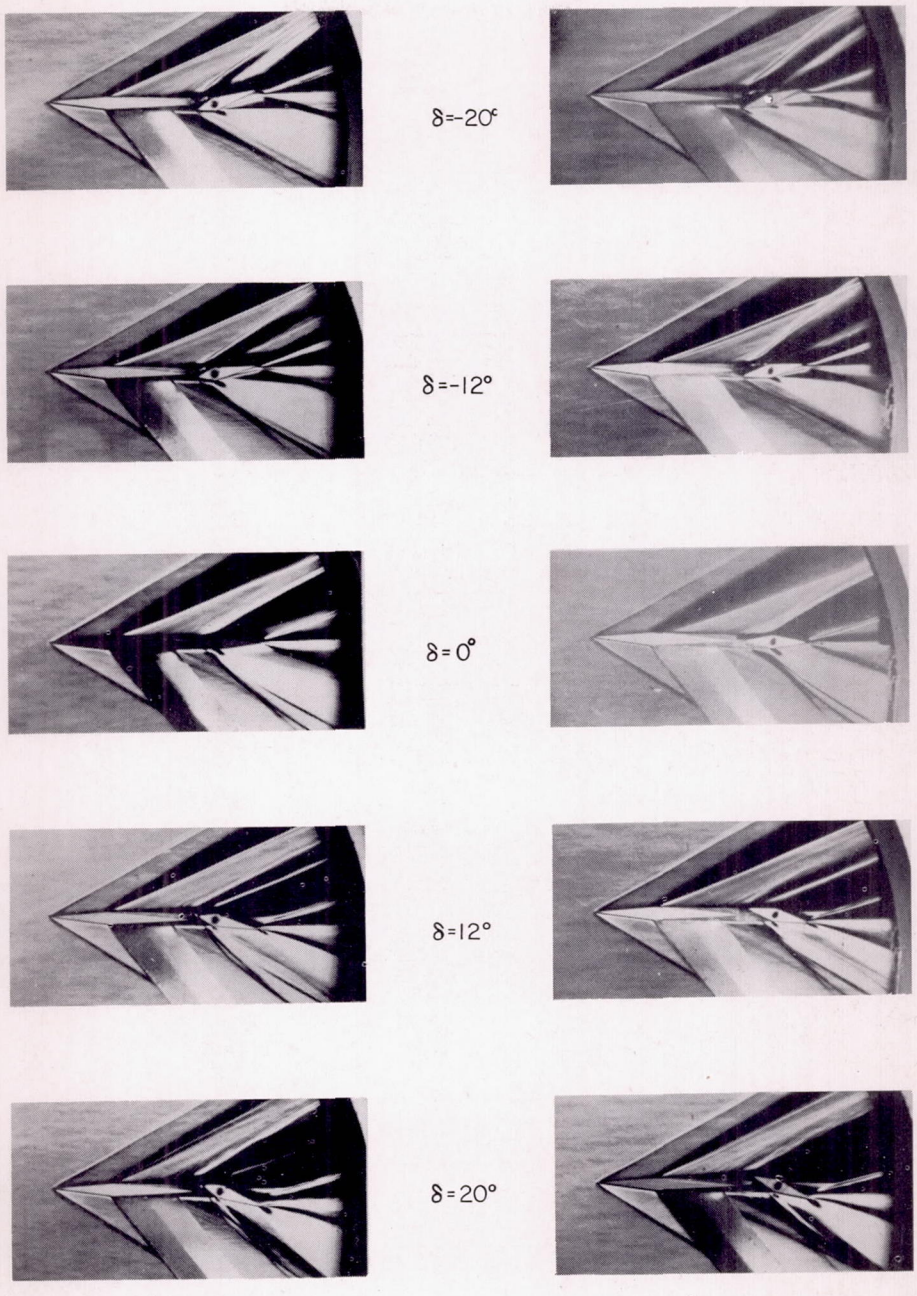
(a) $\alpha = 0^{\circ}$.

Figure 22.- Schlieren photographs of the flow over a 6-percent-thick symmetrical wing equipped with flap-type controls showing some effects of varying percent overhang nose balance. Wing-flap gap size, 0.033c; basic wing 1.



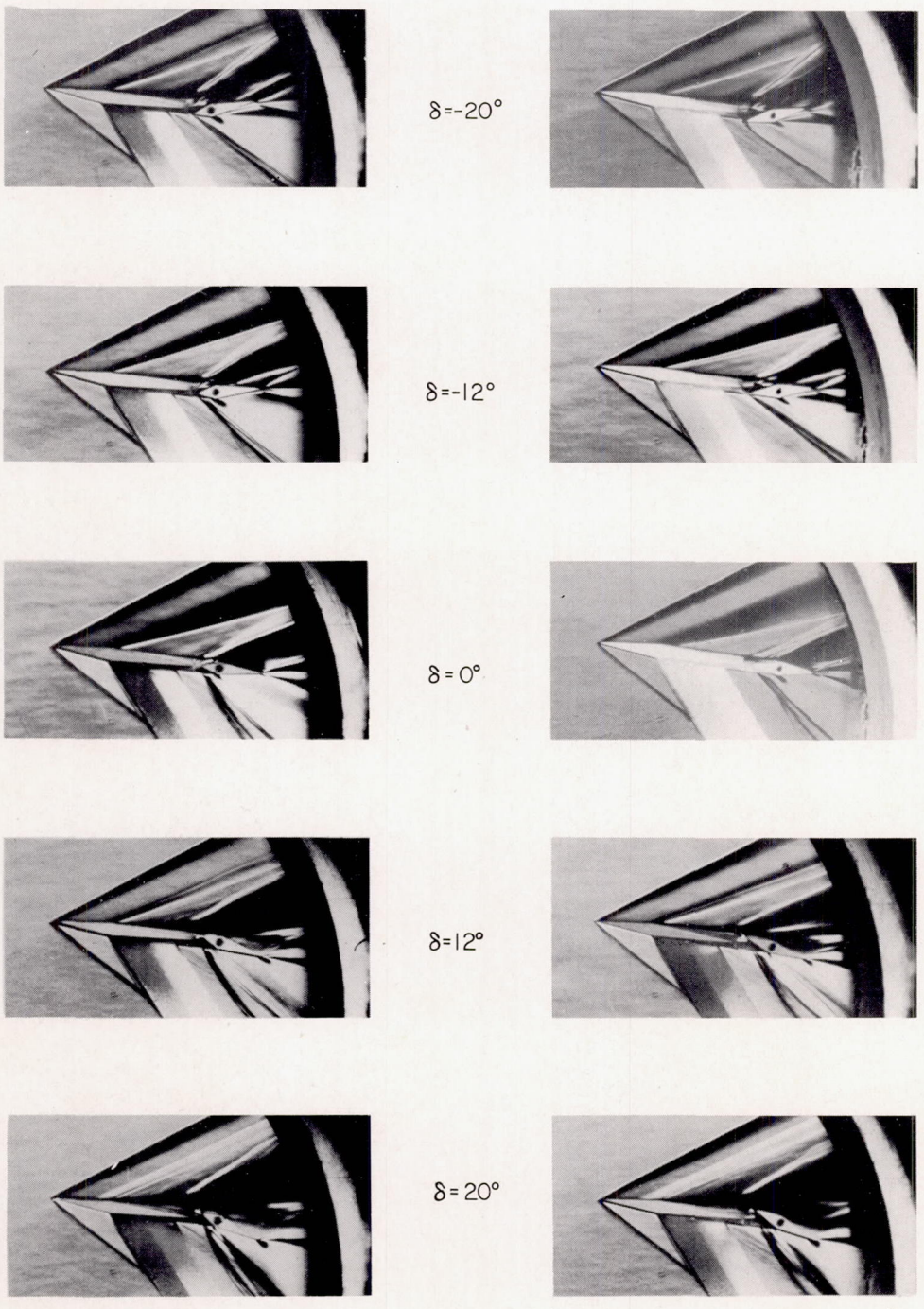
(b) $\alpha = 8^{\circ}$.

Figure 22.- Concluded.



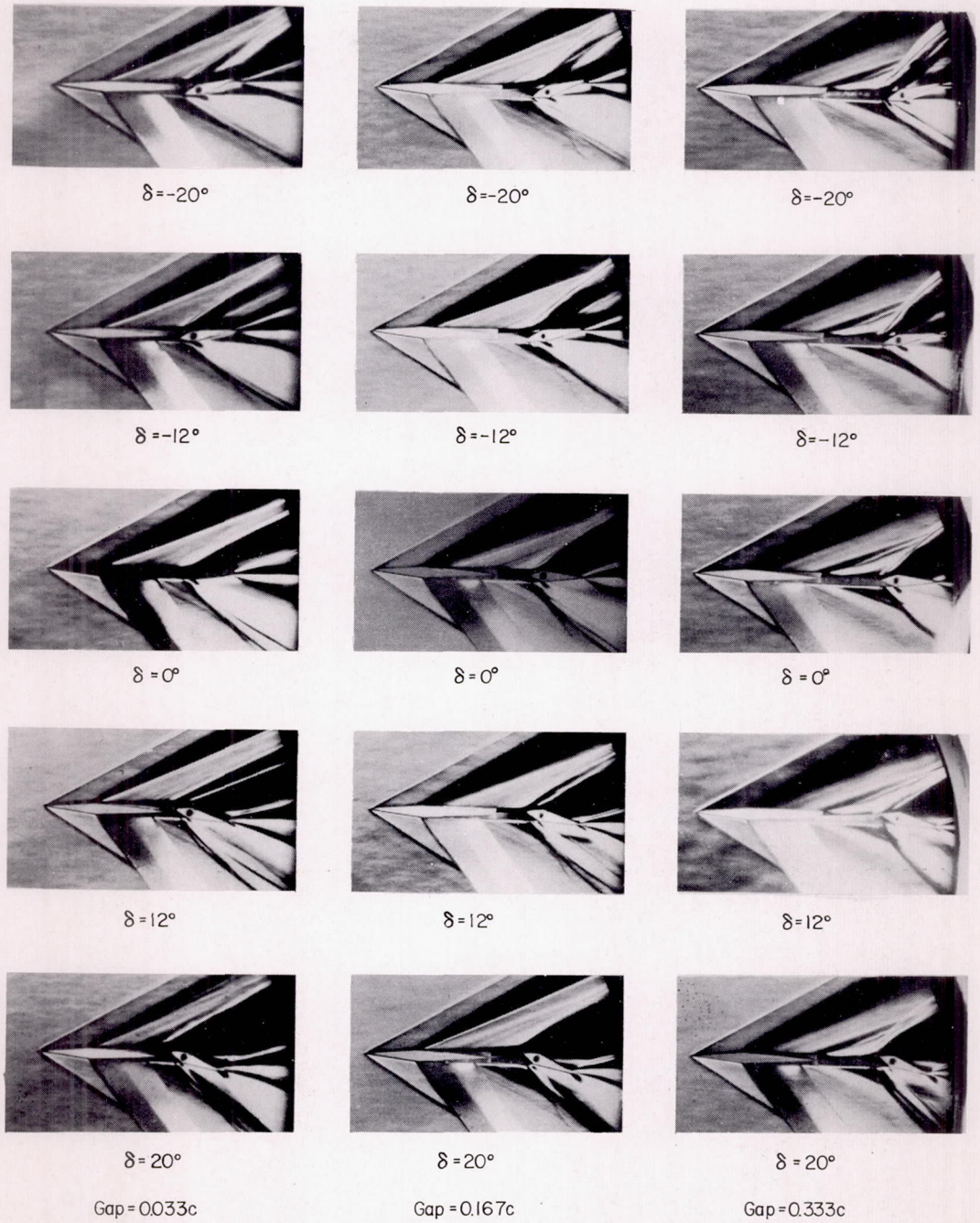
(a) $\alpha = 2^{\circ}$.

Figure 23.- Schlieren photographs of the flow over a 6-percent-thick symmetrical wing equipped with flap-type controls showing some effects of varying percent overhang nose balance. Wing-flap gap size, 0.033c; basic wing 2.



(b) $\alpha = 8^{\circ}$.

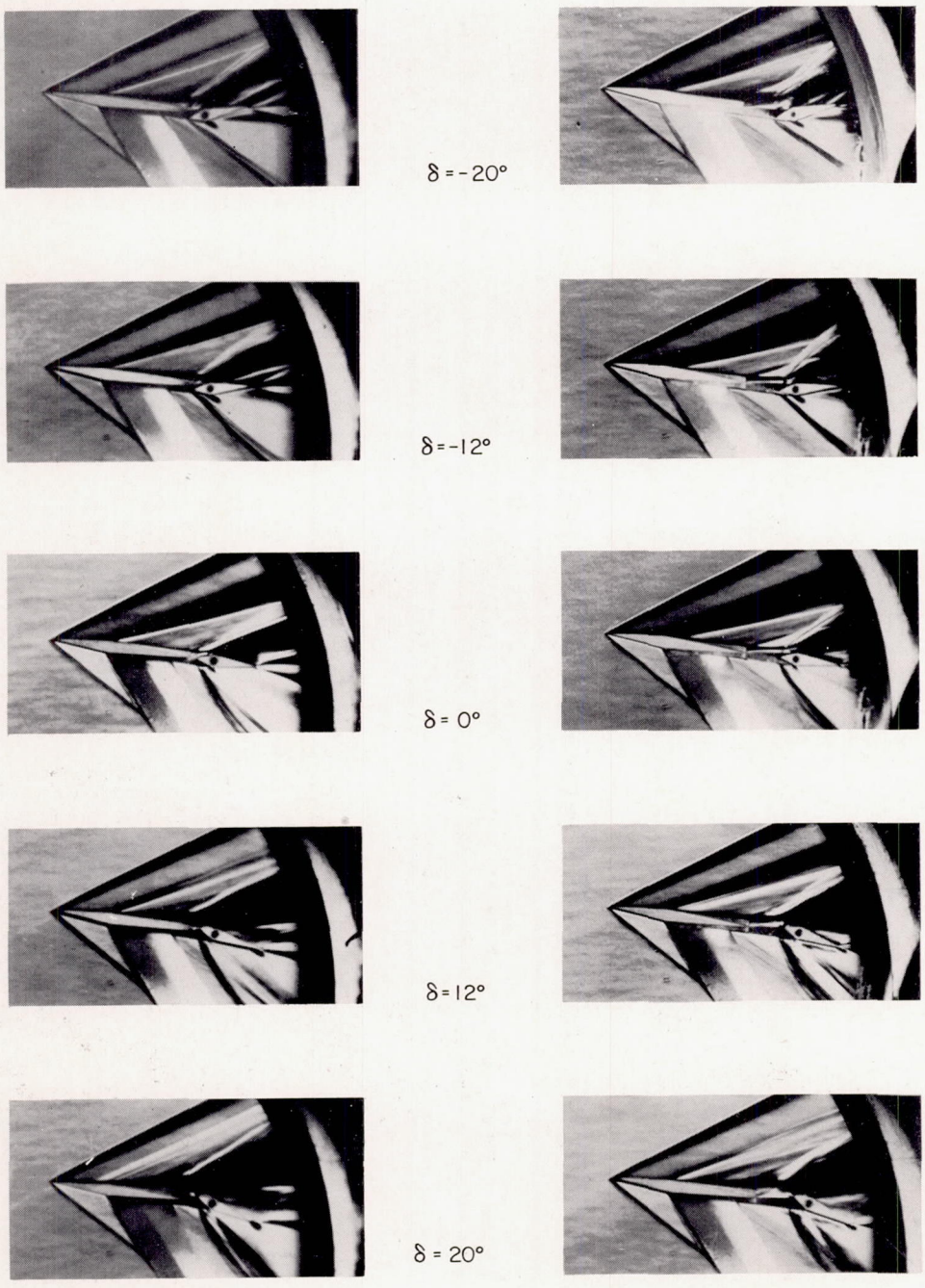
Figure 23.- Concluded.



L-81220

(a) $\alpha = 2^{\circ}$.

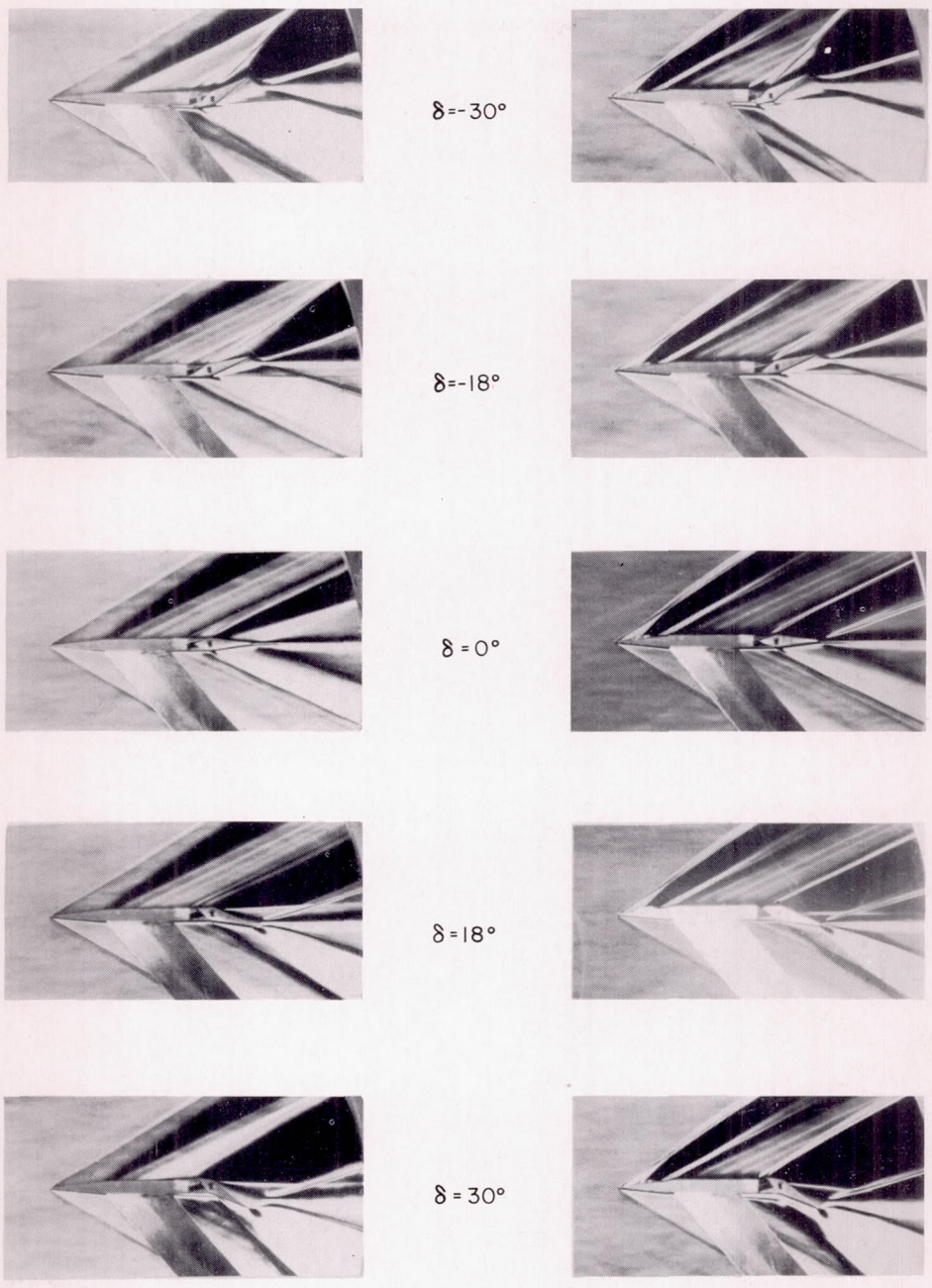
Figure 24.- Schlieren photographs of the flow over a 6-percent-thick symmetrical wing equipped with flap-type controls showing some effects of varying the size of the wing-flap gap. $\frac{c_b}{c_f} = 0.38$; basic wing 2.



L-81221

(b) $\alpha = 8^{\circ}$.

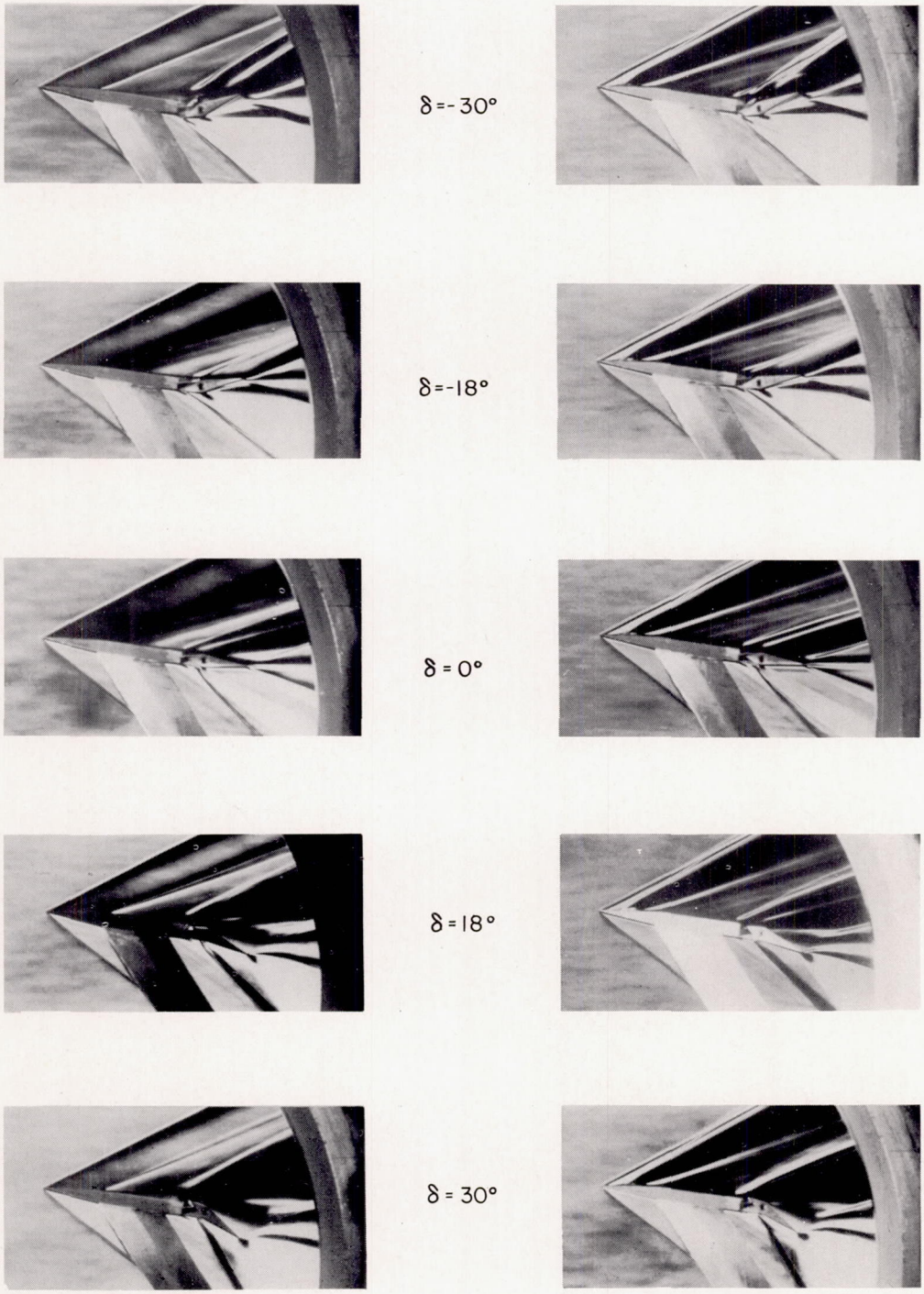
Figure 24.- Concluded.



L-81222

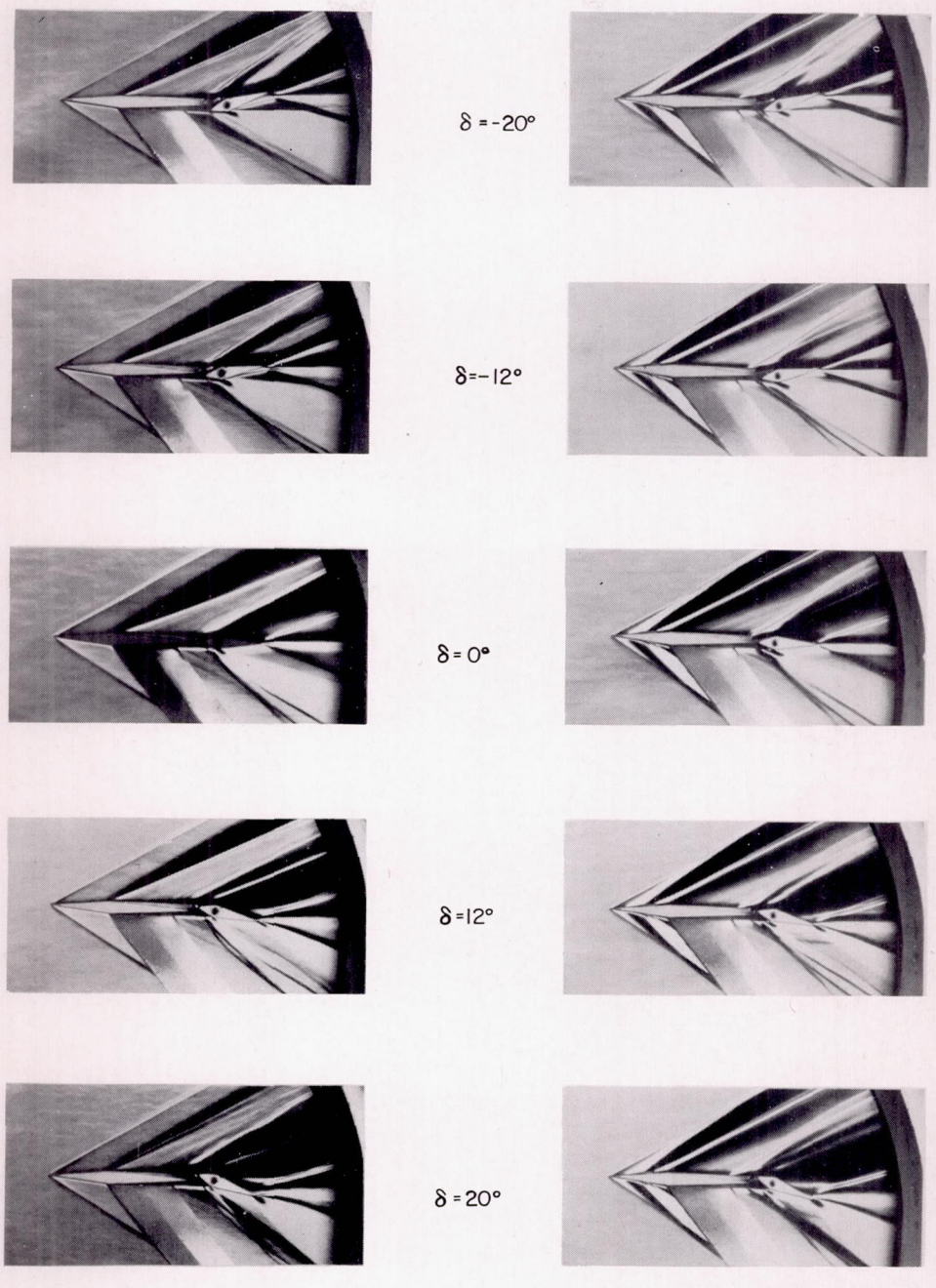
(a) $\alpha = 0^{\circ}$.

Figure 25.- Schlieren photographs of the flow over a 6-percent-thick symmetrical wing equipped with flap-type controls showing some effects of fixed transition. Wing-flap gap size, 0.033c; $\frac{c_b}{c_f} = 0.38$; basic wing 1.



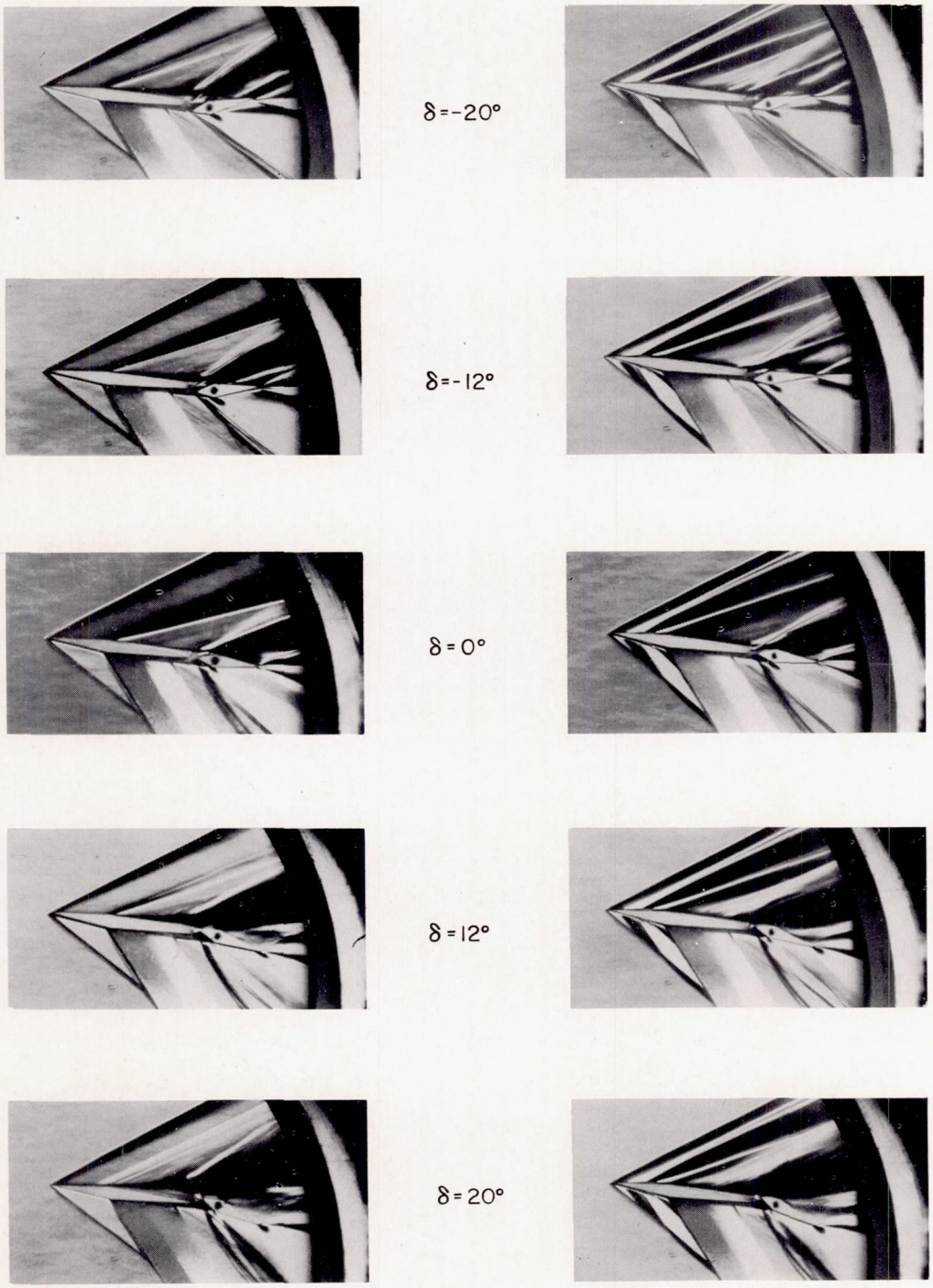
(b) $\alpha = 8^{\circ}$.

Figure 25.- Concluded.



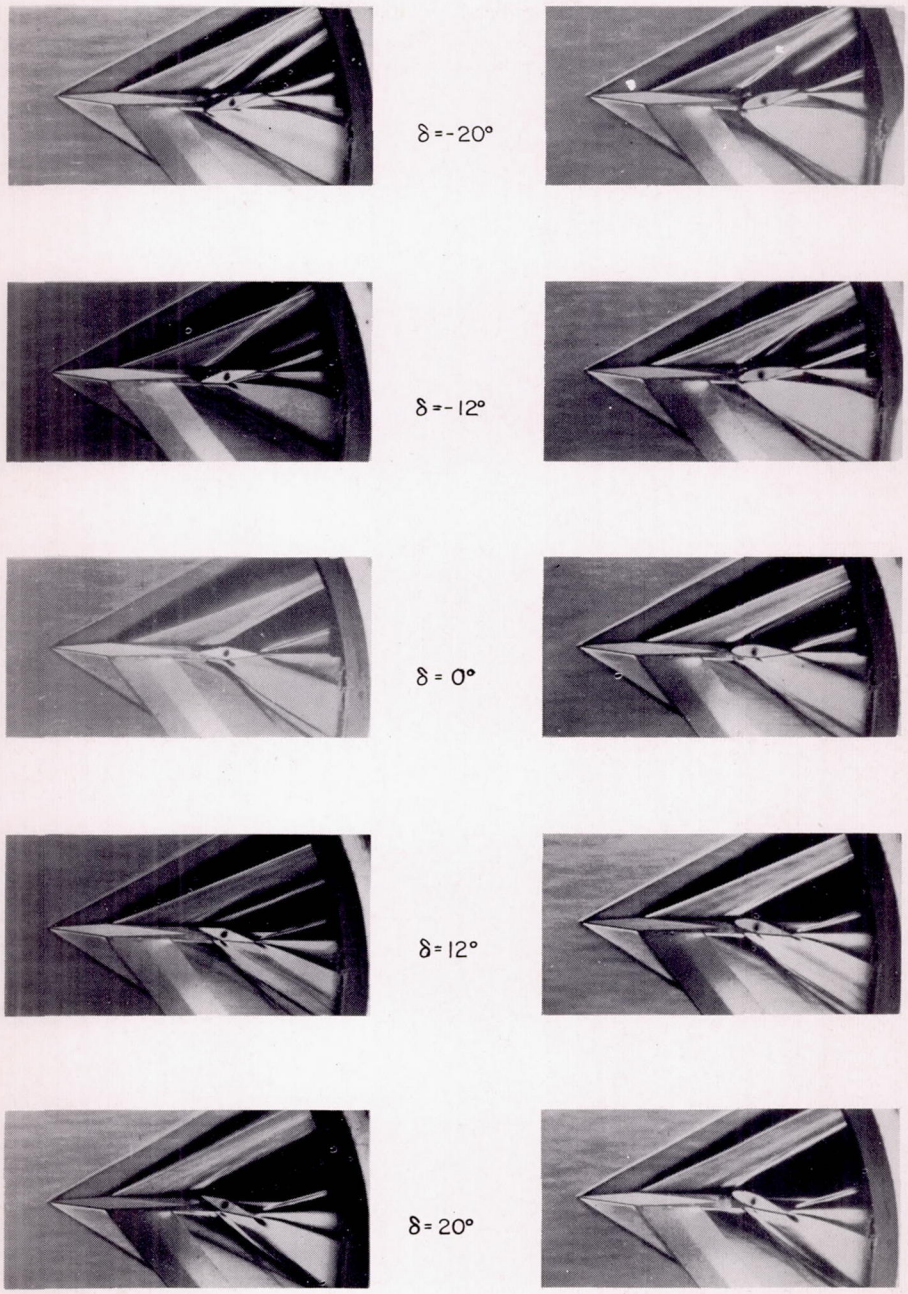
(a) $\alpha = 2^{\circ}$.

Figure 26.- Schlieren photographs of the flow over a 6-percent-thick symmetrical wing equipped with flap-type controls showing some effects of fixed transition: Wing-flap gap size, 0.033c; $\frac{c_b}{c_f} = 0.38$; basic wing 2.



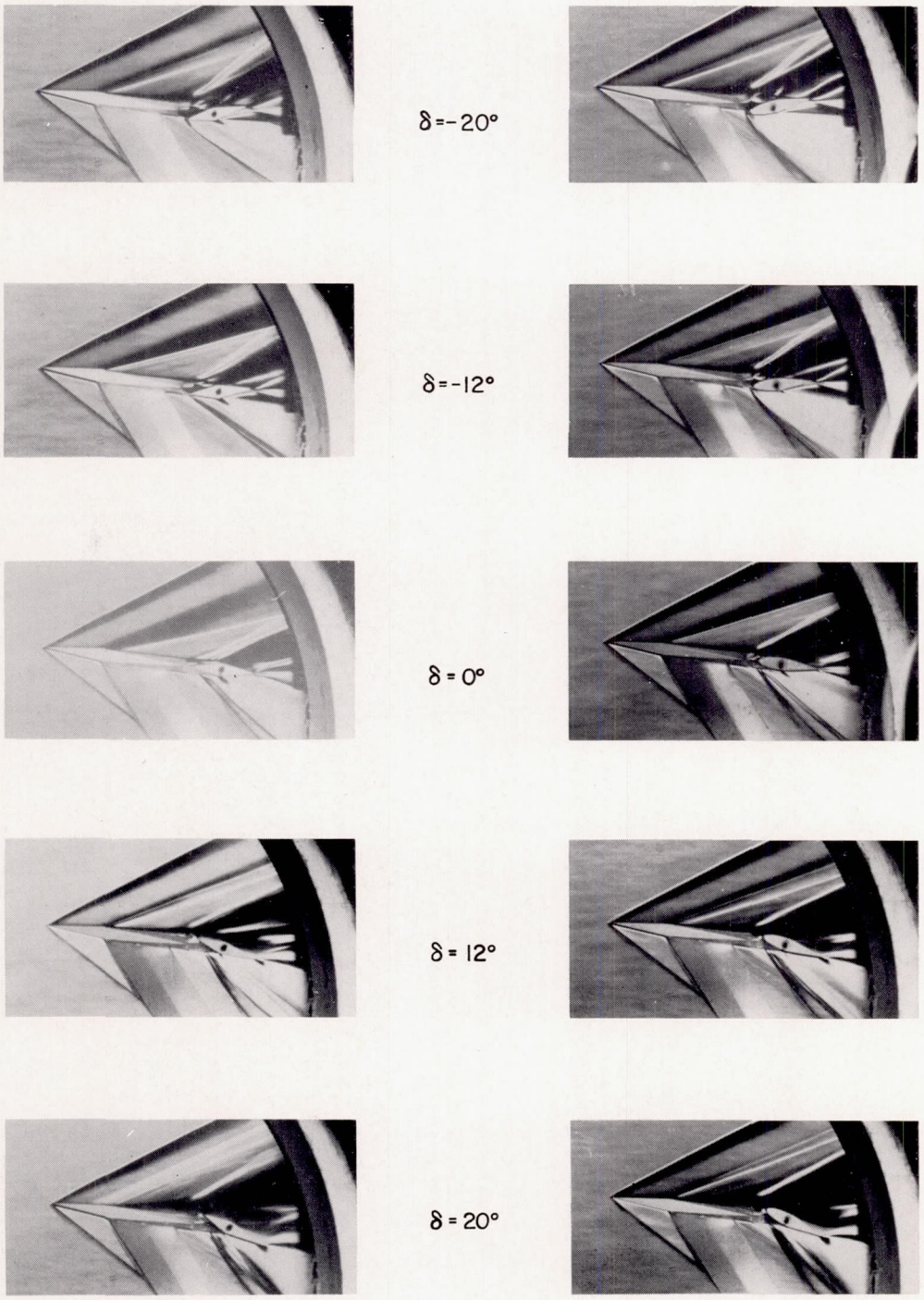
(b) $\alpha = 8^{\circ}$.

Figure 26.- Concluded.



(a) $\alpha = 2^{\circ}$.

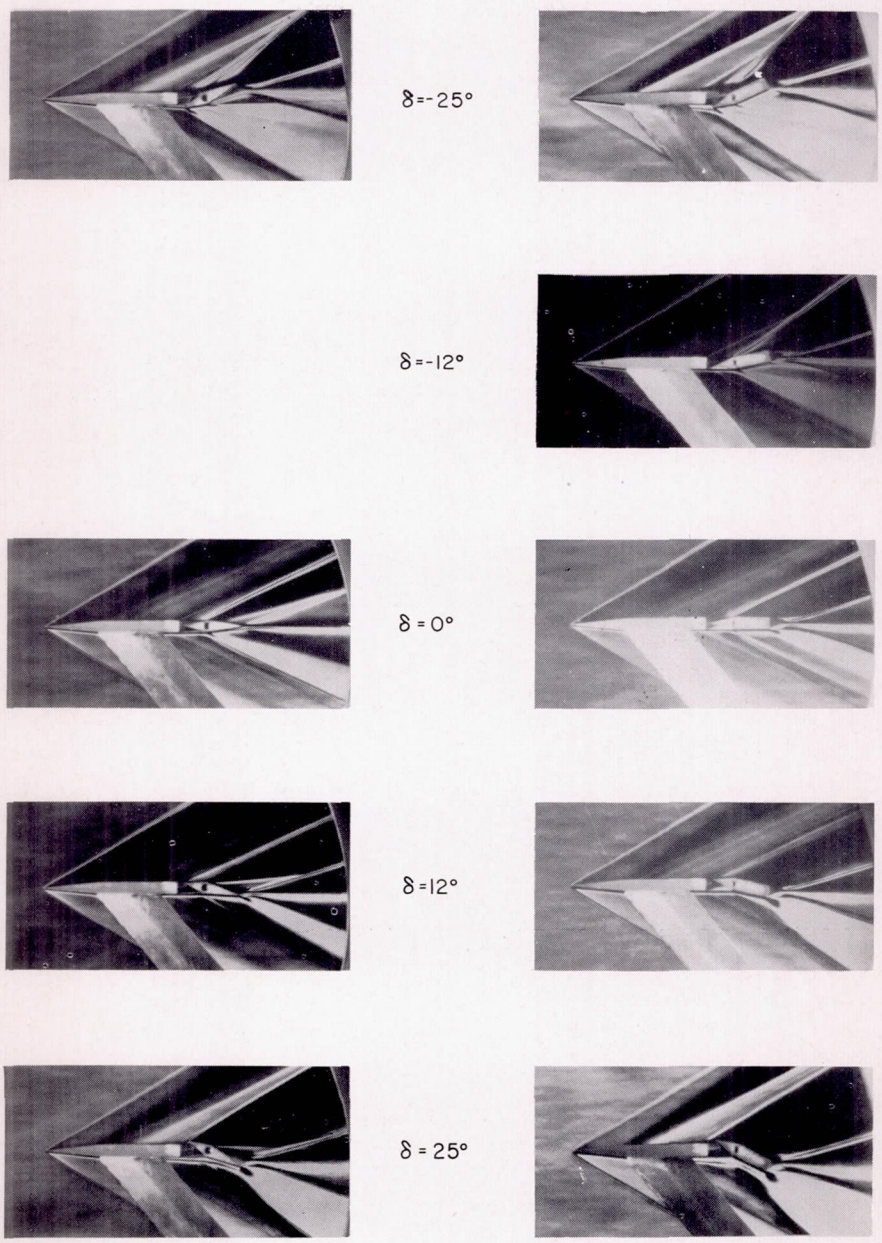
Figure 27.- Schlieren photographs of the flow over a 6-percent-thick symmetrical wing equipped with trailing-edge controls showing some effects of altering the shape of the nose overhang balance. Wing-flap gap size, 0.033c; $\frac{c_b}{c_f} = 0.60$; basic wing 2.



(b) $\alpha = 8^{\circ}$.

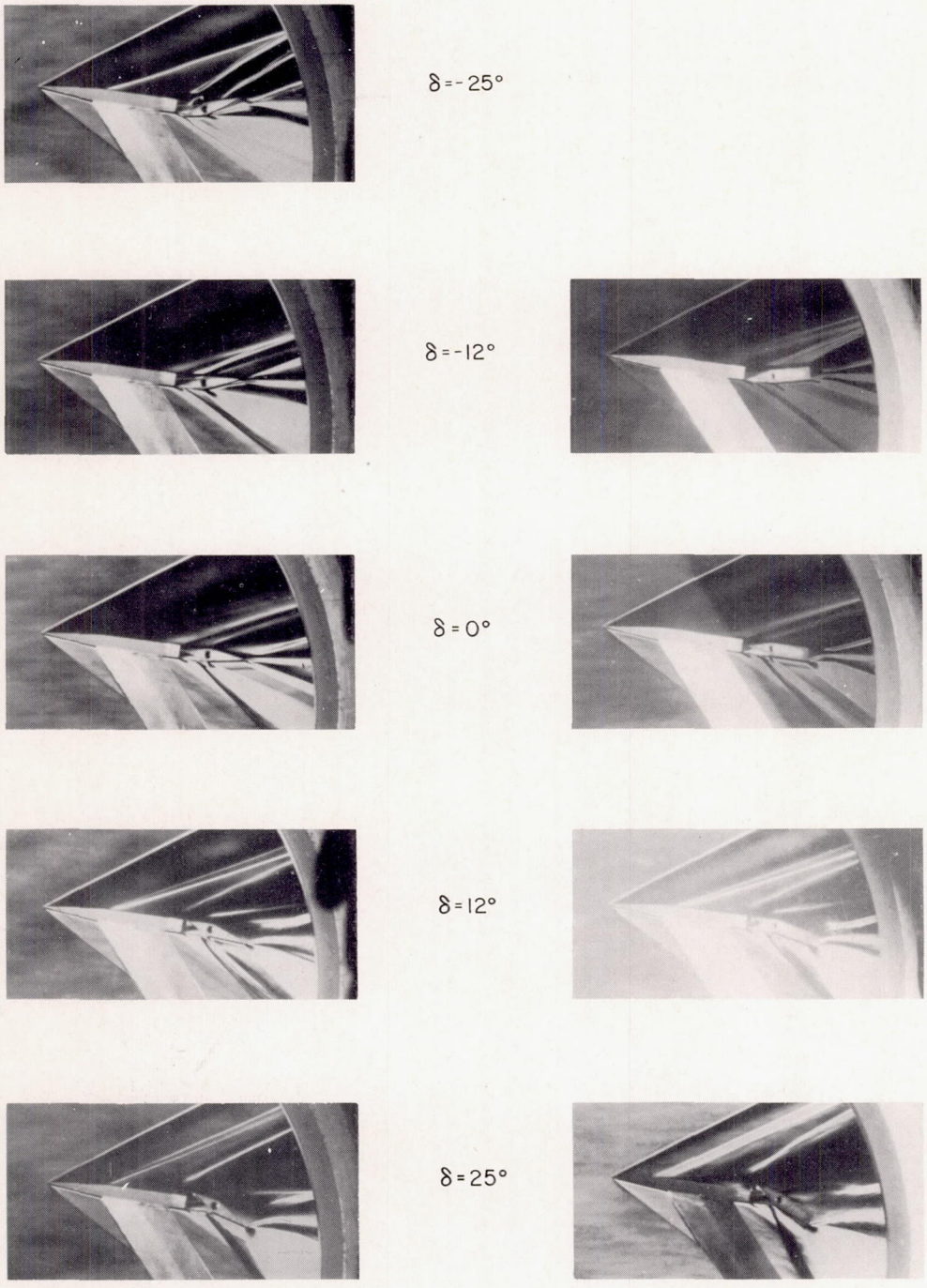
L-81227

Figure 27.- Concluded.



(a) $\alpha = 0^{\circ}$.

Figure 28.- Schlieren photographs of the flow over a 6-percent-thick symmetrical wing equipped with trailing-edge controls showing some effects of varying flap trailing-edge thickness. Wing-flap gap size, 0.033c; $\frac{c_b}{c_f} = 0.60$; basic wing 1.



(b) $\alpha = 8^{\circ}$.

L-81229

Figure 28.- Concluded.

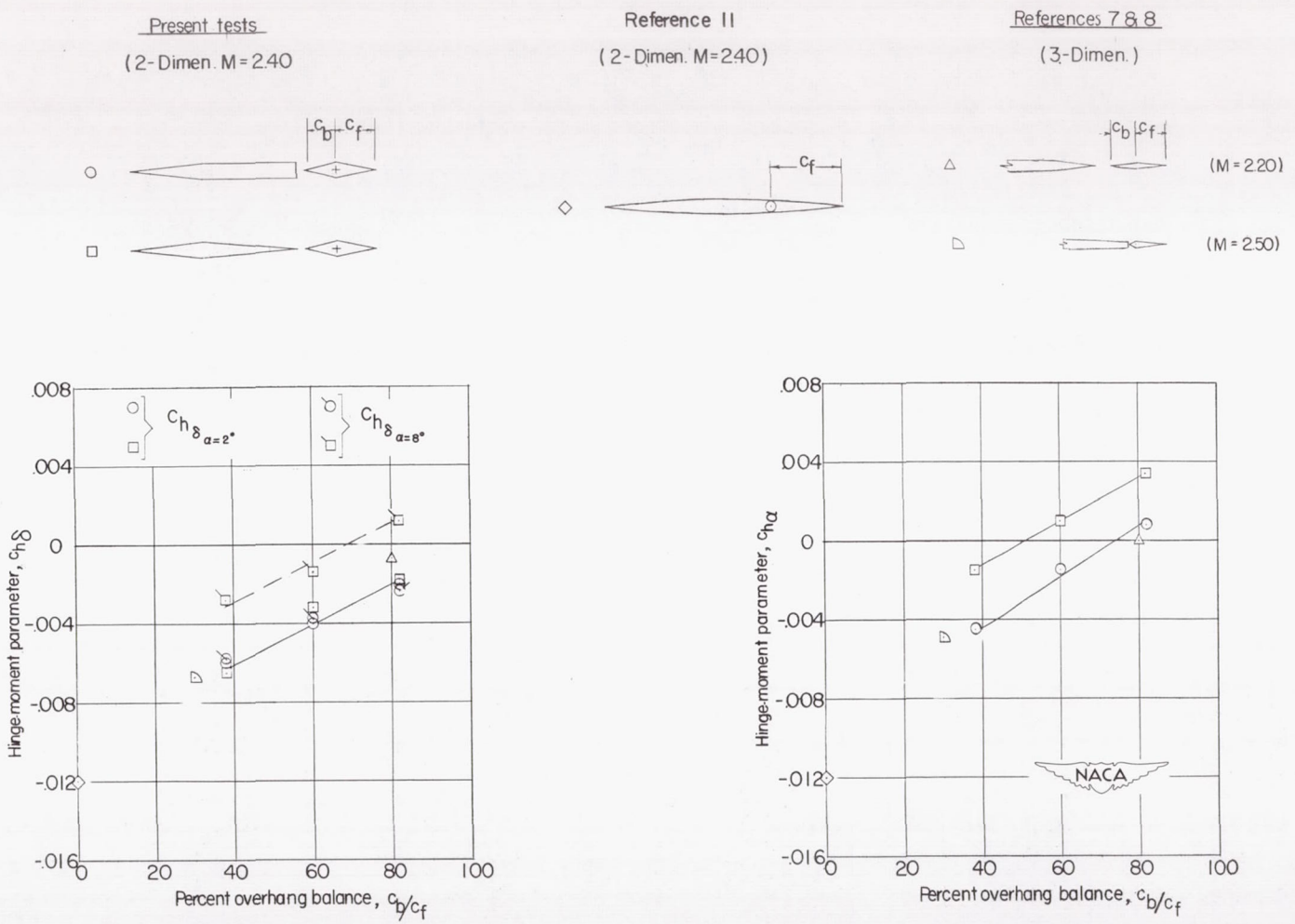
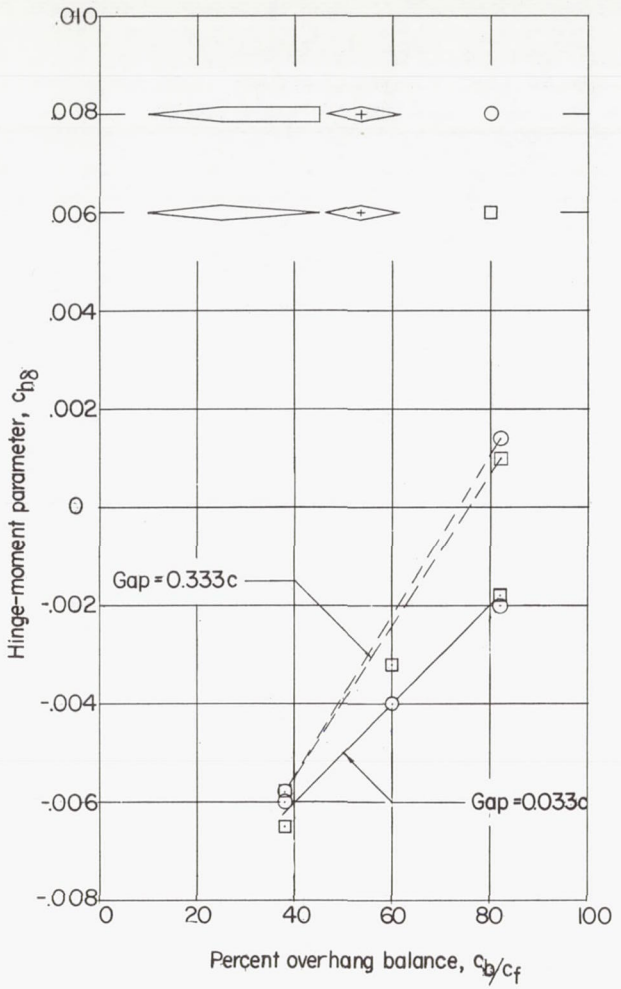


Figure 29.- Comparisons of hinge-moment parameters, c_{h_δ} and c_{h_α}, of basic wing 1 and basic wing 2 equipped with flaps having various amounts of flap-nose overhang. Wing-flap gap size, 0.033c.



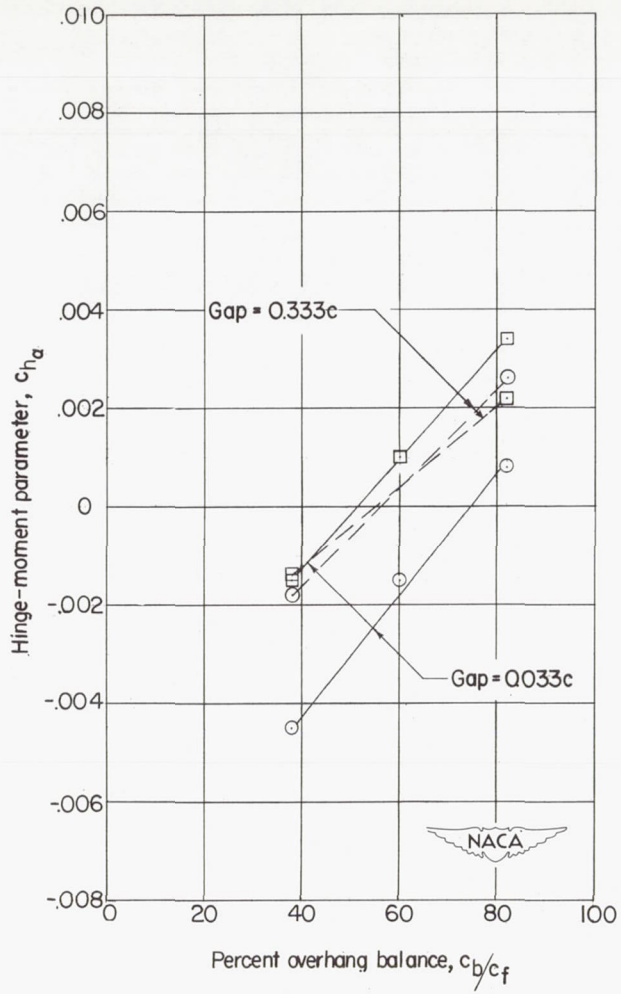
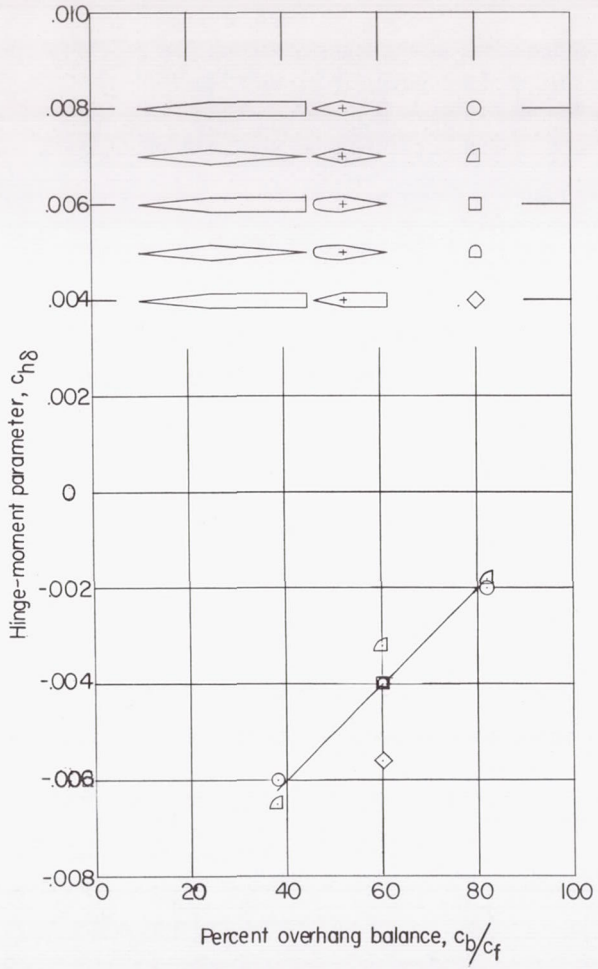


Figure 30.- Comparisons of hinge-moment parameters, c_{h_δ} and c_{h_α}, of basic wing 1 and basic wing 2 equipped with flaps having various amounts of flap-nose overhang at two wing-flap gap sizes.



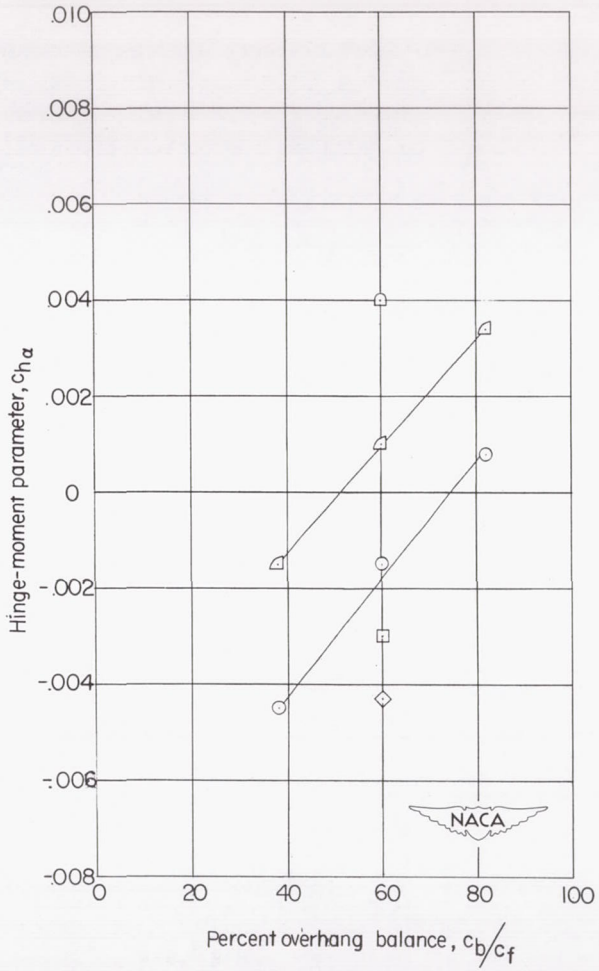
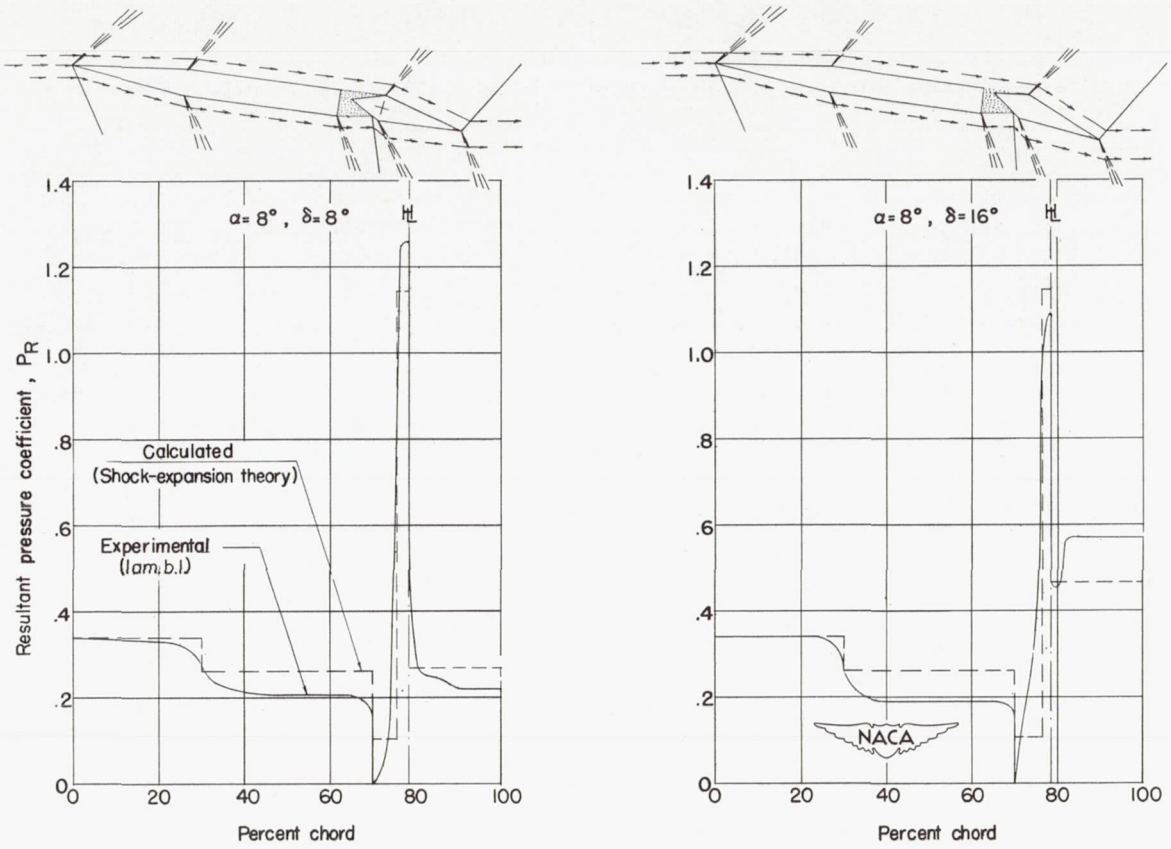
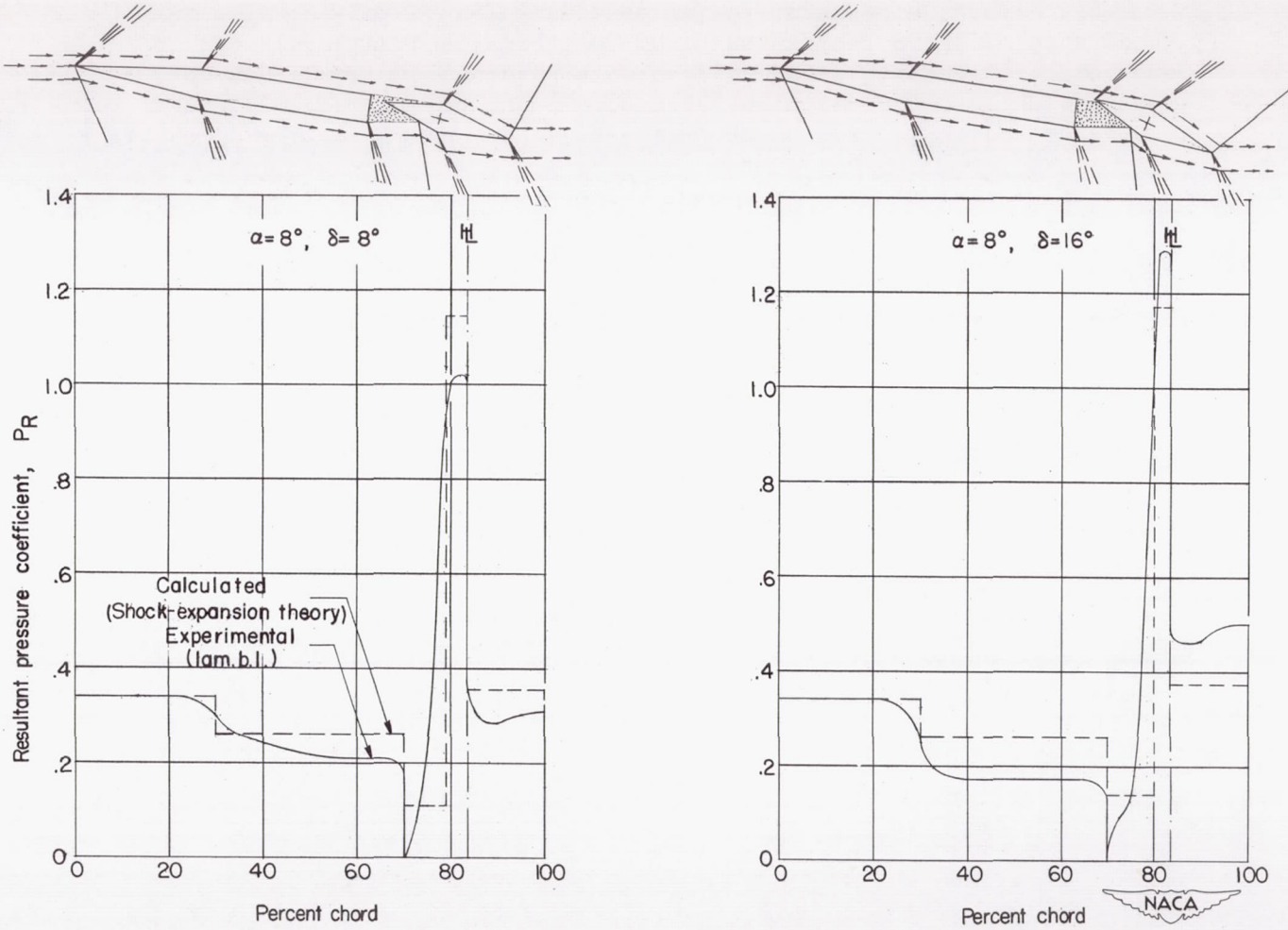


Figure 31.- Comparisons of hinge-moment parameters, c_{h_δ} and c_{h_α}, of basic wing 1 and basic wing 2 equipped with flaps having various amounts of flap-nose overhang and for different overhang shapes and trailing-edge thicknesses. Wing-flap gap size, 0.033c.



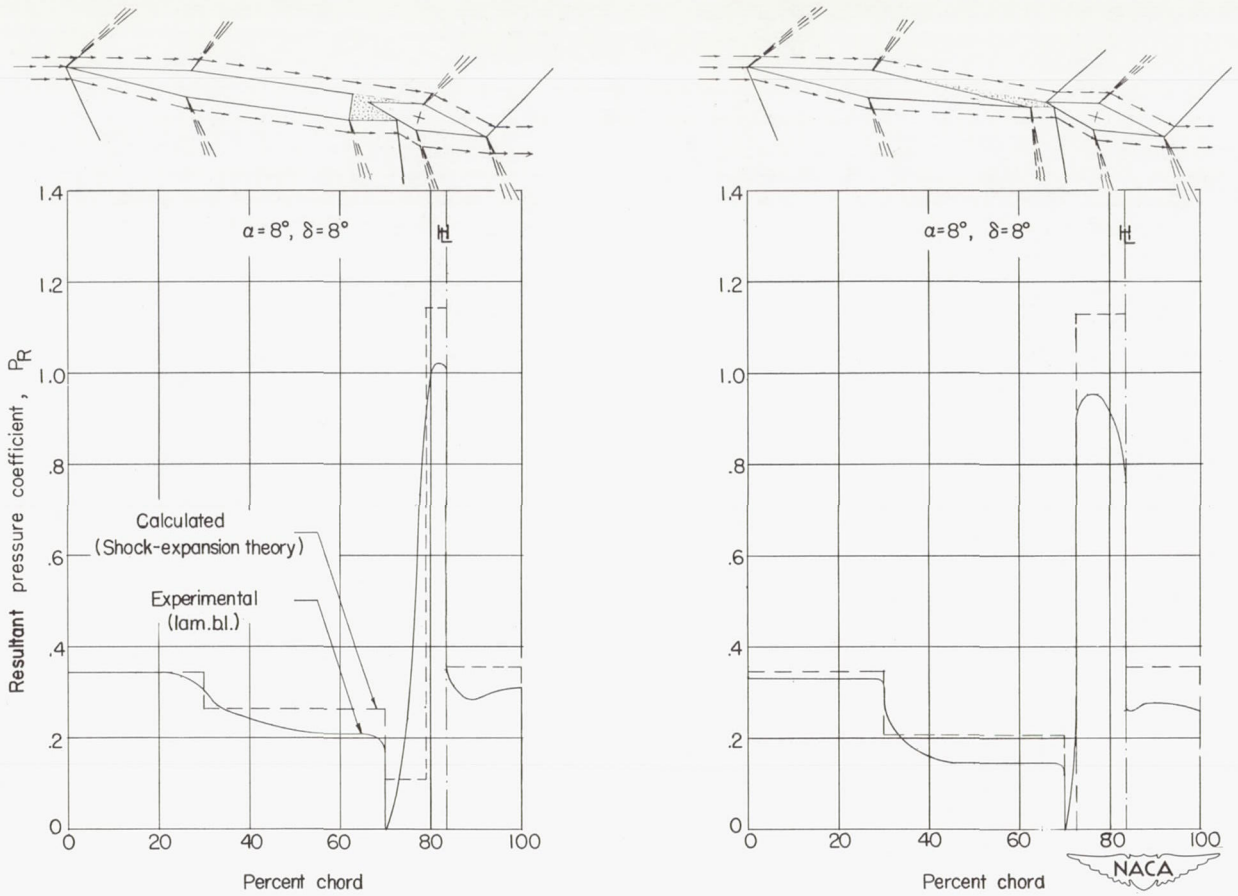
(a) $\frac{c_b}{c_f} = 0.38.$

Figure 32.- Experimental and theoretical aerodynamic-loading diagrams of flap-type controls equipped with overhang nose balances of different chords. Diagrammatic sketches of the wing-flap configurations show the assumed flow patterns upon which the calculation of the theoretical curves are based.



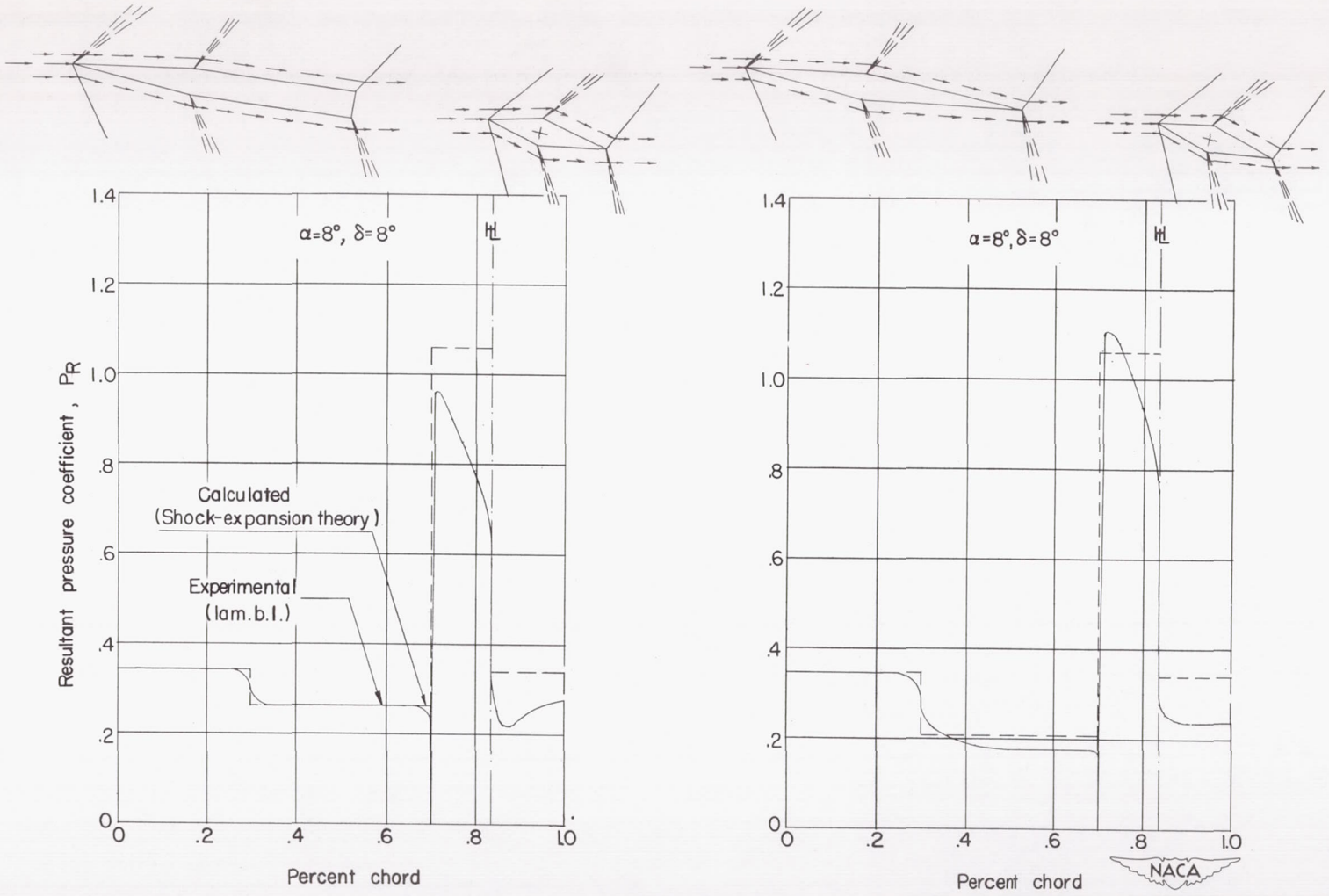
(b) $\frac{c_b}{c_f} = 0.82$.

Figure 32.- Concluded.



(a) Gap = 0.033c.

Figure 33.- Experimental and theoretical aerodynamic-loading diagrams of flap-type controls equipped with overhang nose balances for two wing-flap gap sizes and two wing afterbody shapes. Diagrammatic sketches of the wing-flap configurations show the assumed flow patterns upon which the calculation of the theoretical curves are based.



(b) Gap = 0.333c.

Figure 33.- Concluded.

NACA-Langley - 11-17-53 - 325 CONFIDENTIAL